



UNIVERSITÀ
DEGLI STUDI
FIRENZE

University of Florence

Department of industrial engineering - DIEF

Thesis submitted in fulfilment of the requirements for the degree of

Doctor of Philosophy in
Energy Engineering and Innovative Industrial Technologies

PhD School in Industrial Engineering (ING-IND/09) – XXXI CYCLE (2015-2018)

Thermochemical conversion of wet lignocellulosic biomass for energy and products

Candidate

Eng. Miliotti Edoardo

Edoardo Miliotti

Co-Tutor

Eng. Andrea Maria Rizzo, PhD

Andrea M. Rizzo

Tutor

Prof. Francesco Martelli

Francesco Martelli

Tutor

Prof. Eng. David Chiamonti, PhD

David Chiamonti

PhD Course Coordinator

Prof. Maurizio De Lucia

Maurizio De Lucia

Florence, Italy, October 2018

Declaration

I hereby declare that this submission is my own work, and to the best of my knowledge and belief, it contains no material previously published or written by another person, nor material which to a substantial extent has been accepted for the award of any other degree or diploma at University of Florence or any other educational institution, except where due references are provided in the thesis itself.

Any contribution made to the research by others I have been working with is explicitly acknowledged in the thesis.

Edoardo Miliotti

Florence, October 2018

Acknowledgments

I would like to express my deepest and sincere gratitude to Prof. David Chiaramonti, who gave me the opportunity to work with his research group and to our group leader Prof. Francesco Martelli.

My gratitude goes to Prof. Luca Fiori and Prof. Samir Bensaid, who meticulously revised this manuscript; many thanks for their great effort, valuable suggestions and encouragement.

People working at RE-CORD are simply wonderful and I gratefully acknowledge each of them! A special thanks goes to Andrea, who revised my work and from whom I'll never stop to learn, to Giulia, who patiently performed all the analyses on the HTC aqueous phase with her distinctive kindness and willingness, and to David (Casini), who's the best deskmate ever and greatly contributed to the experimental campaign on digestate conversion.

Thanks to all the students who contributed with their thesis work to bring knowledge and experiences in this research: Leonardo Moricci, Giulia Bisco and especially Alberto Bini (aka *il buon Bini*), who, firstly as a student and then as a very productive collaborator, helped me in the HTC experiments and highly contributed to the calculations in the process integration of AD with HTC and SP.

At last, my gratitude goes to my family – Alberto, Massimo & Patrizia, AnnaMaria Grazia & Mauro, Alba & Augusto – whom love and support has always been invaluable.

Quest'ultima frase di ringraziamenti, in italiano, è tutta per te, Giusy.

Contents

Declaration	I
Acknowledgments	III
Contents	V
List of figures	VIII
List of tables.....	XI
List of acronyms and abbreviations.....	XIII
Summary.....	1
1. Introduction and aim of the study.....	3
1.1 Wet residual biomass	3
1.1.1 Digestate and anaerobic digestion	3
1.1.2 Lignin-rich residue from lignocellulosic ethanol.....	4
1.2 Utilization of char	5
1.2.1 Biochar for agriculture.....	5
1.2.2 Precursor for activated carbons	6
1.3 Aim of the study and technical and scientific objectives	7
2. State of the art of industrial-scale slow pyrolysis and hydrothermal carbonization	9
2.1 Slow pyrolysis	9
2.1.1 Industrial initiatives on biomass slow pyrolysis.....	9
2.2 Hydrothermal conversion of biomass	11
2.2.1 The role of water	13
2.2.2 Industrial initiatives on biomass HTC	13
3. Design and commissioning of the experimental equipment	27
3.1 Micro-Reactor Test-Bench.....	27
3.1.1 Test bench design	27
3.1.2 Characterization and commissioning of the test bench	31
3.2 Commissioning of a horizontal tubular furnace for char activation.....	32
3.2.1 Methodology of the experiments and mass yields	33
3.2.2 Results from the commissioning experiments	34
4. Experimental campaign on Digestate.....	35
4.1 Materials and methods	35
4.1.1 Feedstock.....	35
4.1.2 Experimental equipment and procedure	36
4.1.3 Analytical methods and chemicals	41

4.2	Results and discussion	44
4.2.1	Digestate characterization.....	44
4.2.1	HTC experimental results	44
4.2.2	Solid yields of slow pyrolysis and hydrothermal carbonization	45
4.2.3	Solid product characterization	45
4.2.4	HTC aqueous phase characterization	51
4.2.5	Comparison with EBC, IBI and Italian fertilization decree.....	55
5.	Experimental campaign on lignin-rich residue from 2 nd generation ethanol.....	59
5.1	Materials and methods	59
5.1.1	Feedstock.....	59
5.1.2	Experimental equipment and procedure	60
5.1.2.1	Hydrothermal carbonization	60
5.1.2.2	Physical activation	60
5.1.2.3	Chemical activation	61
5.1.3	Analytical methods and chemicals	62
5.2	Results and discussion	64
5.2.1	LRR characterization	64
5.2.2	HTC experimental parameters.....	65
5.2.3	Preliminary LRR activation.....	66
5.2.4	Solid yields.....	67
5.2.5	Char characterization	68
5.2.6	Activated carbon characterization	69
5.2.7	HTC aqueous phase characterization	74
6.	Process integration and preliminary scale-up design.....	77
6.1	Process integration between anaerobic digestion and hydrothermal carbonization or slow pyrolysis 77	
6.1.1	Reference AD plant.....	77
6.1.2	Integration with fixed bed autothermal slow pyrolysis.....	78
6.1.3	Integration with rotary slow pyrolyzer	80
6.1.4	Integration with hydrothermal carbonization.....	82
6.1.5	Preliminary Economic analysis	86
6.2	Physical activation of LRR at demo-scale: preliminary design and integration with 2 nd generation ethanol and HTC or slow pyrolysis	88
6.2.1	Integration of HTC and physical activation with a demo-scale lignocellulosic ethanol plant .	88
6.2.2	Integration of slow pyrolysis and physical activation with a demo-scale lignocellulosic ethanol plant	89

6.2.3	AC expected incomes	100
7.	Conclusion	101
8.	Appendix.....	103
8.1	MRTB technical drawings	103
8.2	HTC of AD digestate.....	105
8.3	LRR activation	107
8.4	Assessment of digestate compacting (briquetting).....	109
8.5	Proposed P&ID for a pilot rotary plant for physical activation	110
9.	References	111

List of figures

FIGURE 1: GLOBAL INVESTMENT ON NEXT GENERATION BIOFUELS AND BIOCHEMICALS, REPRODUCED FROM [1].	3
FIGURE 2: SIMPLE SCHEME OF A SMALL SCALE BIOGAS PLANT FOR COMBINED HEAT AND POWER GENERATION [6].	4
FIGURE 3: SECOND GENERATION PROCESS FOR ETHANOL PRODUCTION [8].	5
FIGURE 4: TREND OF GLOBAL MARKET SIZE OF ACTIVATED CARBON (PREDICTION FROM 2015 DATA) [27].	6
FIGURE 5: MAIN GLOBAL AC APPLICATION IN 2015 [27].	6
FIGURE 6: BLOCK DIAGRAM SHOWING THE THESIS WORKFLOW.	8
FIGURE 7: ALLOTHERMAL SLOW PYROLYSIS [30].	9
FIGURE 8: AUTOTHERMAL SLOW PYROLYSIS [30].	10
FIGURE 9: LAMBIOTTE (LEFT) AND LURGI (RIGHT) CARBONIZATION PLANTS [31].	10
FIGURE 10: SP ROTARY PILOT PLANT IN DÜRNROHR, AUSTRIA [34].	11
FIGURE 11: PYREG COMMERCIAL CARBONIZATION PROCESS [30].	11
FIGURE 12: COMPARISON BETWEEN HYDROTHERMAL AND CONVENTIONAL THERMOCHEMICAL CONVERSION TECHNOLOGIES (LEFT) AND WATER PHASE DIAGRAM WITH HYDROTHERMAL PROCESSES REGIONS (RIGHT, MODIFIED FROM [35]).	12
FIGURE 13: WORLD MAP OF HYDROTHERMAL CARBONIZATION INDUSTRIAL INITIATIVES.	14
FIGURE 14: INGELIA PLANT IN NAQUERA, SPAIN [71].	15
FIGURE 15: SUNCOAL PILOT PLANT NEAR BERLIN [75].	16
FIGURE 16: CARBONSOLUTIONS HTC PROCESS [76].	16
FIGURE 17: SCHEME OF GRENOL'S HTC PROCESS [80].	17
FIGURE 18: TECHNICAL REPRESENTATION OF LORITUS HTC PLANT [82].	18
FIGURE 19: TERRANOVA HTC PLANT IN JINING, CHINA [83].	19
FIGURE 20: SCHEME OF THE TERRANOVA ULTRA HTC PROCESS WITH PHOSPHOROUS RECOVERY [85].	19
FIGURE 21: AVA-CO ₂ 'S HTC-1 PLANT IN RELZOW, GERMANY [91].	20
FIGURE 22: SCHEME OF THE AVA-CO ₂ MULTI-BATCH HTC PROCESS [92].	21
FIGURE 23: ARTCOAL 3000K PLANT IN HALLE, GERMANY [94].	22
FIGURE 24: REPRESENTATION OF THE SMARTCARBON MULTI-BATCH HTC REACTOR SYSTEM (LEFT) AND ONE HTC MODULE IN LEONBERG (RIGHT) [96].	22
FIGURE 25: SCHEME OF THE SHINKO TECNOS HTC PROCESS [102].	24
FIGURE 26: CARBOREM SIMPLIFIED PROCESS INTEGRATION SCHEME (TOP) AND 3D LAYOUT (BOTTOM) [113].	25
FIGURE 27: SIMPLIFIED SCHEME OF THE MRTB (SINGLE REACTOR CONFIGURATION).	27
FIGURE 28: PRELIMINARY 3D MODEL AND PICTURE OF THE WHOLE BENCH.	28
FIGURE 29: 3D MODEL AND PICTURE OF THE REACTOR (SINGLE AND DOUBLE REACTOR CONFIGURATION).	29
FIGURE 30: FLUIDIZED SAND BED (LEFT) AND INNER VIEW WITH HEATING ELEMENTS AND WELL OF THE TEMPERATURE SENSOR (RIGHT).	29
FIGURE 31: SHAKING DEVICE AND PARTICULAR OF THE ECCENTRIC PIVOT.	30
FIGURE 32: SCREENSHOT OF THE MRTB UI (LABVIEW).	31
FIGURE 33: PRESSURE-TEMPERATURE DIAGRAMS OF SOME OF THE EXPERIMENTS CARRIED OUT WITH ULTRAPURE WATER FOR THE COMMISSIONING OF THE TEST BENCH.	31
FIGURE 34: HORIZONTAL TUBULAR FURNACE USED FOR ACTIVATION EXPERIMENTS (LEFT) AND PARTICULAR OF THE REACTOR (RIGHT).	32
FIGURE 35: SCHEME OF THE EXPERIMENTAL APPARATUS USED FOR ACTIVATION.	32
FIGURE 36: SAMPLES USED FOR THE COMMISSIONING EXPERIMENTS BEFORE AND AFTER ACTIVATION.	33
FIGURE 37: RE-CORD QUANTACHROME NOVA 2200E BET ANALYZER.	34
FIGURE 38: RESULTS FROM THE FURNACE COMMISSIONING EXPERIMENTS.	34
FIGURE 39: WORKFLOW OF THE EXPERIMENTAL CAMPAIGN ON AD DIGESTATE.	35
FIGURE 40: SIMPLIFIED SCHEME OF THE SLOW PYROLYSIS EXPERIMENTAL APPARATUS; PR: PRESSURE REDUCER, FM: FLOW METER, COND: CONDENSER, M: ELECTRIC MOTOR.	36
FIGURE 41: PICTURE OF THE RE-CORD PYROLYSIS APPARATUS.	37
FIGURE 42: BATCH-WISE FEEDING OF THE DRIED DIGESTATE INSIDE THE PYROLYSIS REACTOR.	37
FIGURE 43: PYROCHAR INSIDE THE SLOW PYROLYSIS REACTOR.	38
FIGURE 44: FROM LEFT TO RIGHT: CONDENSER 1, CONDENSER 2 AND BUBBLER AT THE END OF THE SLOW PYROLYSIS EXPERIMENT.	38

FIGURE 45: VACUUM FILTRATION FOR SOLIDS RECOVERY FROM SLOW PYROLYSIS LIQUID PRODUCTS.....	38
FIGURE 46: OVEN-DRIED AND KNIFE-MILLED (4 MM) DIGESTATE FOR HTC EXPERIMENTS.	39
FIGURE 47: INNER VIEW OF THE REACTOR SOON AFTER ITS DISCONNECTION FROM THE MRTB.	40
FIGURE 48: PROCEDURE FOR COLLECTION OF HTC PRODUCTS.	40
FIGURE 49: TYPICAL ASPECT OF DILUTED HTC LIQUID AFTER FILTRATION.	41
FIGURE 50: EXTRACTION OF HTC AQUEOUS PHASE. THE DCM-SOLUBLE ORGANICS ARE CONCENTRATED IN THE BOTTOM FRACTION.....	43
FIGURE 51: METHODOLOGY FOR GAS-CHROMATOGRAPHIC ANALYSES.....	43
FIGURE 52: OPERATING DIAGRAM OF A TYPICAL EXPERIMENT CARRIED OUT AT 250 °C - 3 H.	45
FIGURE 53: COMPARISON BETWEEN THE SOLID YIELDS FROM THE EXPERIMENTS. ERROR BARS REPRESENT ABSOLUTE STANDARD DEVIATION. .	45
FIGURE 54: PYROCHAR (LEFT) AND HYDROCHAR [250 °C-3 H] (RIGHT).....	46
FIGURE 55: COMPARISON BETWEEN HYDROCHAR SAMPLES OBTAINED AT 3 H AND DIFFERENT TEMPERATURE: LEFT 200 °C, RIGHT 250 °C. .	46
FIGURE 56: COMPARISON OF ELEMENTAL COMPOSITION OF DIGESTATE, HYDROCHAR (250 °C-3 H) AND PYROCHAR.....	47
FIGURE 57: VAN KREVELEN DIAGRAM OF DIGESTATE, HYDROCHAR (250 °C-3H) AND PYROCHAR COMPARED TO NATURAL COALS (COALS DATA REPRODUCED FROM [134]).	49
FIGURE 58: SELECTED AQUEOUS PHASE FROM THE HTC EXPERIMENTS.	51
FIGURE 59: CONCENTRATION OF INORGANIC ELEMENTS IN THE HTC LIQUID PHASE.	51
FIGURE 60: CHROMATOGRAMS FROM GC-MS OF HTC AQUEOUS PHASE FROM THE HTC OF AD DIGESTATE.	52
FIGURE 61: CONCENTRATION OF ORGANICS IN THE HTC AQUEOUS SAMPLES MEASURED BY GC-FID.	54
FIGURE 62: WORKFLOW OF THE EXPERIMENTAL CAMPAIGN ON LIGNIN-RICH RESIDUE.	59
FIGURE 63: LIGNIN-RICH RESIDUE AS RECEIVED (LEFT) AND AFTER DRYING, MILLING AND SIEVING (RIGHT).....	60
FIGURE 64: LECO 701 THERMOGRAVIMETRIC ANALYZER USED FOR SP AND CHEMICAL ACTIVATION EXPERIMENTS.	61
FIGURE 65: IMPREGNATION OF THE LRR WITH KOH AT TWO DIFFERENT MASS RATIOS: 1:1 (LEFT) AND 2:1 (RIGHT).	62
FIGURE 66: WATER-SOLUBLE EXTRACTIVES (LEFT), ETHANOL-SOLUBLE EXTRACTIVE (CENTER) AND LIGNIN (RIGHT) OBTAINED FOR THE EVALUATION OF THE LIGNIN CONTENT FROM THE LRR.	63
FIGURE 67: EXTRACTION OF AN AQUEOUS PHASE SAMPLE; THE DEE-SOLUBLE ORGANICS ARE CONCENTRATED IN THE TOP-PHASE.....	64
FIGURE 68: OPERATING DIAGRAM OF A TYPICAL EXPERIMENT CARRIED OUT AT 200 °C - 2 H.	66
FIGURE 69: CHEMICALLY ACTIVATED CARBONS FROM LRR; AS REMOVED FROM THE TGA (LEFT, THE <i>MUFFIN EFFECT</i> IS CLEARLY VISIBLE) AND AFTER WASHING AND DRYING (RIGHT).	67
FIGURE 70: SOLID YIELDS FROM THE PHYSICAL ACTIVATION EXPERIMENTS (THE ERROR BAR REPRESENTS THE ABSOLUTE STANDARD DEVIATION).	68
FIGURE 71: SOLID YIELDS FROM THE CHEMICAL ACTIVATION EXPERIMENTS (THE ERROR BAR REPRESENTS THE ABSOLUTE STANDARD DEVIATION).	68
FIGURE 72: CHAR SAMPLES OBTAINED AFTER THE CARBONIZATION PRETREATMENT.	69
FIGURE 73: ADSORPTION ISOTHERMS (N ₂ , 77 K) OF THE PHYSICALLY (LEFT) AND CHEMICALLY (RIGHT) ACTIVATED CARBONS.....	70
FIGURE 74: ISOTHERMS CLASSIFICATION [143].....	70
FIGURE 75: COMPARISON BETWEEN THE ADSORPTION-DESORPTION ISOTHERMS (N ₂ , 77 K) OF SELECTED ACTIVATED CARBON SAMPLES.....	71
FIGURE 76: CLASSIFICATION OF HYSTERESIS LOOPS [143].....	71
FIGURE 77: BET AREA OF FEEDSTOCK, HYDROCHARS, PAC AND CAC (WITH PAC 500-2 IT IS DENOTED THE ACTIVATED CARBON SUBJECTED TO THE PYROLYSIS PRETREATMENT).	72
FIGURE 78: TOTAL PORE VOLUME OF THE PRODUCED ACTIVATED CARBONS.....	72
FIGURE 79: PERCENTAGE OF THE MICROPORE VOLUME IN THE PRODUCED ACTIVATED CARBONS.....	73
FIGURE 80: PORE SIZE DISTRIBUTION OF SELECTED PHYSICALLY-ACTIVATED CARBONS.	73
FIGURE 81: PORE SIZE DISTRIBUTION OF SELECTED CHEMICALLY-ACTIVATED CARBONS.	74
FIGURE 82: CHROMATOGRAMS FROM GC-MS OF HTC AQUEOUS PHASE FROM THE HTC OF LRR.	75
FIGURE 83: RESULTS FROM THE GC-MS OF THE AQUEOUS PHASE FROM THE HTC OF LRR.	75
FIGURE 84: RESULTS FROM THE HPLC OF THE AQUEOUS PHASE FROM THE HTC OF LRR.....	76
FIGURE 85: SCHEME OF THE AD REFERENCE PLANT WITH MASS AND POWER VALUES.	78
FIGURE 86: SCHEME OF THE AD + AUTOTHERMAL SP PLANT WITH MASS AND POWER VALUES.....	80
FIGURE 87: SCHEME OF THE AD + ROTARY SP PLANT WITH MASS AND POWER VALUES.	81
FIGURE 88: SCHEME OF THE AD + HTC PLANT WITH MASS AND POWER VALUES.....	83
FIGURE 89: SCHEME OF THE ADOPTED SOLUTION FOR THE HEAT FLOW MATCHING.....	84

FIGURE 90: LAYOUT OF THE CONTINUOUS HTC PLANT.....	85
FIGURE 91: NPV TRENDS FOR THE THREE EVALUATED CASES.....	87
FIGURE 92: BLOCK DIAGRAM REPRESENTING THE INTEGRATION WITH HTC.....	88
FIGURE 93: SCHEME OF THE WHOLE PROCESS INTEGRATION WITH HTC WITH ADDITIONAL DATA.....	89
FIGURE 94: BLOCK DIAGRAM REPRESENTING THE INTEGRATION WITH SLOW PYROLYSIS.....	90
FIGURE 95: MASS FLOW OF THE LIGNOCELLULOSIC ETHANOL PLANT.....	90
FIGURE 96: SIMPLIFIED SCHEME OF A CO-CURRENT ROTARY DRYER, MODIFIED FROM [183] AND EXAMPLE OF BIOMASS SHOWERING DUE TO INNER FLIGHTS.....	91
FIGURE 97: MASS FLOW SCHEME OF THE DRYING PLANT.....	92
FIGURE 98: ROTARY KILN BED MOTIONS AND FROUDE NUMBER RANGES (WITHOUT FLIGHTS) [33].....	93
FIGURE 99: PARTICULAR OF THE ROLLING FLOW REGIME [33].....	93
FIGURE 100: MASS FLOW SCHEME OF THE SP PLANT.....	94
FIGURE 101: MASS FLOW SCHEME OF THE ACTIVATION PLANT.....	95
FIGURE 102: SCHEME OF THE WHOLE PROCESS INTEGRATION WITH SP WITH ADDITIONAL DATA.....	96
FIGURE 103: PIVOT TECHNICAL DRAWING.....	103
FIGURE 104: CLAMP 1 TECHNICAL DRAWING.....	103
FIGURE 105: CLAMP 2 TECHNICAL DRAWING.....	104
FIGURE 106: CLAMP 3 TECHNICAL DRAWING.....	104
FIGURE 107: DRIED DIGESTATE EXTRUSION DURING BRIQUETTING.....	109
FIGURE 108: BRIQUETTES PRODUCED FROM DIGESTATE.....	109
FIGURE 109: P&ID OF A PHYSICAL ACTIVATION PILOT UNIT.....	110

List of tables

TABLE 1: COMPARISON BETWEEN TYPICAL YIELDS OF CONVENTIONAL THERMOCHEMICAL AND HYDROTHERMAL PROCESSES OF BIOMASS. VALUES ARE EXPRESSED AS MASS FRACTION (D.B.).	12
TABLE 2: INDICATIVE TIME NEEDED TO REACH A CERTAIN SAND TEMPERATURE (4 kW POWER).	30
TABLE 3: RESULTS IN TERMS OF YIELDS OF THE COMMISSIONING ACTIVATION EXPERIMENTS.	33
TABLE 4: EXPERIMENTAL CONDITIONS OF DIGESTATE SLOW PYROLYSIS AND HYDROTHERMAL CARBONIZATIONS EXPERIMENTS.	36
TABLE 5: DISTRIBUTION OF RECOVERED PYROCHAR.	39
TABLE 6: CHARACTERISTICS OF THE DIGESTATE.	44
TABLE 7: AVERAGE EXPERIMENTAL RESULTS OF THE DIGESTATE HTC TESTS.	44
TABLE 8: CARBON, HYDROGEN AND NITROGEN MASS PERCENTAGE ON DRY BASIS OF THE HYDROCHAR SAMPLES (ABSOLUTE STANDARD DEVIATION IS REPORTED IN BRACKETS).	46
TABLE 9: COMPARISON BETWEEN HYDROCHAR (250 °C-3 H) AND PYROCHAR PHYSICO-CHEMICAL PROPERTIES.	48
TABLE 10: PAHS CONCENTRATION IN THE PYROCHAR SAMPLE. VALUES ARE ON DRY BASIS (ABSOLUTE STANDARD DEVIATION IS REPORTED IN BRACKETS).	50
TABLE 11: INORGANIC ELEMENTS CONCENTRATION IN MG KG ⁻¹ (D.B.) IN THE DIGESTATE, HYDROCHAR (250 °C-3 H) AND PYROCHAR.	51
TABLE 12: CONCENTRATION, IN MG L ⁻¹ , OF MAJOR ORGANIC COMPOUNDS IN THE HTC AQUEOUS SAMPLES (ABSOLUTE STANDARD DEVIATION IS GIVEN IN BRACKETS).	54
TABLE 13: CHAR PROPERTIES AND THRESHOLD VALUES FROM EBC, IBI AND D.L. 29 APRILE 2010, N. 75.	56
TABLE 14: CHAR CONCENTRATION OF INORGANICS AND THRESHOLD VALUES FROM EBC, IBI AND D.L. 29 APRILE 2010, N. 75. VALUES ARE EXPRESSED IN MG KG ⁻¹ (D.B.).	57
TABLE 15: EXPERIMENTAL CONDITIONS OF LRR HYDROTHERMAL CARBONIZATIONS EXPERIMENTS.	60
TABLE 16: RESULTS FROM THE EVALUATION OF THE DEE EXTRACTION EFFICIENCY FROM THE AQUEOUS PHASE.	63
TABLE 17: PROPERTIES OF THE LIGNIN-RICH RESIDUE FROM POPLAR FERMENTATION.	64
TABLE 18: RESULTS FROM THE LIGNIN CONTENT EVALUATION.	65
TABLE 19: AVERAGE EXPERIMENTAL RESULTS OF THE LRR HTC TESTS.	65
TABLE 20: RESULTS FROM THE PRELIMINARY PHYSICAL ACTIVATION OF LRR.	66
TABLE 21: RESULTS FROM THE PRELIMINARY CHEMICAL ACTIVATION OF LRR.	67
TABLE 22: RESULTS FROM THE ELEMENTAL ANALYSIS OF THE CHARS.	69
TABLE 23: MASS FLOW OF THE REFERENCE AD PLANT.	77
TABLE 24: POWER VALUES OF THE REFERENCE AD PLANT.	78
TABLE 25: MASS FLOW OF THE AD AND AUTOTHERMAL SP PLANT.	79
TABLE 26: POWER VALUES OF THE AD AND AUTOTHERMAL SP PLANT.	80
TABLE 27: POWER VALUES OF THE AD AND ROTARY SP PLANT.	81
TABLE 28: MASS FLOW OF THE AD AND HTC PLANT.	82
TABLE 29: POWER VALUES OF THE AD AND HTC PLANT.	83
TABLE 30: GLOBAL EFFICIENCIES OF THE INTEGRATION WITH AD.	83
TABLE 31: INPUT VALUES USED FOR THE CALCULATION OF THE HTC PLANT.	85
TABLE 32: RESUME OF THE PRELIMINARY ECONOMIC ANALYSIS (VALUES ARE EXPRESSED IN K€).	87
TABLE 33: PROFITABILITY INDEX FOR THE THREE EVALUATED CASES.	87
TABLE 34: MASS FLOW OF THE DEMO LIGNOCELLULOSIC ETHANOL PLANT.	91
TABLE 35: MASS FLOW OF THE DRYING PLANT.	92
TABLE 36: MASS FLOW OF THE SP PLANT.	94
TABLE 37: MASS FLOW OF THE ACTIVATION PLANT.	95
TABLE 38: ASSUMED DATA TAKEN FOR THE ROTARY DRYER EVALUATION.	97
TABLE 39: ASSUMED DATA TAKEN FOR THE ROTARY KILN PYROLYZER EVALUATION.	98
TABLE 40: ASSUMED DATA TAKEN FOR THE ROTARY KILN ACTIVATOR EVALUATION.	99
TABLE 41: ANNUAL INCOME FROM AC SELLING FOR THE SP AND HTC SCENARIO.	100
TABLE 42: LIST OF COMPOUNDS THAT WERE IDENTIFIED IN THE AQUEOUS PHASE FROM HTC OF AD DIGESTATE.	105
TABLE 43: DETAILED RESULTS FROM THE PRELIMINARY PHYSICAL ACTIVATION OF LRR.	107

TABLE 44: DETAILED RESULTS FROM THE PRELIMINARY CHEMICAL ACTIVATION OF LRR.	107
TABLE 45: DETAILED RESULTS FROM THE PHYSICAL AND CHEMICAL ACTIVATION OF LRR-HYDROCHAR.	108

List of acronyms and abbreviations

AC:	Activated Carbon
ACS:	American Chemical Society
AD:	Anaerobic Digestion
BET:	Brunauer–Emmett–Teller
b.q.l.:	Below quantification limit
CAC:	Chemically-Activated Carbon
CHP:	Combined Heat and Power
CHNS:	Carbon, Hydrogen, Nitrogen, Sulphur
COD:	Chemical Oxygen Demand
CSTR:	Continuously-Stirred Tank Reactor
d.b.:	Dry basis
DCM:	DiChloroMethane
DEE:	DiEthyl Ether
DFT:	Density Functional Theory
EBC:	European Biochar Certificate
GC-MS:	Gas Chromatography – Mass Spectroscopy
GC-FID:	Gas Chromatography – Flame Ionization Detector
HE:	Heat Exchanger
HHV:	Higher Heating Value
HMF:	HydroxyMethylFurfural
HPLC:	High Performance Liquid Chromatography
HR:	Heating Rate
HTC:	HydroThermal Carbonization
HTL:	HydroThermal Liquefaction
HTG:	HydroThermal Gasification
IBI:	International Biochar Initiative
ICP-OES:	Inductively Coupled Plasma - Optical Emission Spectrometry
IUPAC:	International Union of Pure and Applied Chemistry
LHV:	Lower Heating Value
LRR:	Lignin-Rich Residue
MC:	Moisture Content
MFC:	Mass Flow Controller
MRTB:	Micro-Reactor Test Bench
MSW:	Municipal Solid Waste
n.a.:	Not available
NIST:	National Institute of Standards and Technology
n.m.:	Not measured
NPV:	Net Present Value
NREL:	National Renewable Energy Laboratory
PAC:	Physically-Activated Carbon
PAH:	Polycyclic Aromatic Hydrocarbon
P&ID:	Piping and Instrumentation Diagram
PID:	Proportional-Integral-Derivative
RH:	Relative Humidity
SP:	Slow Pyrolysis
TGA:	ThermoGravimetric Analyzer
TRL:	Technology Readiness Level
UI:	User Interface
US EPA:	Environmental Protection Agency
u.m.:	Unity of measure

UV-VIS: Ultra Violet – Visible
WWT: WasteWater Treatment
w.b.: Wet basis

Summary

The aim of this study is to assess the valorization of wet residual biomass into value-added bioproducts by slow pyrolysis, hydrothermal carbonization (HTC) and physical and chemical activation; in particular, char from anaerobic digestion digestate was intended to soil amelioration, while char from lignin-rich residue from lignocellulosic ethanol was activated for the production of activated carbons. This work deals with experimental investigation in the production and characterization of char from the thermochemical conversion of these wet residual biomasses.

Within the period of the doctorate, a dedicated test bench for hydrothermal conversion experiments and an activation reactor in a specifically adapted ceramic furnace were built for this purpose. The char from slow pyrolysis and hydrothermal carbonization, together with physical and chemical activated carbons and HTC aqueous phase, were comprehensively characterized in laboratory.

The first chapter introduces the issues and the opportunities related with wet residual biomass, in particular with anaerobic digestion digestate and lignin-rich residue from lignocellulosic ethanol, and describes the potential applications of char derived from these feedstocks.

The second chapter deals with a description of hydrothermal carbonization and slow pyrolysis, together with a comprehensive state of the art of industrial initiatives on these thermochemical conversion processes.

The third chapter is related to the design and commissioning of the experimental apparatus, which was used for the hydrothermal carbonization and activation experiments: a micro-reactor test bench (MRTB) and an activation reactor for a tubular ceramic furnace.

In the fourth and in the fifth chapters are respectively reported a detailed description of the experimental campaign on anaerobic digestion digestate and lignin-rich residue. These chapters follow a classic paper structure, with the *material and methods* and *results and discussion* sections.

The sixth chapter focuses on the process integration at industrial/farm scale of the investigated thermochemical processes (slow pyrolysis, hydrothermal carbonization and activation) with the technology that produced the wet residual biomass (lignocellulosic ethanol and anaerobic digestion). A preliminary economic analysis and reactors design is also reported.

1. Introduction and aim of the study

The 21st Conference of Parties (COP21) was held in 2015 in Paris, where more than 190 nations committed themselves to keeping the increase in global average temperature 2 °C below pre-industrial levels, limiting its increase to 1.5 °C. In order to reach this goal, our dependence from fossil fuels has to be heavily reduced and one of the main sector where this can be potentially achieved is the transport sector. Lignocellulosic or 2nd generation ethanol production is a technological process where lignocellulosic biomass, such as wood or agricultural residues (e.g. straw), is converted into this biofuel, which has a relatively well-established downstream infrastructure. However, as recently reported by Lynd [1], this technology is facing a slower growth than initially expected, as can be depicted by the trend of its annual global investments (Figure 1).

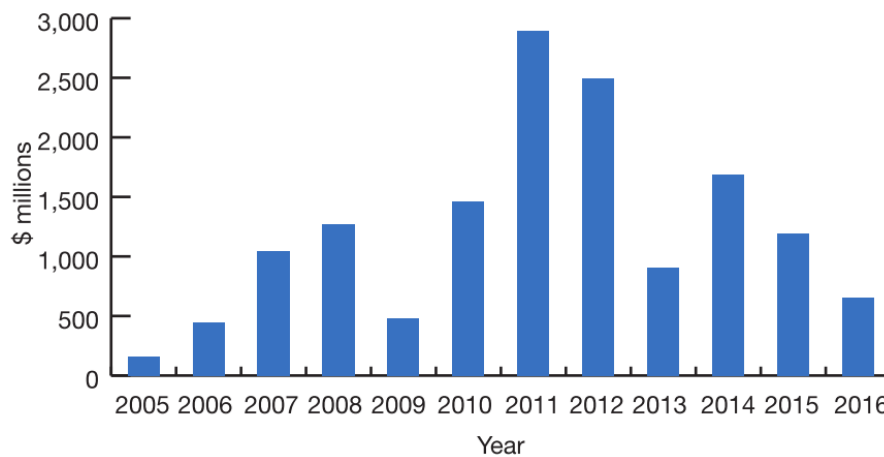


Figure 1: Global investment on next generation biofuels and biochemicals, reproduced from [1].

Partly because of underestimation of technological readiness, partly due to the global financial crisis and collapse of oil prices, and mostly because of the lack of adequate supporting policies, many advanced biofuel startups have failed and those who survived have changed their focus from biofuel to biomass-derived value-added products. More than half of the actual global investment in biofuels and biochemicals is dedicated to the latter [1]. And this is the key point. In a zero-waste biorefinery concept, all products derived from biomass have to be exploited and the production of biofuels (low selling price) should follow that of biochemicals (high selling price).

If 2nd generation ethanol is a well-established technology, which can process agro-industrial and forestry residues at big industrial/biorefinery scale, its small and decentralized farm-scale equivalent is represented by anaerobic digestion for biogas/biomethane production. Between 2009 and 2016, the number of biogas plants in Europe has greatly increased, rising from 6227 to 17662, especially thanks to the increase in plants running on agricultural substrates (12496 in 2016) [2].

Both technologies produce a biofuel and end up with a large amount of a very wet co-product: lignin-rich residue (LRR) in the former case and the so-called digestate in the latter.

1.1 Wet residual biomass

1.1.1 Digestate and anaerobic digestion

Anaerobic digestion (AD) is a commercially well-known technology, in which biomass is directly converted into a flammable gas, the so called biogas, that is mainly composed of methane (50 - 75 % v/v) and carbon dioxide (25 - 50 % v/v). It is one of the few biotechnologies that can simultaneously produce bio-energy and

recycle nutrients. AD is particularly suitable for the processing of very wet feedstock and waste such as municipal sludge, manure and agricultural and food industry residues [3]. In addition, it provides an opportunity for pollutants removal from liquid and solid wastes in a more feasible way than the aerobic processes [4].

The produced biogas can be exploited for local heating in small boilers or for combined heat and power (CHP) in internal combustion engines (see Figure 2) or, rarely, in gas turbines. However, a cleaning step is needed in order to remove H_2S , water vapor, NH_3 and siloxanes, which could cause damage to engines. A further upgrade, in which the CH_4 concentration is increased by means of CO_2 removal, is needed in order to reach the natural gas network requirements in terms of heating value; in this case the gas is referred as biomethane and it is considered a biofuel [5]. A typical Italian AD plant for biogas production is fed with corn silage and has a gross installed power of about 1 MW.

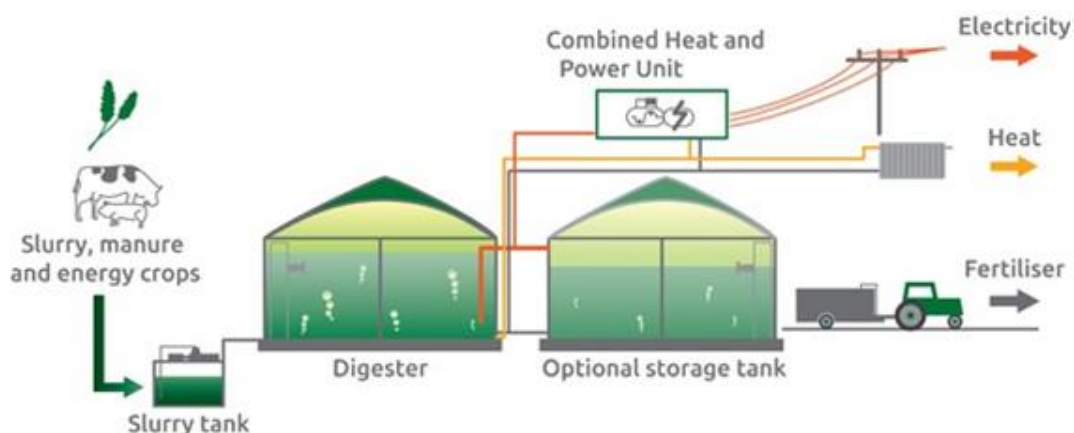


Figure 2: Simple scheme of a small scale biogas plant for combined heat and power generation [6].

As a result of the digestion process, the fraction of the feedstock that is not converted in biogas is called digestate. It is a very wet material that is rich in nutrients and therefore can be used for fertilization; however, its management often represents a critical issue, with problems related to nutrient leaching and environmental pollution, as well as odors and hazards for human health [7]. In this context, the digestate is a material to be disposed, representing a cost rather than a useful product.

Carbonization of the digestate by slow pyrolysis or hydrothermal carbonization can produce a carbonaceous material (char or biochar), which is more stable in soil and more resistant to biological degradation; moreover, any biological hazards for human health are destroyed during the carbonization process.

1.1.2 Lignin-rich residue from lignocellulosic ethanol

The conversion of lignocellulosic biomass to fermentable sugars is a very complex process, due to the highly structured chemical composition of woody biomass. Cellulose and hemicellulose, indeed, have to be firstly separated, as different microorganisms are needed to efficiently ferment their respective sugars, glucose and xylose, to ethanol. A conceptual scheme of 2nd generation ethanol production is depicted in Figure 3.

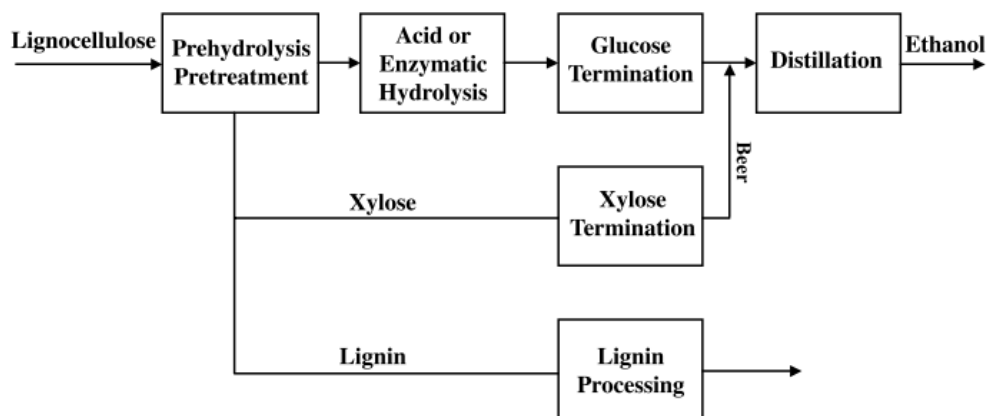


Figure 3: Second generation process for ethanol production [8].

Lignin is not fermentable and, consequently, a large amount of a very wet lignin-rich residue is produced, which in the current management is dried and co-burned for heat and power generation [9]. Lignin is the most abundant source of aromatics in nature and its valorization offers unparalleled opportunity for the green chemistry and circular economy, especially when the feedstock is recovered as a residue from an industrial process. Finding a more profitable way to exploit this co-product stream is fundamental in order to improve the overall biorefinery efficiency and a possible alternative to energy production can be represented by activated carbons. The conventional activation process involves biomass carbonization through slow pyrolysis, but, due to the very high amount of the LRR water content, hydrothermal carbonization represents an interesting option.

1.2 Utilization of char

Char is a solid carbonaceous material originated by biomass carbonization, which can be used for a very wide variety of application; the main ones are the following:

- Solid fuel
- Soil amendment/conditioning for agriculture, where the char is often referred as *biochar* [10–13]
- Advanced carbon material [14]
- Precursor for activated carbons [15–21]

In general, even if char from HTC has often a lower amount of fixed carbon than pyrochar, its potential applications are the same.

1.2.1 Biochar for agriculture

Char application to soil has the potential to mitigate global warming by reducing net greenhouse gas emissions through carbon stabilization and sequestration into soil, it is the so-called “carbon-negative” concept [22], while simultaneously providing energy and increasing crop yields. However, substantial uncertainties exist regarding the impact, capacity and sustainability at the global level, but the use of char for agriculture has indeed also other direct advantages: it improves soil characteristics by increasing water and nutrient retention capacity and microbial activity, reducing the impact of agriculture on the environment [23–26]. Because of the improvement in water retention capacity, the use of char in agriculture is particularly suited to arid lands, e.g. the Mediterranean area, where water availability represents a serious issue. In addition, a sustainable use of agricultural fields with char can help to mitigate our carbon footprint by replacing peat, which is a fossil-derived material, and by reducing the use of energy involved in fertilization.

1.2.2 Precursor for activated carbons

Due to the continuous increase of global population and environmental pollution, the need for clean air and clean water is becoming a relevant issue and governments across the globe are offering subsidies and issuing new stringent environmental regulations and directives for water as well as air purification. Considering also the rapid industrialization of emerging countries, such as the Asia Pacific region, the reasons behind the growth of the activated carbon market (over 3 M\$ in 2015, Figure 4) is explained [27].

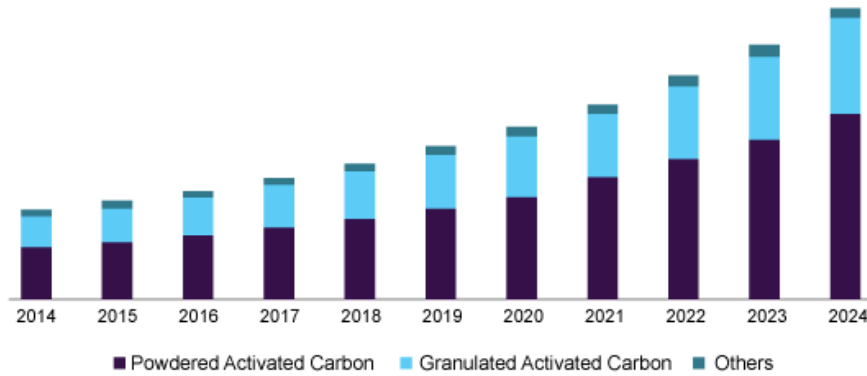


Figure 4: Trend of global market size of activated carbon (prediction from 2015 data) [27].

The main AC applications are indeed referred to water and air treatment as depicted in Figure 5.

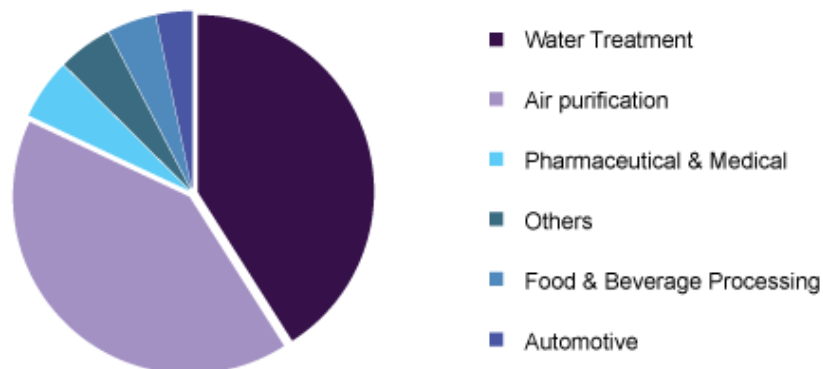


Figure 5: Main global AC application in 2015 [27].

Activated carbons are produced from lignocellulosic biomass (coconut shell, wood, etc.) and from coal, lignite and peat [27]. In order to decrease the dependence from fossil sources, the production of AC from LRR represents an optimal opportunity to exploit a residual and renewable material in the perspective of sustainable bioeconomy.

AC are amorphous organic materials with high adsorption potential, industrially produced via two different processes: physical and chemical activation. In physical activation, an activating agent (steam, carbon dioxide, air or a combination thereof) gasify at elevated temperatures part of the carbon structure, creating a porous structure; in chemical activation, the feedstock is impregnated with a reagent (KOH, ZnCl₂, H₃PO₄, K₂CO₃, etc.) and then it is heated in an inert atmosphere. A combination of physical and chemical methods can be adopted for producing AC with finely tuned porosity [28]. In general, physical activation is carried out on a pre-carbonized material (char, double-step activation), while, in the chemical process, carbonization occurs during activation.

1.3 Aim of the study and technical and scientific objectives

The aim of the present study, whose workflow is depicted in Figure 6, is to assess the valorization of AD digestate and LRR through thermochemical conversion by either slow pyrolysis (SP) or hydrothermal carbonization (HTC) and perform both chemical and physical activation on the LRR char for activated carbon production. The so-produced chars and activated carbons were comprehensively characterized and compared. In addition, also an in-depth characterization of the aqueous phase from the HTC of the two materials was performed in order to investigate its possible reuse.

In particular, due to the very different scale of anaerobic digestion and lignocellulosic ethanol, two distinct end-products were considered for the two wet residual feedstock:

- To transform and stabilize AD digestate into char for soil amelioration
- To valorize LRR by means of activated carbon production, investigating HTC as a pretreatment to activation, in place of conventional slow pyrolysis, and assess if its process conditions affect the AC morphological characteristics

To the author's knowledge, the reported experiences of lignin or lignin-rich biomass in HTC have been carried out on lignin from pulp and paper processes or high-purity model compounds, both of them structurally differing from LRR from advanced lignocellulosic ethanol. The present work aims also at partially filling this gap by preliminary assessing the viability of converting this promising feedstock in batch, subcritical hydrothermal conditions and providing a comprehensive characterization of products.

In order to perform the required experimental campaign, a test bench for hydrothermal carbonization was entirely designed, built, commissioned and operated. In addition, a ceramic tubular furnace was modified and a stainless steel reactor was designed and built in order to carry out the activation experiments.

An investigation on the influence of char addition to soil and plant growth, as well as the adsorption capacity of the produced activated carbons is out of the scope of this thesis, whose focus is related to the technological processes: slow pyrolysis and hydrothermal carbonization, and to the characterization of the related products.

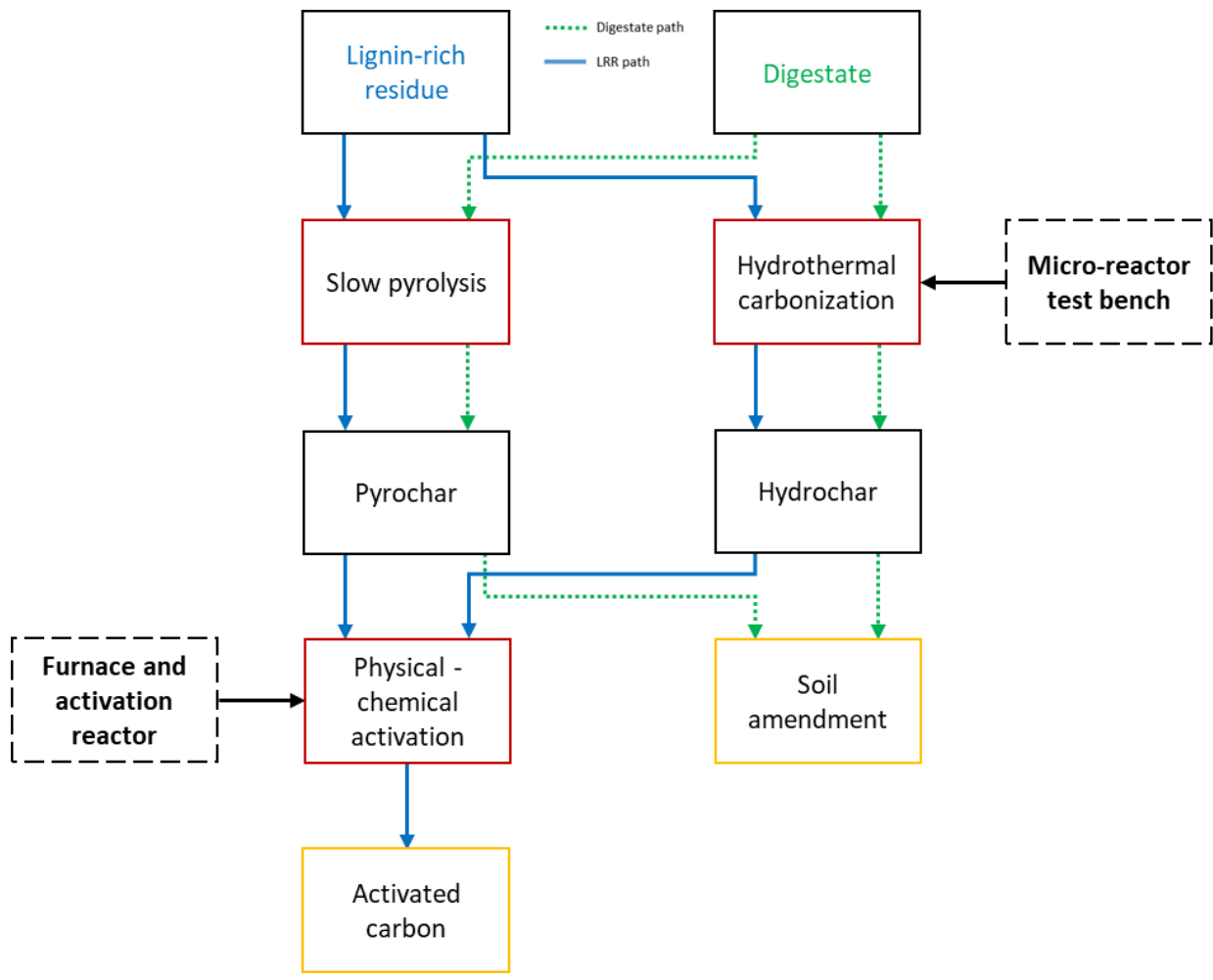


Figure 6: Block diagram showing the thesis workflow.

2. State of the art of industrial-scale slow pyrolysis and hydrothermal carbonization

2.1 Slow pyrolysis

Slow pyrolysis (SP) is an ancient technology, converting biomass material into char by heating (400 - 600 °C) in absence of oxygen or in a limited oxygen atmosphere; together with the main product, also non-condensable gases, water and condensable vapors (tars) are produced. Slow pyrolysis is characterized by slow heating rates and very long solids retention times; differently, the yield of condensable vapors is maximized when very high heating rates and very short vapors residence times are adopted, this is the case of fast pyrolysis for biocrude production.

2.1.1 Industrial initiatives on biomass slow pyrolysis

The carbonization process is operated at a very wide scale: from simple and rudimental batch earth mounds to large continuous industrial systems. Carbonization reactors can be classified in a large number of ways, one of which is the way the reactor is heated: in this case, allothermal and autothermal reactors are defined. In the former reactor typology, the heat for the pyrolysis reactions is provided by an external source, often by the combustion of the pyrogas (Figure 7), while in the latter case, heat is supplied by partial oxidation of the feedstock, due to controlled and limited injection of an oxidizing agent (Figure 8). In general, all commercial processes are operated at ambient pressure, due to economic and operating issues, but it was proven that the char yield is improved when elevated pressures are applied due to increased polymerization of tarry vapors [29].

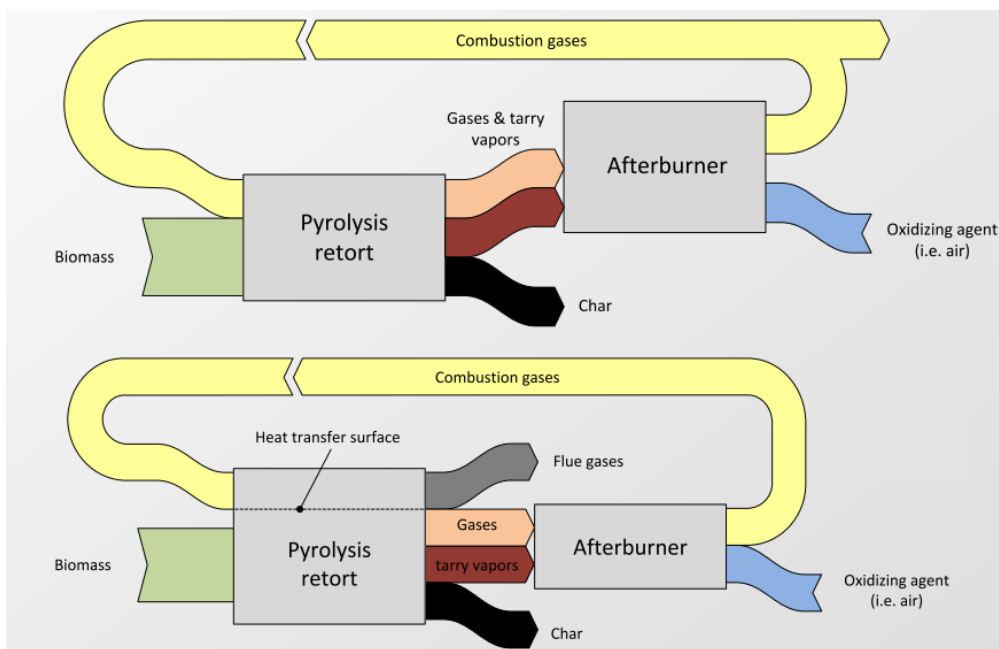


Figure 7: Allothermal slow pyrolysis [30].

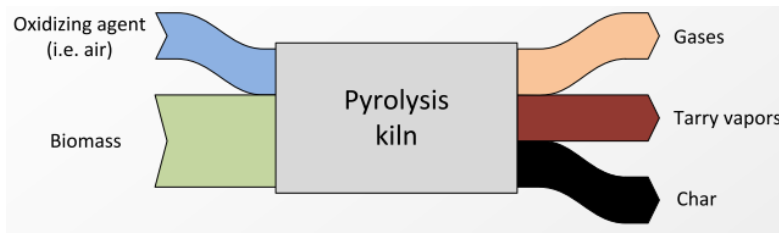


Figure 8: Autothermal slow pyrolysis [30].

The majority of industrial carbonization units are characterized by an allothermal retort configuration, in which the hot vapors and gases are directly combusted around the reactor for producing the heat needed for pyrolysis. One of the SP plant with the highest throughput (6 kt y^{-1} of char, now shut down) was the Lambiotte retort process. It was an autothermal fixed bed process where the hot gases were recirculated in the reactor for temperature control; up to 25 % of conversion efficiency could be achieved. A similar process, operating on the same principle, is the so-called Lurgi process; a plant with a capacity of 26 kt y^{-1} was installed in Bunbury, Western Australia [31]. Both processes are shown in Figure 9.

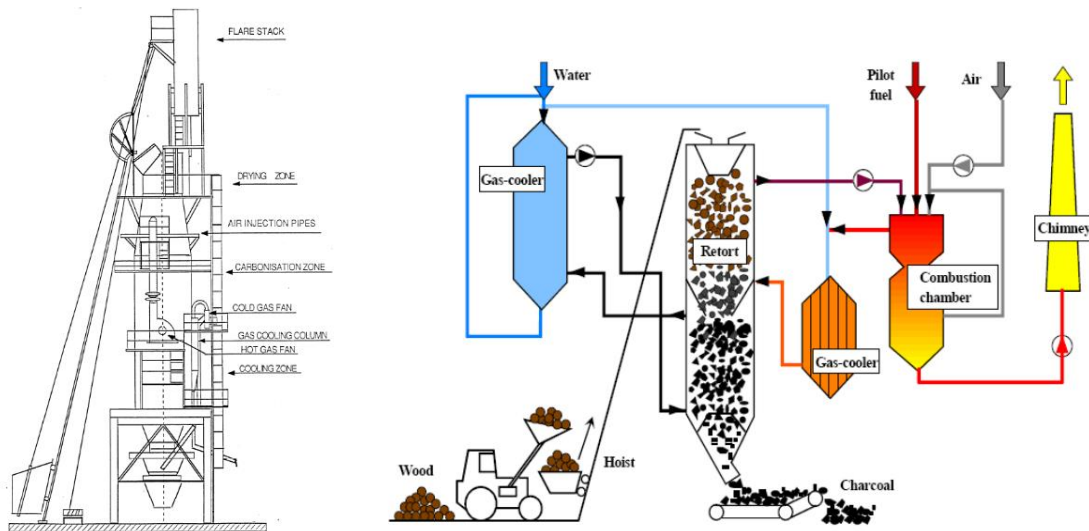


Figure 9: Lambiotte (left) and Lurgi (right) carbonization plants [31].

Another type of reactor used for biomass carbonization is the rotary kiln. Being mainly used in waste incineration and in the cement industry as dryer, it was recently adopted for biomass conversion [32]. They consist in cylindrical shells, which are inclined and rotated to allow biomass to flow down the length of the kiln; the heat for pyrolysis can be supplied by heating the shell from the outside or from the inside by means of hot gas flow. Their main advantages are feedstock flexibility, scalability and maturity of the technology. The main drawback is represented by the complexity in maintaining an inert atmosphere inside the reactor due to rotating seals [33]. As an example, in Figure 10 it is reported a picture of a rotary kiln pyrolyzer, which was installed and operated since 2009 in Dürnröhr, Austria, for the production of char from agricultural residues for co-firing with biomass in a 3 MW thermal power plant [34].



Figure 10: SP rotary pilot plant in Dürnröhr, Austria [34].

A different kind of reactor is the auger one: a commercial example of which is the Pyreg process (1 t d⁻¹ of char, Figure 11). It is a continuous plant where the reactor is externally heated by hot gases from pyrogas combustion and its average char yield is around 27 % w/w [30].

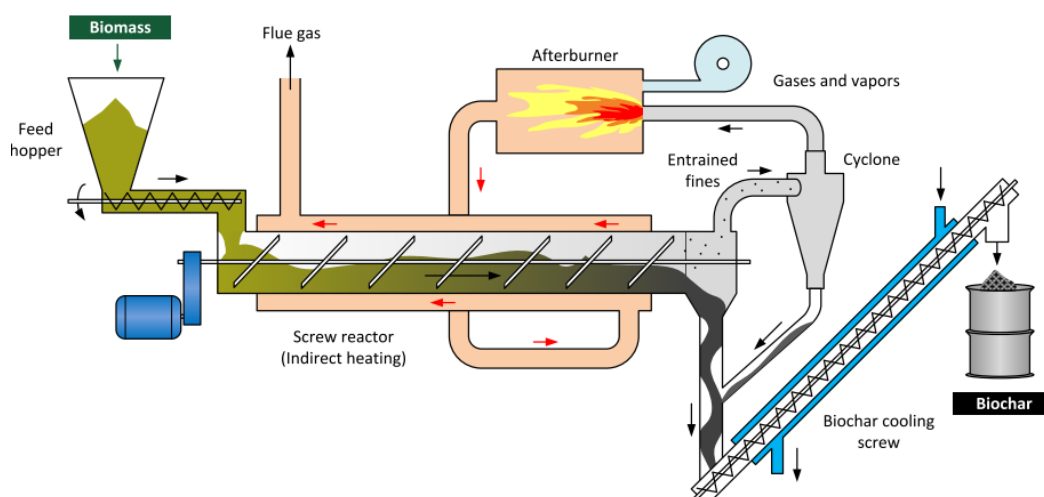


Figure 11: Pyreg commercial carbonization process [30].

2.2 Hydrothermal conversion of biomass

Just like other thermochemical processes such as pyrolysis and gasification, hydrothermal conversion routes transform biomass into a solid, a liquid and a gaseous product; nevertheless, they differentiate from conventional thermochemical technologies by the reaction medium: hot compressed water. This condition makes them highly indicated for treating very wet materials, like micro/macroalgae, sewage sludge, digestate and manure, which cannot be easily converted with conventional technologies, unless energy-consuming pre-treatment steps are taken, as mechanical dewatering and drying [35].

Similarly to pyrolysis and gasification, by varying residence time at reaction conditions and reaction temperature three possible hydrothermal processes occur. At low temperatures (180 - 250 °C) and long residence times (hours) the process is referred to as *hydrothermal carbonization* (HTC) and predominantly produces a lignite-like solid (hydrochar) [36–39]. At intermediate temperatures (200 - 370 °C) and short residence times (minutes) the process is referred to as *hydrothermal liquefaction* (HTL) and predominantly produces an oil/tarry liquid product [35,37,40–44]. At high temperatures (> 350 °C) and short residence times (minutes, highly depending on the catalyst adopted) *hydrothermal gasification* (HTG) reactions occur,

predominantly producing a gaseous phase [35,37,45–47]. A comparison between the operating conditions in terms of temperature and time of conventional thermochemical and hydrothermal processes is presented in Figure 12, together with hydrothermal processing zones in the pressure-temperature diagram of water.

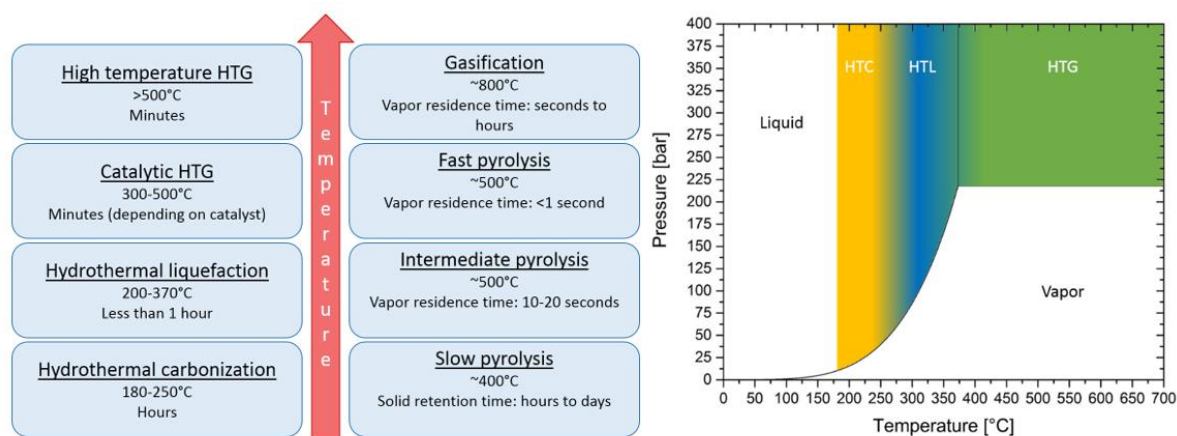


Figure 12: Comparison between hydrothermal and conventional thermochemical conversion technologies (left) and water phase diagram with hydrothermal processes regions (right, modified from [35]).

Typical products' yields are reported in Table 1; these values are highly dependent on the type of biomass used as feedstock and on process conditions and therefore have to be considered as indicative values.

Table 1: Comparison between typical yields of conventional thermochemical and hydrothermal processes of biomass. Values are expressed as mass fraction (d.b.).

Process	Typical yields	Reference
Slow pyrolysis	Solid 35%, Liquid 30%, Gas 35%	[48]
Intermediate pyrolysis	Solid 20%, Liquid 50%, Gas 30%	[48]
Fast pyrolysis	Solid 12%, Liquid 75%, Gas 13%	[48]
Gasification	Solid 10%, Liquid 5%, Gas 85%	[48]
HTC	Solid 60%, Liquid 35%, Gas 5%	[35]
HTL	Solid 5%, Liquid 80%*, Gas 15%	[35,49–51]
Catalytic HTG	Gas 66%	[35,37,45,52]
High-temperature HTG	Gas > 90%	[35,37,45,53]

* Liquid: biocrude 30%, aqueous organics 50%

Hydrothermal carbonization recently gained a renewed interest, but its origin can be dated back to the first years of the 20th century, when Germany started to reduce petroleum dependency by synthesizing liquid fuels from its abundant reserves of coal [54]. In particular, the work of the chemist Friedrich Bergius, although mainly focused on hydrocarbons and coal hydrogenation [55], i.e. on synthetic liquid fuel production, opened the road to the development of the hydrothermal carbonization of biomass [56]. A brief but accurate description of the relation between Bergius findings and hydrothermal carbonization can be found in Titirici et al. [36]. Although in those years the production of coal-like fuel gained less interest than liquid and gaseous fuel synthesis, some of the main reactions involved in hydrothermal carbonization have been exploited also in industrial applications such as thermal dewatering of lignite and peat, where partial carbonization of the feedstock occurred [57,58]. In addition, hydrothermal liquefaction shares similar subcritical water reaction medium with HTC and, therefore, these two processes are strictly related, even if in the former the solid

product has to be minimized. In particular, hydrothermal carbonization of biomass gained renewed interest not only as a process capable of producing renewable solid fuel, but also for the production of high value-added carbon materials. In 2001 carbon nano-spheres were produced via HTC from sugar for the first time [59] and, by accurately tuning the process parameters and/or by means of specific post treatment on the hydrochar, it is possible to obtain highly porous nano-structured materials [36,60–62]. Another aspect that brought notable attention to this technology is that hydrothermal carbonization of fast growing plants was regarded as the most efficient process for atmospheric CO₂ sequestration [63]. Thorough reviews have been made on this subject, which may be useful also for the carbonization process [35,37,42].

2.2.1 The role of water

Although the reaction mechanisms occurring during hydrothermal carbonization are still not completely understood, they can be considered as the sum of hydrolysis, dehydration, decarboxylation, polymerization and aromatization [39]. In this context, water plays a key role as it simultaneously acts as heat transfer medium, reactant, catalyst and solvent.

The reason why hydrothermal conversion processes occur at lower temperature compared to dry thermochemical processes is that the presence of hot compressed water outside and especially inside the biomass structure leads to an enhancement in heat and mass transfer, increasing temperature homogeneity. In addition, water properties such as density, dielectric constant, ionic product and transport properties change drastically with respect to ambient conditions when the critical point is approached (374 °C, 221 bar). These changes in water properties make subcritical water to act as a nonpolar solvent, as water solvation power at 300 °C is roughly similar to that of acetone at 25 °C. The improvement of hydrocarbon solubility in water further enhances their contact with H⁺ ions, accelerating hydrolysis reactions [64]. Hence, water acts as a solvent with changing properties and thus process conditions can be set in order to favour reaction selectivity to the desired products [37,65].

2.2.2 Industrial initiatives on biomass HTC

The majority of hydrothermal carbonization tests have been conducted batch-wise in lab-scale autoclaves; however, various pilot and demonstration-scale plants have been recently built and operated by different firms. Many companies possess their own patented HTC technology and offer commercial or pre-commercial solutions including feasibility studies, design, engineering, construction, testing and after-sales services. The majority of these companies are European, in particular from Germany, but commercial interest in HTC is growing also in Asia (China, Japan, and Indonesia) and new start-ups are emerging also in the United States (Figure 13).



Figure 13: World map of hydrothermal carbonization industrial initiatives.

Ingelia SL

Ingelia SL is a Spanish company located in Valencia; since 2007, it developed a continuous hydrothermal carbonization process, leading to the inauguration in December 2010 of one of the first continuous demonstration HTC plant, in Nàquera, Spain (Figure 14). The plant has a modular design and consists of two continuous reactors for a total annual biomass input of 14 kt and a lignite-like hydrochar and fertilizer production of 3500 and 750 t y⁻¹ respectively. Ingelia's technology, thanks to its modular design, can process different kinds of feedstock (the minimum plant capacity is 6000 t y⁻¹). The process consists in three main steps: feedstock pretreatment (removal of inert material, crushing, sieving), carbonization (at 180 - 210 °C, 10 - 20 bar for 8 - 10 hours) and products post-treatment (hydrochar drying, nutrients separation, etc.). In the case of the Valencia plant, the process water after hydrochar separation is utilized to fertilize citrus trees, however also a solid fertilizer can be extracted from the water phase. Some of the main characteristics of the Ingelia hydrochar, depending on the feedstock used, are higher heating value higher than 24 MJ kg⁻¹, carbon content higher than 60 % w/w and volatile matter between 50 and 70 % w/w [66,67]. Currently, the hydrochar produced at the Valencia plant is used by CPL Industries Ltd., a society leader in production and distribution of solid fuels [68–70].

Three plants are planned to be built in Italy by Ingelia Italia srl in Capannori, Piombino (both in collaboration with CREO srl) and Lecce. These facilities will be characterized by 10 reactors, producing 15 kt y⁻¹ of hydrochar and 3 kt y⁻¹ of fertilizer from 60 kt y⁻¹ of input biomass [66]. A CHP engine and a boiler, both fed with natural gas, will fulfill the energy demand of the plant situated in Capannori [68].



Figure 14: Ingelia plant in Naquera, Spain [71].

SunCoal Industries GmbH

SunCoal Industries GmbH is a German company founded in 2007; in the same year it patented its HTC technology: the CarbonREN process. In 2008 the first continuous HTC pilot plant (Figure 15) was built and operated in Koenigs Wusterhausen, Germany, in 2010 the company moved to Ludwigsfelde, Germany. In 2011 submitted the permit application for the first industrial plant with an annual capacity of about 60 kt of biomass, for a production of approximately 20 kt of hydrochar. In the CarbonREN process a wide range of biomass feedstocks can be converted, such as straw, wood chips, rice husks, waste from palm oil and fruit juice mills, bagasse and so on, with a moisture content ranging from 20 to 75 % w/w [72].

Prior to hydrothermal carbonization, biomass is pretreated to remove impurities and to reduce its size to 60 mm. Then biomass is preheated and pressurized by mixing with recycled process water and low-pressure steam. The stirred reactor receives the biomass mash from the top and charred particles are removed from the bottom. Reaction conditions (200 °C, 20 bar) are reached inside the reactor by means of high-pressure steam injection; residence times are comprised between 6 - 12 hours. The resulting slurry is depressurized, cooled and, subsequently, a hydrochar cake with 50 % w/w moisture content is obtained by mechanical dewatering with a filter press. Separated water is recycled into the process and used for steam production. The hydrochar is finally dried in a fluidized bed to a water content near 5 % w/w and processed into granules, powder or pellets. The energy demand of the process is evaluated to be only 7 % of the energy contained in the hydrochar [72,73]. The CarbonREN HTC process developed by SunCoal Industries is actually commercialized by Valmet for organic sludge treatment and technical carbons production [74].



Figure 15: SunCoal pilot plant near Berlin [75].

CarbonSolutions GmbH

CS CarbonSolutions GmbH is a German company founded in 2007, which has a close collaboration with the Max Plank Society. The company developed and operated in 2010 in Teltow, Germany, a 10 kt y⁻¹ capacity continuous plant, named CS-HTC90. Carbon Solutions claims to convert any type of biomass in 90 minutes thanks to its particular 2-stage countercurrent HTC reactor. Biomass is initially mixed with water and specific additives and it is preheated by means of HTC waste heat. Then the slurry is pumped into the first reaction stage, where it is subjected to a countercurrent flow of steam, generated by the purified process water, and rapidly heats up. In the second-stage reactor, the conversion completes and a filter press subsequently dewateres the char suspension. Hydrochar is sent to a drying step in order to remove its residual water content, whereas the process water is purified in the so-called carbonPure process (COD < 2 g l⁻¹). A fraction of purified water is sent to a steam generator for heating the first stage-reactor (Figure 16) [76].

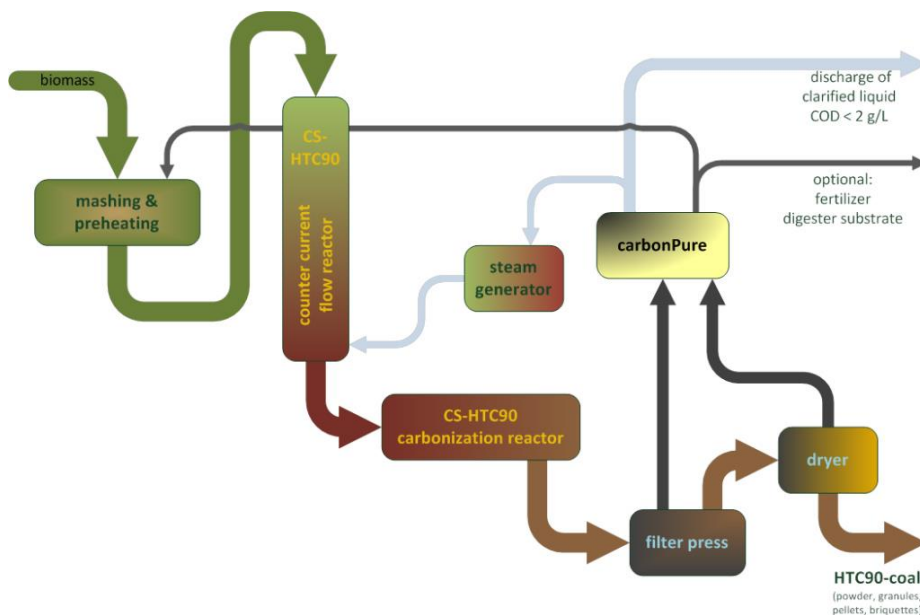


Figure 16: CarbonSolutions HTC process [76].

Grenol GmbH

Grenol GmbH is a German company established in 2007 in Ratingen-Meiersberg [77]. Its services include consulting, engineering, delivery and maintenance of its patented HTC continuous process. In 2012 Grenol operated a prototype plant in Kalkar, Germany, able to process 1 t of biomass waste per year [78]. Recently Grenol presented a HTC base module with the capacity of 10 t day⁻¹ of biomass input (20 - 30 % w/w dry matter content). The plant is set on a 40' container frame for easy transportation. Reactor volume is approximately 2.5 m³, leading to a processing time of 4 - 6 hours; maximum reaction temperature and pressure are, respectively, 230 °C and 30 bar. Depending on the feedstock, the hydrochar output is 1 - 2 t day⁻¹. The process (Figure 17) consists in the following main steps: biomass slurry is pumped and initially preheated in a heat exchanger, then it enters a screw conveyor which is externally heated by a heating medium. Biomass is conveyed into an unstirred reactor and extracted by another heated screw. An exit pump delivers the slurry to a heat exchanger, which is cooled by the thermal medium of the first preheater, and the hydrochar is eventually separated and briquetted. Grenol tested the hydrochar briquettes in their 115 kW gasifier along with wood chips [79]. The company states that its process is thermally self-sustained and only an initial amount of heat has to be given to the system, as approximately 1/3 of the chemical energy of the biomass is released as thermal energy [77,80].

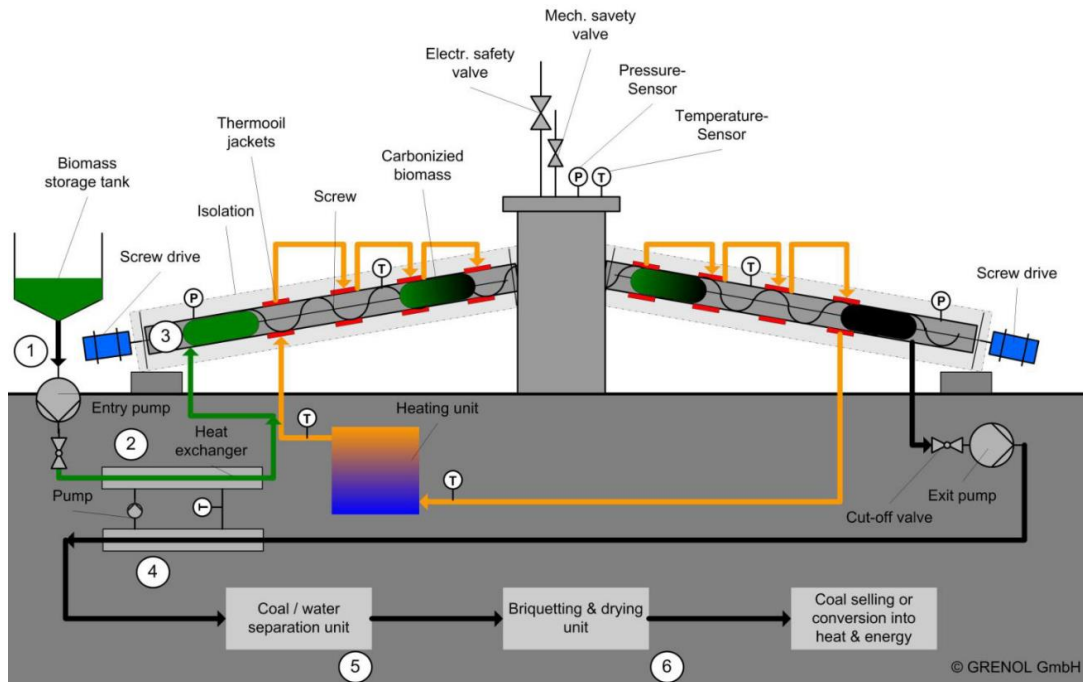


Figure 17: Scheme of Grenol's HTC process [80].

Loritus GmbH

Loritus GmbH is a German company, which claims to be one of the first company to receive patents in HTC reactor designs in Europe. Its continuous process is able to treat any kind of biological waste. Similarly to Grenol, its process is thermally self-sustained thanks to the exothermic nature of the hydrothermal carbonization reactions and residence time can be adjusted in order to obtain different products (hydrochar similar to brown/black coal or nutrients). The company targets input streams between 5 and 6 kt per year. Loritus continuous process utilizes continuously stirred tank reactor (CSTR, Figure 18) with citric acid addition [81].

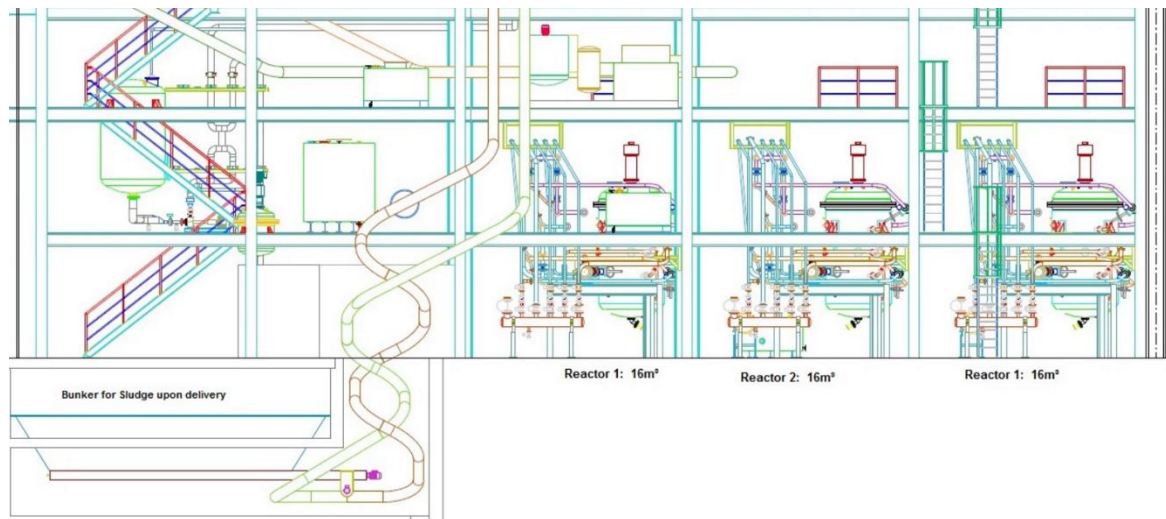


Figure 18: Technical representation of Loritus HTC plant [82].

TerraNova Energy GmbH

TerraNova Energy GmbH is a German company who developed the so-called TerraNova Ultra process: a continuous HTC system for sewage sludge treatment. The main goal of this company is to offer a feasible and efficient alternative to the expensive wastewater and sewage sludge disposal. Indeed, the TerraNova HTC process sterilizes sewage sludge and converts it into a lignite-like coal. The non-organic toxic waste, such as heavy metals, are bound to the char, which can be safely disposed through incineration. The liquid fraction contains a large amount of phosphor, which can be recovered in order to produce fertilizers [83].

The TerraNova HTC method has been proven since 2010, when a pilot plant was implemented in the Kaiserslautern (Germany) wastewater central treatment plant. This facility has been active until the end of 2012. In 2014, other two plants have been operated in Düsseldorf, Germany and in Maribor, Slovenia. On December 2016 the first large scale plant (14 kt of sewage sludge) has been inaugurated in Jining, China (Figure 19); an expansion to the capacity of 40 kt has been planned [83].

As said, the TerraNova Ultra method (Figure 20) consists in a continuous hydrothermal carbonization process: a high-pressure pump pressurizes sewage sludge with 5 – 30 % w/w dry matter content into a tubular heat exchanger, where it reaches nearly reaction temperature, and enters a CSTR. The reaction condition is approximately 3 hours residence time, 200 °C and 20 - 35 bar; catalyst and/or additives are injected in the reactor. From the bottom of the tank, where the charry particles have sunk, the slurry is released to another tubular heat exchanger and then dewatered in a mechanic filter press to a 65 - 70 % w/w solid content. The filtrate is rich in nutrient and it can either be directly used as liquid fertilizer or processed in a phosphor recovery process [84,85]. The heat exchange is carried out by means of diathermic oil. The use of oil-heated tubular heat exchanger upstream and downstream the CSTR avoids the most important disadvantage of a continuously stirred tank: the leaving of early-unconverted material from the reactor. The heat exchanger act indeed as tubular reactor ensuring high conversion efficiency [86].

The company states that their process can be easily integrated with an anaerobic sludge digestion plant, by exploiting the waste heat from the biogas CHP engine to meet the HTC heat demand and by recycling the excess water from the HTC to the digester. In this way TerraNova says that the biogas yield can be increased by an additional 10 % [83].



Figure 19: TerraNova HTC plant in Jining, China [83].

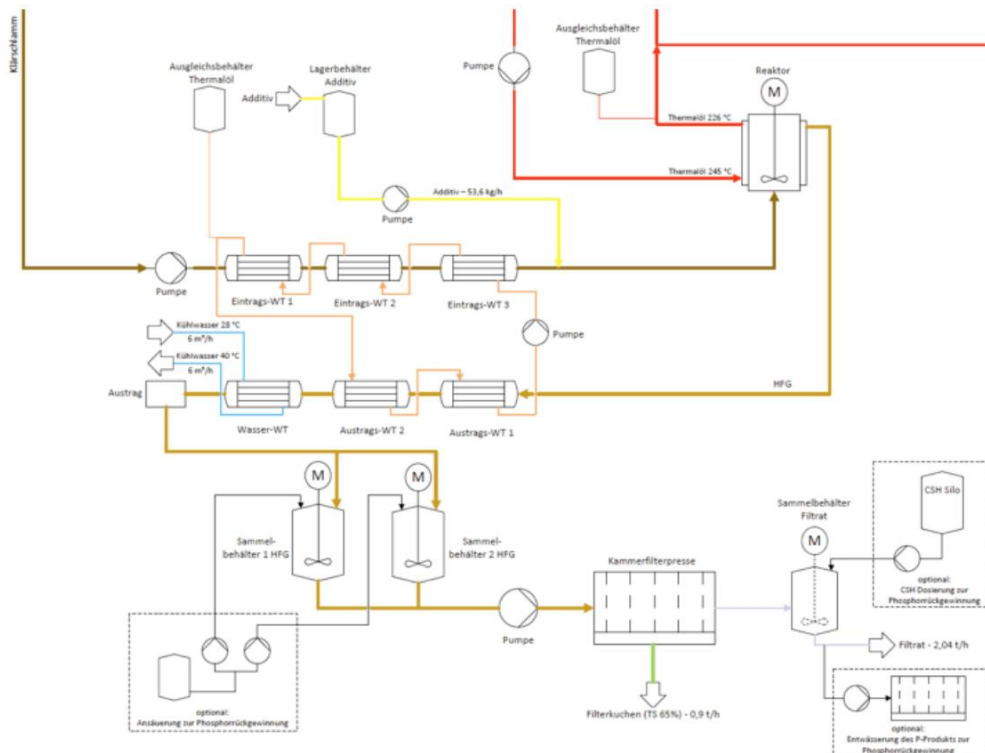


Figure 20: Scheme of the Terranova Ultra HTC process with Phosphorous recovery [85].

AVA-CO2 Schweiz AG

AVA-CO2 Schweiz AG is a Swiss company founded in 2009, which is a pioneer of the hydrothermal carbonization technology. In the same year of its foundation, it operated a HTC pilot plant (K3-335) in collaboration with the Karlsruhe Institute of Technology (KIT). On October 2010 AVA-CO2 and KIT put into operation the first demonstration HTC plant in Karlsruhe (Germany), the so-called HTC-0, capable of processing 8.4 kt of biomass per year [87]. After two years, AVA-CO2 commissioned for Eurosolid the HTC-1 (Figure 21), a commercial-scale hydrothermal carbonization plant, set in Relzow (Germany), with a production capacity of 8200 t y⁻¹ (dry matter) of “AVA cleancoal” [88].

The AVA-CO2 HTC process (Figure 22) is based on a multi-batch concept: biomass is crushed and separated from impurities, then it enters a tank where it is preheated by mixing with high and low pressure steam and

process liquid. After the reaction condition is attained (nearly 220 °C, 22 bar), the slurry is transferred to the reactor. The produced hydrochar settles to the bottom of the reactor and the reacted slurry is then sent to high and low pressure flash tanks by a pump, where heat storage and depressurization is achieved by steam generation. The hydrochar is cooled, dewatered and stored [73]. The multi-batch layout of the plant combines the ease of handling typical of batch systems with the uninterrupted production of continuous processes. While a reactor is filled, another is emptied, ensuring a constant throughput [86]. Moreover, this design is modular and can be adapted to a variety of plant capacities.

AVA-CO2 states that a wide variety of biomass feedstock can be processed by its HTC process, but indicates that the more the cellulose and hemicellulose content and the less the lignin content, the better the hydrochar quality. For instance, spent grains, grassy materials, oil-producing plants, cereal husks, sugar beet and so on are well suited for AVA-CO2 HTC, while woody biomass, meat by-products and animal waste are more difficult to process. AVA cleancoal has a 65 % w/w carbon content, a higher calorific value between 25 and 30 MJ kg⁻¹ and possesses a very small particle size (99 % < 300 μm). Carbon efficiency and net energy efficiency of the process are respectively > 90 % and > 70 % [88].

Although the achieved success in hydrothermal carbonization technology, AVA-CO2 is focusing its efforts on biochemistry, in particular in renewable 5-Hydroxymethylfurfural (5-HMF) production by means of a modified version of the HTC process. In 2014 AVA Biochem, a subsidiary of AVA-CO2, operated Biochem-1, the world's first industrial plant for the production of renewable 5-HMF, in Muttenz, Switzerland. In order to follow the increasing demand of 5-HMF, in 2016 the company AVALON Industries was created, taking over all bio-based chemistry activities from AVA-CO2. The HTC-0 demonstration plant in Relzow and all relevant intellectual property rights of AVA-CO2's hydrothermal carbonization technology have been sold to International Power Invest, a holding company active in the renewable energy field [89,90].



Figure 21: AVA-CO2's HTC-1 plant in Relzow, Germany [91].

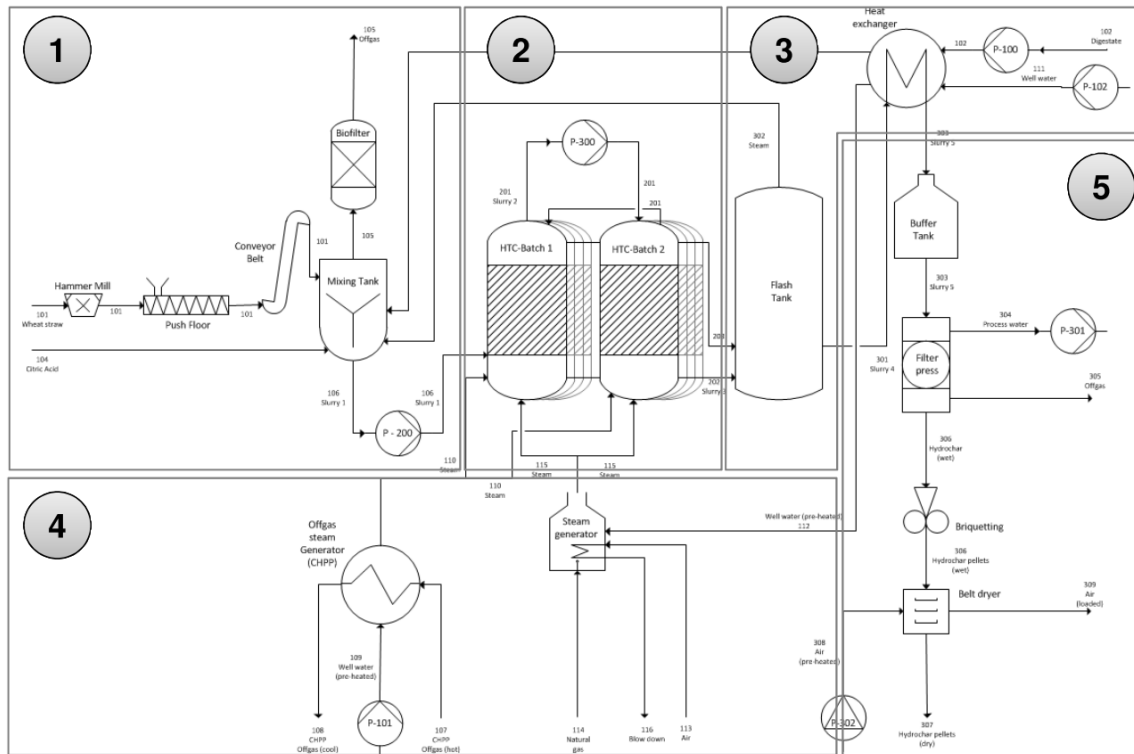


Figure 22: Scheme of the AVA-CO₂ multi-batch HTC process [92].

Artec Biotechnologie GmbH

Artec Biotechnologie GmbH is a German company located in Bad Königshofen and founded in 2009; its shareholders are Renergiesysteme GmbH & Co.KG and Agrokraft GmbH. The company offers development and construction of HTC plants from lab-scale autoclaves to continuous pilot plants [93].

The first continuous pilot plant developed by Artec Biotechnologie is the MOLE I (180-liter reactor), which has accomplished more than 3000 hours of operation. The core of the plant consists in a tubular 180 liter-reactor (9 m length, 150 mm internal diameter) assembled as S-shaped tubes; external heat is provided by means of diathermic oil tube-in-tube heat exchangers as the thermal energy released by the reaction was not sufficient to sustain the process. Maximum reaction condition is 220 °C and 24 bar; reactor dimensions have been selected in order to achieve 8 hours reaction time and the input dry matter is limited to 13 % w/w in order to avoid plugging. The biomass feeding system consists in a funnel, leading the feedstock to a two-ball-valve pressure lock, combined with a piston pump. An equivalent system is placed at the end of the reactor, maintaining the reaction pressure and ensuring continuous processing. The cooling of the reaction products is obtained by means of another diathermic oil heat exchanger. The next project conducted by Artec was the design and construction of a downsized version of the MOLE I (20 l, 3 m length and 120 mm internal diameter); in this lab-scale plant the reactor is heated by electric resistors and the cooling step is achieved by air natural convection. The biggest-scale plant developed by the company is the so-called Artcoal 3000k (Figure 23), a 3 m³ reactor with 250 mm internal diameter and 40 m long, installed in the waste management facility of Halle, Germany. The reactor tubes are U-shaped and distributed in three vertical layers; biomass is inserted from the top in order to allow a higher solid input [86]. The plant is able to process 2.5 kt y⁻¹ of input material and produces about 1 kt y⁻¹ of hydrochar [94].



Figure 23: Artcoal 3000k plant in Halle, Germany [94].

SmartCarbon AG

SmartCarbon AG provides solutions for the conversion of waste biomass into hydrochar and nutrients via hydrothermal carbonization. The company was founded as a spin-off from the non-profit research initiative THINKenergy [95]. SmartCarbon developed a multi-batch design, similar to that of AVA-CO₂, in which biomass is mixed with water and catalytic substances (citric acid) and processed for 4 - 8 hours. In 2012 one-reactor module has been put into operation in Leonberg, Germany, and successfully tested with fermentation residues, sewage sludge, organic fraction of municipal solid waste and other feedstocks (Figure 24) [96].

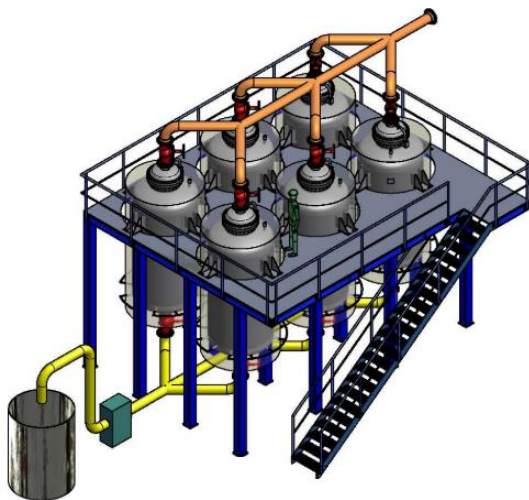


Figure 24: Representation of the SmartCarbon multi-batch HTC reactor system (left) and one HTC module in Leonberg (right) [96].

Antaco UK Ltd

Antaco UK Ltd has been founded in 2011; the company offers design, engineering, construction, servicing and maintenance of its continuous HTC plant. They claim their process is able to convert any type of biomass in 4 - 10 hours at reaction temperature of approximately 200 °C, producing a hydrochar with a heating value of 23 MJ kg⁻¹. In Antaco's process, biomass is mixed with water, pumped, preheated in a heat exchanger and converted in a tubular reactor. The reacted slurry is then cooled in another heat exchanger and finally dewatered [97].

ECN

The Energy Research Centre of the Netherlands (ECN) is a not-for-profit research institute founded in 1955. In 2006 ECN reported the proof of principle of the so-called TORWASH (torrefaction + washing) process [98], which can be effectively assumed to be hydrothermal carbonization. The purpose of this technology is to produce a solid fuel in the form of pellet and biogas from digestion of the organics contained in the process water. The combustion properties of the converted pellets are highly enhanced with respect to the original biomass thanks to the reduction of ash content.

After demonstrating the principle of TORWASH, ECN established a consortium in 2010 to test the technique at lab scale. On May 2015, ECN signed a collaboration with Felda Global Ventures Holdings Berhad (FGV), the world's largest producer of Crude Palm Oil, to build a TORWASH pilot plant at the Mill and Biomass Technology Centre (MBTC) in FGV's Research Complex in Tekam, Pahang (Malesia). The pilot will convert palm empty fruit bunch into fuel pellets for coal plant co-firing [99].

Recently, the TORWASH process has been focused on the conversion of sewage sludge, with the possibility to recover phosphorus. By changing the process conditions, it is possible to obtain a 95 % recovery of P in the solids as well as a 95 % recovery in the liquid phase [100].

Shinko Tecnos Co. Ltd

Shinko Tecnos is a Japanese company founded in 1996. It started producing machinery for the clothes dyeing industry, but recently developed processes for waste treatment [101]. In close collaboration with prof. Yoshikawa from Tokyo Institute of Technology, the company developed a particular hydrothermal treatment (HTT), concerning steam injection (220 °C, 25 bar) into a stirred reactor, capable of converting the input material in less than 1 hour. The hydrochar can be naturally dried and used as a fuel for co-firing with coal in cement kiln, while the process water is cleaned and sent to a boiler for steam production.

Many feedstocks have been tested like municipal solid waste (MSW), lignocellulosic residues, hospital waste, sewage sludge, paper sludge, palm empty fruit bunch, antibiotic bacterial residue and microalgae. Shinko Tecnos possesses two overseas offices (China and Indonesia) and had implemented several commercial HTT plants: in Japan a 5 m³ reactor treating hospital waste and a 12 m³ reactor treating MSW were installed. A 25 t day⁻¹ plant (10 m³ reactor) was also built in Jakarta (Indonesia) for solid fuel production from MSW. Other plants, regarding fertilizer production from food waste and sewage sludge were built in China, Thailand and Sri Lanka [102,103].

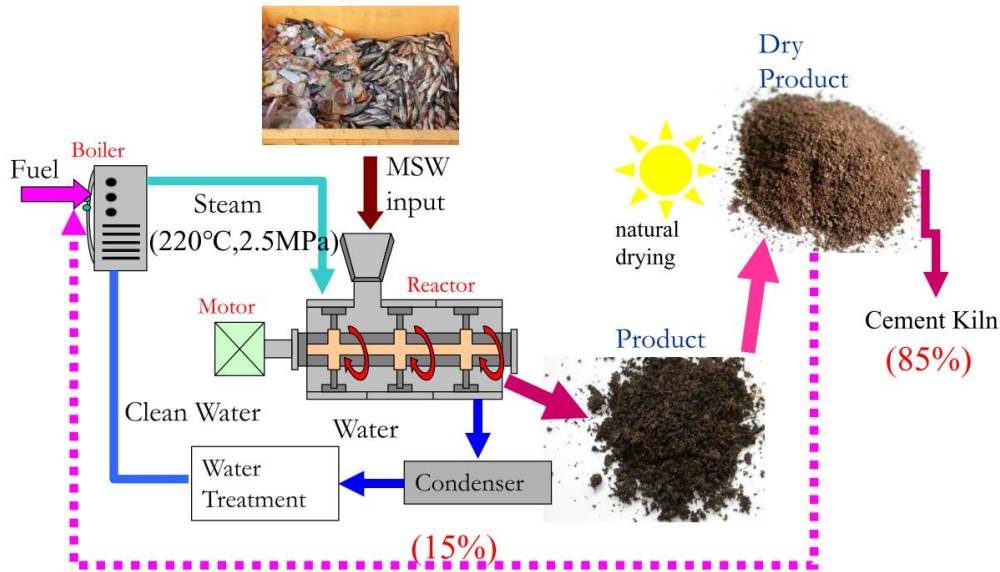


Figure 25: Scheme of the Shinko Tecnos HTC process [102].

HydroTORR

HydroTORR is a US start-up enterprise, which developed the Zero Input Process Carbonization (ZIP-Carb): a continuous HTC process capable of producing a phosphorus-rich hydrophobic solid and a nitrogen-rich liquid fertilizer at the operating conditions of 250 °C and 40 bar. The ZIP-Carb system is modular, scalable and skid-mounted. A nearly 19 l h⁻¹ semi-continuous pilot plant has been developed and demonstrated at the University of Nevada, Reno [104,105].

ThermChem

ThermChem is a start-up company based on University of Minnesota, launched in October 2015. The company is based in Portland, Oregon, USA and has exclusive U.S. patented hydrothermal carbonization technology, including the extraction of Phosphorus for fertilizer production [106]. In April 2017 ThermChem has been selected to collaborate with researchers at the Department of Energy's Pacific Northwest National Laboratory to address technical challenges concerning bio-coal production [107].

EnerTech Environmental, Inc

EnerTech Environmental was a US company based in Atlanta, founded in 1992. Although its core technology, the SlurryCarb process, had never been addressed to as hydrothermal carbonization, this company was one of the first firm to develop a hot-pressurized biosolids conversion process. The main goal of the process was to produce a renewable solid fuel, called E-fuel, from sewage sludge to be sold for co-firing in cement kilns. Biosolids with a water content of 70 - 80 % are firstly macerated to a particle size lower than ½ inch and then pressurized in high pressure slurry pumps. Before entering the reactor, the slurry is heated to 230 °C in a heat exchanger and, after the reaction step, partial cooling and depressurization, it is conveyed to a centrifuge where nearly 50 % w/w of water is removed. The converted slurry could be used as a fuel or eventually dried and pelletized, resulting in a 60 % reduction of energy, if compared to conventional drying of the starting material. The liquids from the centrifuge could be filtered and sent to anaerobic digestion or aerobic treatment [108]. The company operated a 54.5 l h⁻¹ pilot facility in Atlanta and started a collaboration with Mitsubishi Corporation in 1994: a 20 t day⁻¹ plant was commissioned in 2007 in Ube City, Japan. Initially, municipal solid waste was selected as feedstock, but soon technical issues showed up, i.e. pipes clogging, due to the high plastic content of the Japanese waste, which was not taken into account during design calculation. At last, the demonstration was completed, but commercial use in Japan was indefinitely delayed.

After the lesson learned in Japan, EnerTech focused its attention to a simpler waste to be processed: sewage sludge [109]. In June 2009, a 160 M\$ plant including a wastewater treatment facility and a sewage sludge SlurryCarb process was launched in Rialto, California, serving five municipalities in the Los Angeles area and producing 170 t day⁻¹ of E-fuel. The plant suffered from several technical problems and never reached full capacity. In October 2012, the facility was closed and EnerTech was sold to the Canadian firm Anaergia Inc out of bankruptcy in 2013. From its launch, the Rialto plant processed approximately 250 kt of sludge, producing 75 kt of E-fuel [110–112].

CarboREM s.r.l.

CarboREM (Recovery of Energy and Materials) is a recent Italian startup, located in Rovereto (TN), which designs and realizes HTC plants for processing of sludge from wastewater treatment, digestate and organic waste, such as the organic fraction of municipal solid waste and agro-industrial residues. They boast the collaboration with international universities, such as Boston, Hohenheim and Penn State University, but their HTC technology was developed by University of Trento and consists in using a closed reactor, operating at temperatures and pressures lower than 200 °C and 20 bar, respectively, with a residence time from 1 to 3 hours. Their technology is scalable, reduces sludge pathogens, allows the recovery of nitrogen and phosphor and is thermally self-sustainable. The highly hydrophobic hydrochar can be used as a solid fuel or as a soil amendment, while the aqueous phase can be used to boost biogas production. When combined with a wastewater treatment plant, it allows rapid and efficient sludge sterilization and dewatering, as the produced hydrochar is highly hydrophobic, reducing transport volumes and, consequently, disposal costs. In Figure 26 a simplified scheme and a 3D layout of the plant is represented [113].

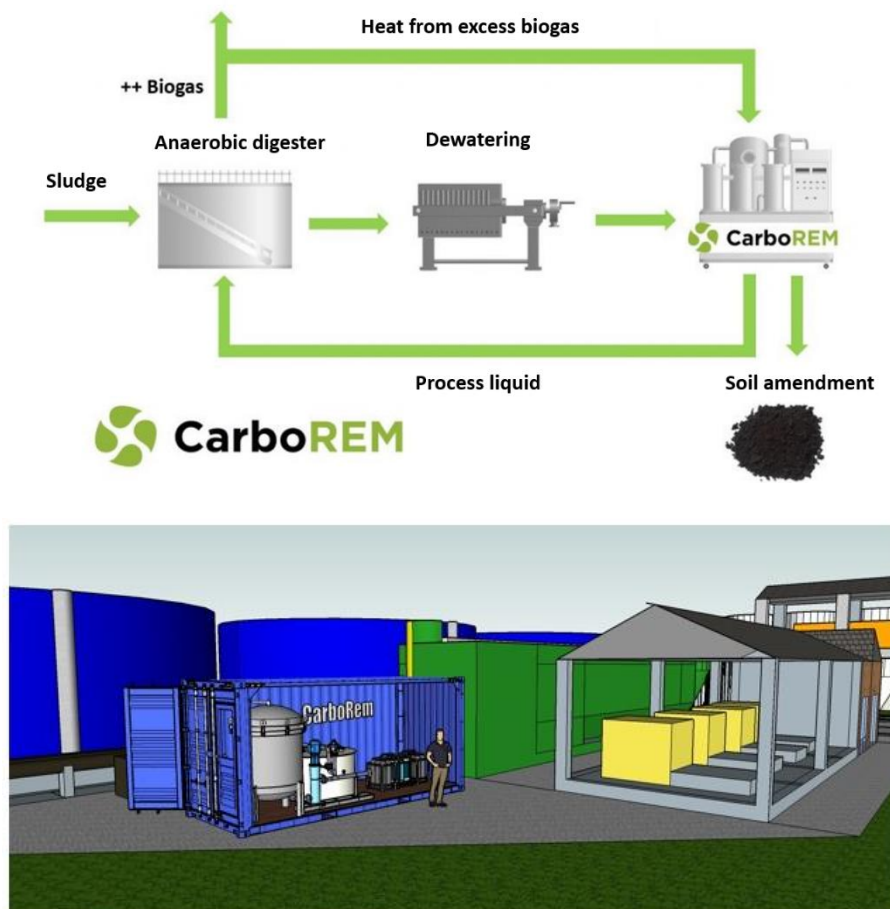


Figure 26: CarboREM simplified process integration scheme (top) and 3D layout (bottom) [113].

3. Design and commissioning of the experimental equipment

3.1 Micro-Reactor Test-Bench

The Micro-reactors test bench (MRTB) was completely designed and assembled during the first year of the doctorate. More details regarding technical drawings are reported in the Appendix.

The MRTB allows performing batch experiments of biomass conversion (pressurized pyrolysis, HTC, HTL, etc.) under a wide range of operating conditions. Its fully modular architecture and small scale permits to rapidly screen the effect of distinct process parameters, allowing the systematic investigation of their effect on products relative distribution, quality or properties. Leveraging its flexibility, moderate operating cost and high availability, the bench is particularly suited for research, from preliminary screening to process optimization.

3.1.1 Test bench design

The Micro-Reactor Test Bench consists in a lab-scale plant on a five-wheeled modular aluminum structure (Robotunits). Its main components are:

- Reactor(s)
- Air-fluidized sand bed
- Water bath
- Shaking device
- Gas cylinder
- Temperature and pressure sensors
- Data acquisition system

In Figure 27 and Figure 28, the piping and instrumentation diagram (P&ID), 3D model and a picture of the whole bench are shown.

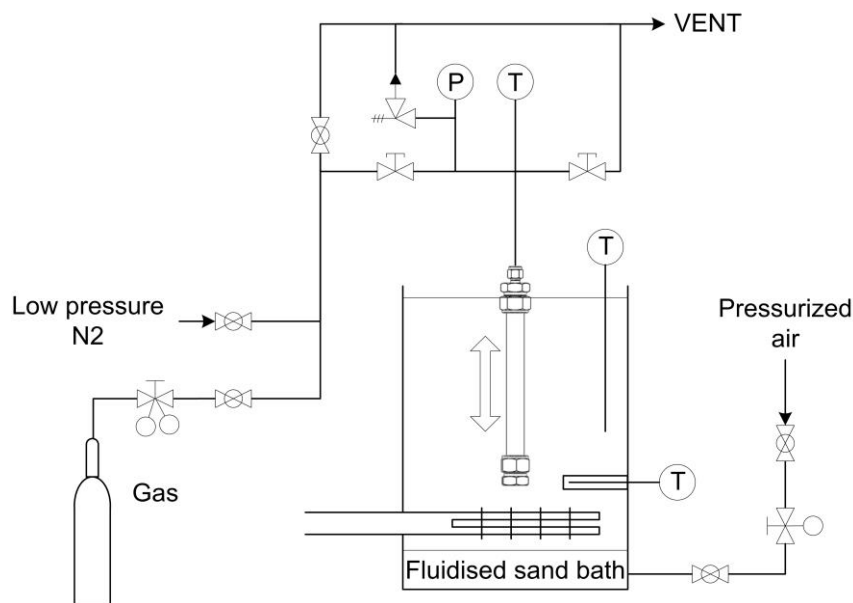


Figure 27: Simplified scheme of the MRTB (single reactor configuration).

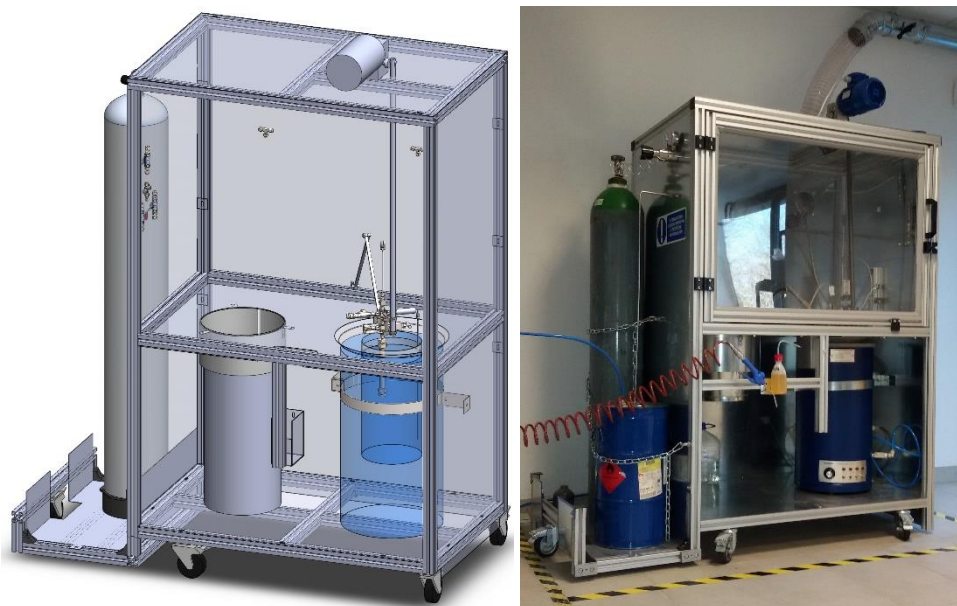


Figure 28: Preliminary 3D model and picture of the whole bench.

The operative principle is the following: once the feedstock is inserted in the reactor, the latter is connected to the bench and is pressurized by means of the gas cylinder, which is located on the bench itself. The typology of gas can be changed by substituting the cylinder, but in general an inert gas, e.g. argon, is used for HTC experiments when a high initial pressure is needed. The reaction temperature is achieved thanks to immersion into the air-fluidized sand bed; pressure is autogenous and its final value is due to temperature increase and gas formation. Once the user-defined reaction time is expired, the reactor is removed from the sand bed and is put into the water bath for fast quenching; after reaching room temperature, the reactor is depressurized and disconnected for products collection.

The reactor is the heart of the MRTB, and it was designed to withstand to 300 bar at 400 °C, in order to be able to investigate both HTC and HTL reaction conditions. The reactor consists of a $\frac{3}{4}$ " AISI 316 Sandvik tube (0.109" thickness), which is connected to the bench by means of Swagelok stainless steel fittings. Because it is composed of commercially available items, it is modular and the length, thickness and number of the reactors can be varied according to the specific needs of the experiment; in a single reactor configuration, the inner volume can be set up to nearly 50 ml. In Figure 29, the preliminary 3D model and a picture of the reactor are shown.



Figure 29: 3D model and picture of the reactor (single and double reactor configuration).

The reactor is equipped with two needle valves for initial pressurization and final depressurization, a conveniently calibrated high-pressure relief valve, a pressure transducer and a temperature sensor, which measure the inner slurry temperature.

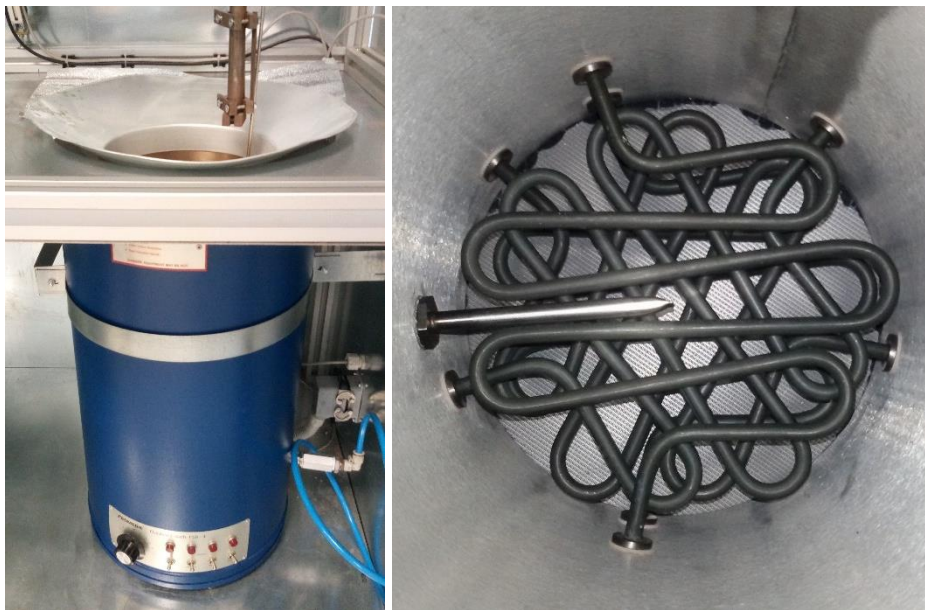


Figure 30: Fluidized sand bed (left) and inner view with heating elements and well of the temperature sensor (right).

The air-fluidized sand bed (FSB-4, Omega Engineering, Figure 30) is equipped with four 1 kW electric heaters and is able to reach a maximum temperature of 600 °C. Due to the high amount of sand (F0885 Alundum, brown aluminum oxide), the inertia of the system is relevant and the higher the desired set temperature the longer the heating time. In Table 2, the indicative heating times are reported for 4 kW heating power at a fixed airflow.

Table 2: Indicative time needed to reach a certain sand temperature (4 kW power).

<i>Time from start [hh:mm]</i>	<i>Sand temperature [°C]</i>
00:00	20
00:16	100
00:29	150
00:45	200
01:00	250
01:22	300
01:48	350
02:11	400
03:12	450
04:55	500
05:20	540

The air pressure should not exceed 0.2 bar and, in order to keep an acceptable fluidization (bubbles diameter near to 2 cm), the former has to be decreased while temperature is increasing, due to greater air expansion. The advantage of using a fluidized bed is that a fast and very high homogeneity of temperature can be achieved. The shaking system (Figure 31) consists in an electric motor (2 pole pairs, 0.37 kW) coupled to a gearbox (transmission ratio 7:1); the gearbox is then connected to a custom-made eccentric pivot, which moves a shaft where the reactor is tightened by means of a custom-made clamp system. An inverter (7 - 140 Hz) controls the speed of the motor and, consequently, the shaking frequency of the reactor can be varied from 0.5 to 10 Hz.

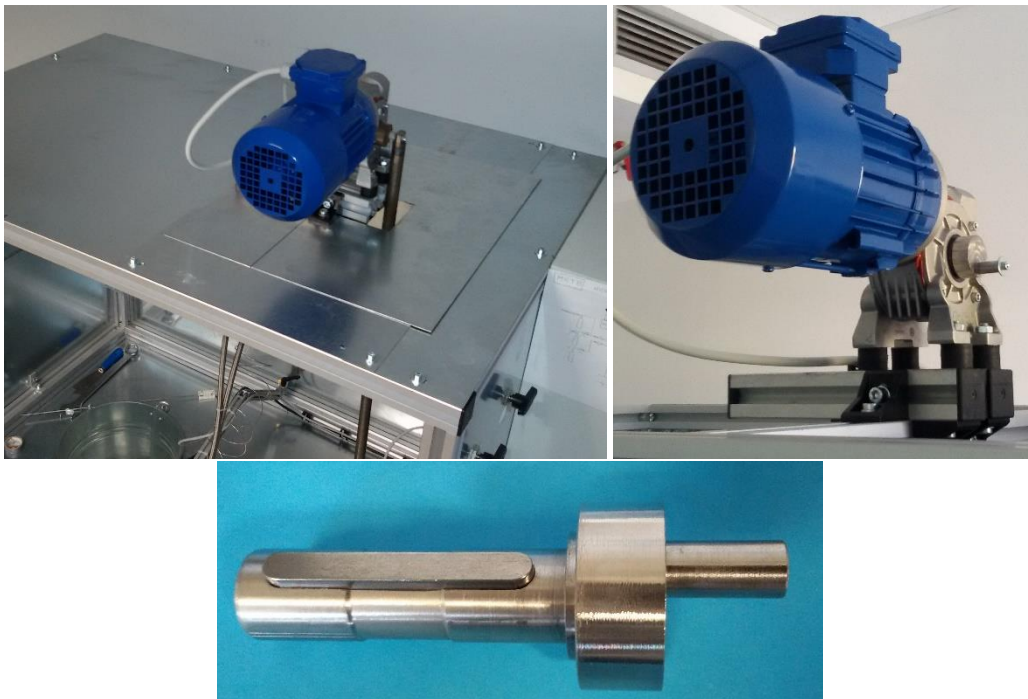


Figure 31: Shaking device and particular of the eccentric pivot.

The pressure sensor is a 0 - 400 bar strain gauge pressure transducer (Trafag); its sensitive membrane is made of stainless steel, making it able to tolerate harsh conditions. The reaction temperature is measured inside the reactor by means of an immersed 3-wire RTD sensor (100 Ohm, 1/10 DIN accuracy class), while the sand temperature is monitored by two 3-wire RTD sensors (B accuracy class). The data acquisition system consists

in a NI cDAQ-9178 (National Instruments), with digital and analog I/O modules; the control logic and the user interface (UI) were specifically developed in LabVIEW environment (Figure 32).

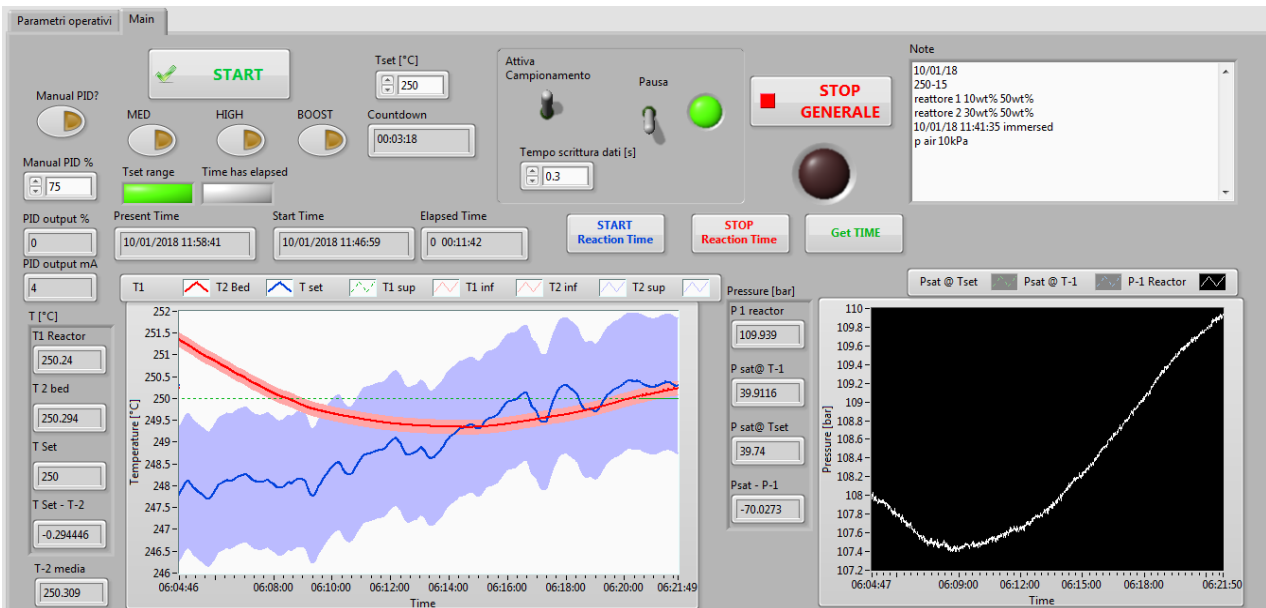


Figure 32: Screenshot of the MRTB UI (LabVIEW).

3.1.2 Characterization and commissioning of the test bench

Ten experiments with ultrapure water were carried out for the characterization and commissioning of the test bench in order to test the MRTB performance. Five set temperatures (150, 200, 250, 300, and 350 °C) and four initial pressures (0, 5, 20, 55 bar gauge) were investigated, with and without the shaker action. In Figure 33, pressure-temperature diagrams of some selected experiments are reported.

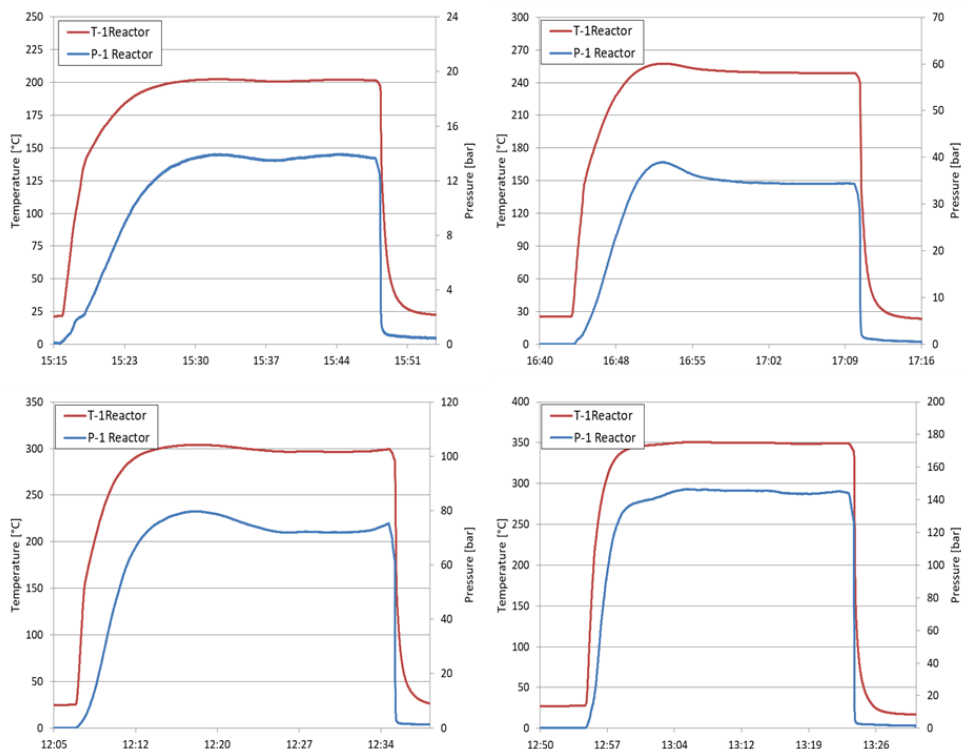


Figure 33: Pressure-temperature diagrams of some of the experiments carried out with ultrapure water for the commissioning of the test bench.

3.2 Commissioning of a horizontal tubular furnace for char activation

A horizontal ceramic tubular furnace (1.3 kW, max temperature 1200 °C, Figure 34) was adapted to RE-CORD experimental facilities for the activation experiments. In particular, an AISI 316 tubular reactor (3/4" outer diameter, 300 mm length) was built and connected to RE-CORD gas mass flow meters (nitrogen and carbon dioxide, 99.999% purity), according to the scheme reported in Figure 35. At the end of the reactor, a glass fiber filter was used in order to prevent carbon particles to be removed due to gas flow; in the same zone, temperature is measured by means of a K-type thermocouple, with which the temperature of the furnace is controlled by a PID controller. After the reactor, an AISI 316 water bubbler was used for further gas cleaning. Prior to the reaction zone of the reactor, a 1/8" coiled tube was built and connected for increasing the gas residence time in the furnace and guarantee the achievement of reaction temperature. Data acquisition and gas flowrate control were carried out with the same LabVIEW hardware adopted for the MRTB; again, the software had been specifically programmed for this purpose.



Figure 34: Horizontal tubular furnace used for activation experiments (left) and particular of the reactor (right).

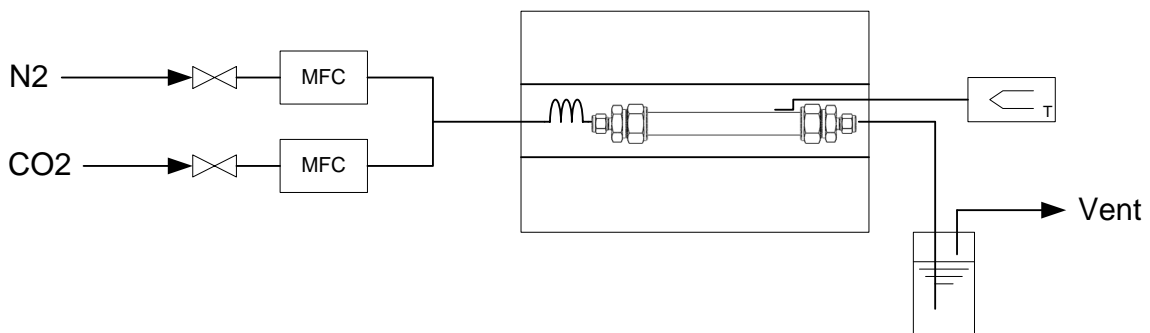


Figure 35: Scheme of the experimental apparatus used for activation.

In order to evaluate the furnace performance, four samples were physically activated with a CO₂ flow:

- Olive stone char produced in RE-CORD intermediate pyrolysis reactor
- Chestnut wood chip char produced in RE-CORD slow pyrolysis plant
- Lignite
- Anthracite

3.2.1 Methodology of the experiments and mass yields

The sample was inserted into the reactor, which is then weighed and located in the tubular furnace. Once connected to the gas line, N₂ flow was activated for air purging. The heating was started and, when set temperature was reached (800 °C), the gas flow (250 ml min⁻¹) was switched from N₂ to CO₂; activation time started (2 h) at this point. After the expire of activation time, nitrogen was switched back until a relatively low temperature was reached. The reactor was then disconnected and removed from the furnace, weighed and opened for activated carbon collection.

In Table 3, the obtained mass yields are reported: the olive stone char and lignite exhibited similar yields, being their mass more than halved; the chestnut slow pyrolysis char was slightly more resistant to mass loss and anthracite led only to an 8.9 % w/w mass loss. In Figure 36 are reported the pictures of the samples before and after activation.

Table 3: Results in terms of yields of the commissioning activation experiments.

Parameter	Olive stone char	Chestnut wood chip char	Anthracite	Lignite
Sample mass [g]	10.8	10.5	10.9	10.1
Activated mass [g]	4.6	5.3	9.9	4.19
Yield [% w/w] d.b.	42.6%	50.5%	91.2%	41.5%
Mass loss [% w/w] d.b.	57.4%	49.5%	8.8%	58.5%

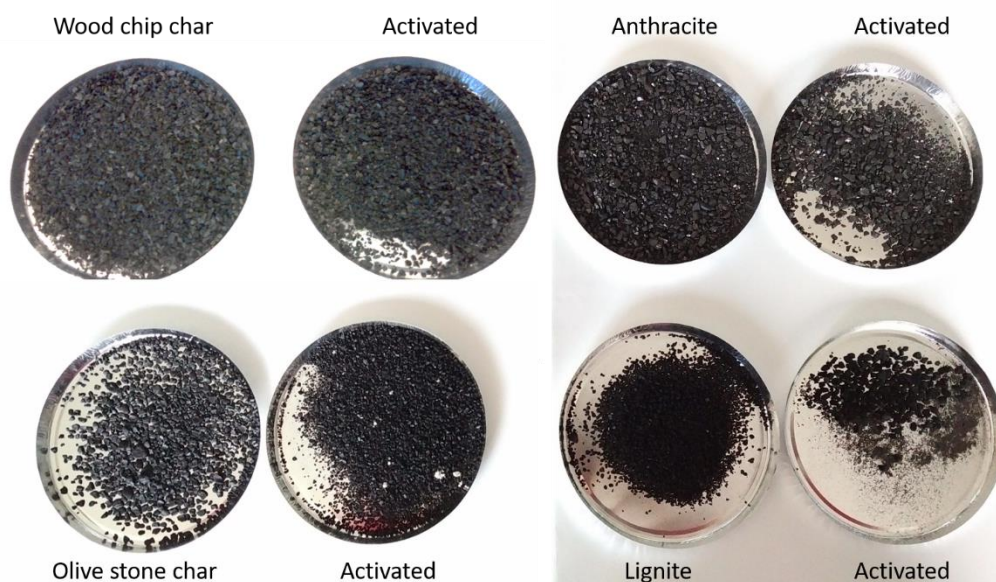


Figure 36: Samples used for the commissioning experiments before and after activation.

A BET (Brunauer–Emmett–Teller) analysis was performed to the samples before and after the physical activation in order to evaluate the increase in the apparent surface area. This analysis was performed in a Quantachrome Nova 2200E analyzer (Figure 37) with N₂ at 77 K. Samples were put in an oven at 160 °C for 48 h in order to remove moisture and volatile compounds and then were degassed in the Nova 2200E

analyzer at 160 °C for 24 h under vacuum. The samples were then weighed and analyzed in a bulb cell immersed in liquid nitrogen.



Figure 37: RE-CORD Quantachrome NOVA 2200E BET analyzer.

3.2.2 Results from the commissioning experiments

The BET results together with the activation yield are reported in Figure 38. Wood char reached the highest BET value (greater than 1000 m² g⁻¹), followed by olive stone and lignite. Anthracite led to a negligible increase in surface area due to its very low devolatilization, being substantially inert during the activation. The BET values of the “not activated” olive stone char and anthracite are, indeed, so small that are not visualized in Figure 38, due to its scale.

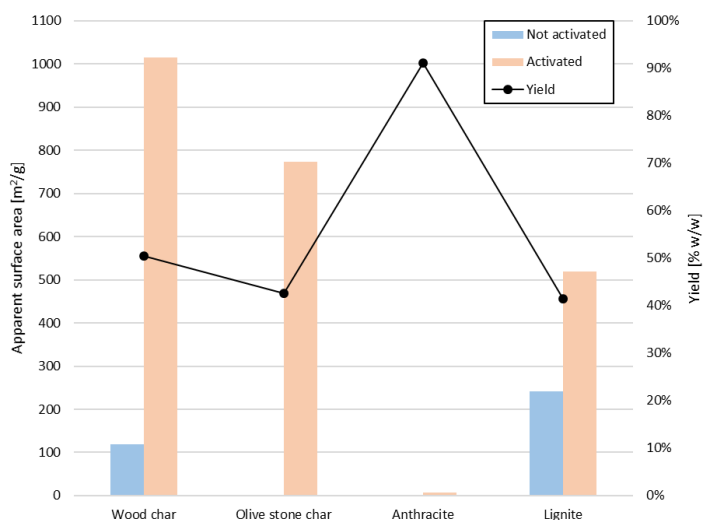


Figure 38: Results from the furnace commissioning experiments.

4. Experimental campaign on Digestate

The content of this chapter was partially published in:

E. Miliotti, D. Casini, G. Lotti, L. Bettucci, S. Pennazzi, A. M. Rizzo, D. Chiaramonti; Valorization of solid residues from anaerobic digestion through thermal and hydrothermal carbonization process; European Biomass Conference and Exhibition Proceedings, Volume 2017, Issue 25thEUBCE, June 2017, Pages 1063-1069, doi:10.5071/25thEUBCE2017-3DO.3.4 [114].

E. Miliotti, D. Casini, M. Prussi, G. Lotti, L. Bettucci, A.M. Rizzo, D. Chiaramonti, Lab-scale pyrolysis and hydrothermal carbonization of biomass digestate : Characterization of solid products, in: F. Berruti, R. Ocone, O. Masek (Eds.), Biochar: Production, Characterization and Applications, ECI Symposium Series, Alba (CN), 2017, <http://dc.engconfintl.org/biochar/54> [115].

The following experimental campaign was part of the work for Agrochar project, funded by MIPAAF (Ministero per le politica agricole, alimentari e forestali).

Previous studies regarding a comparison between the characteristics of SP and HTC char from digestate are reported in [16,116–119].

4.1 Materials and methods

In Figure 39 it is represented a scheme referring to the workflow of the experimental campaign.

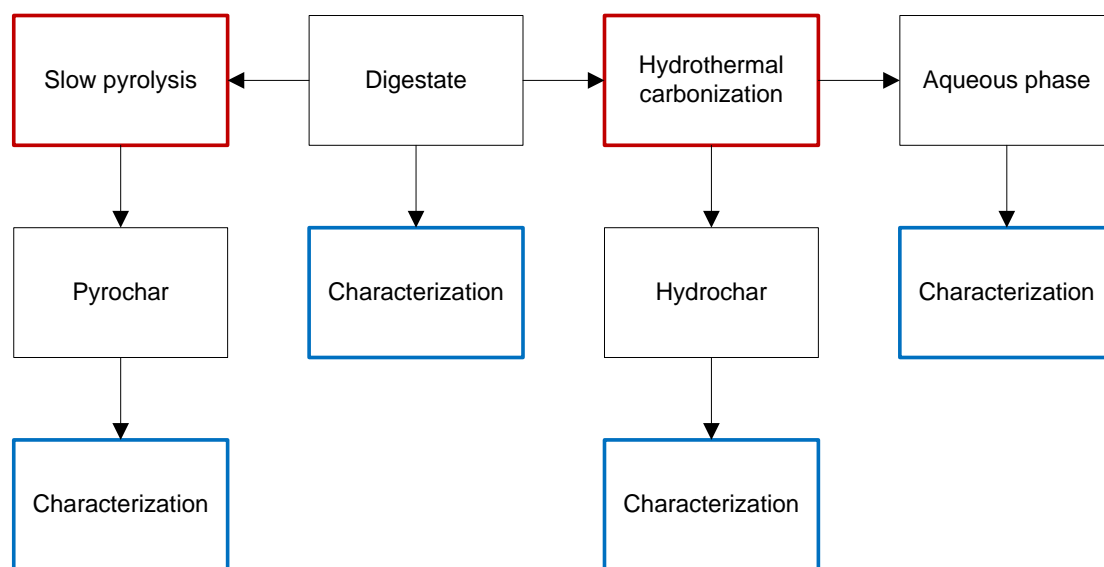


Figure 39: Workflow of the experimental campaign on AD digestate.

4.1.1 Feedstock

The digestate sample was supplied by a farm located in central Italy (Grosseto, Tuscany), from a mesophilic anaerobic digester, whose diet consisted in herbaceous biomass and agro-industrial residues. The sample was collected after water mechanical separation, however the digestate water content was still relatively high (greater than 70 % w/w). Prior to the thermochemical experiments, the digestate was dried to ensure good storage; in the case of HTC it was also milled and sieved at 4 mm in order to guarantee homogeneity of batches, due to the small size of the hydrothermal reactor.

4.1.2 Experimental equipment and procedure

In Table 4, the experimental operating conditions are reported. For simplicity, from here on the char produced by the slow pyrolysis process will be addressed as *pyrochar*, while the one obtained from hydrothermal carbonization will be named *hydrochar*. The yield of the solid products was calculated as:

$$\text{Yield of solid} = \frac{\text{dry weight of solid}}{\text{dry weight of digestate}} \cdot 100 \quad \text{Eq. 1}$$

Table 4: Experimental conditions of digestate slow pyrolysis and hydrothermal carbonizations experiments.

Operating condition	Slow pyrolysis	HTC
Pretreatment	Drying	Drying, milling ($\leq 4\text{mm}$)
Digestate input (d.b.)	1047 g	2 g
Temperature	500 °C	200-250 °C
Time	1 h	0.5-3 h
Biomass/Water mass ratio (d.b.)	-	10 % w/w

Slow pyrolysis

In order to identify the minimum solid residue obtainable by slow pyrolysis, a preliminary thermogravimetric test was carried out at 900 °C with 5 °C min⁻¹ heating rate and 3.5 l min⁻¹ nitrogen flow in the LECO TGA 701 thermogravimetric analyzer.

The experimental apparatus utilized for slow pyrolysis experiments is described in [120]: it consists in a stirred tubular stainless steel reactor (~ 31 l of inner volume), a vapors' catalytic cracking system and a double counter-flow water condensing system. The heating of the reactor is achieved by means of electric heaters and inert atmosphere is ensured by a constant flow of nitrogen or argon. A simple scheme and a picture of the plant are reported in Figure 40 and Figure 41. It is a continuous pilot plant, which was operated batch-wise in this study.

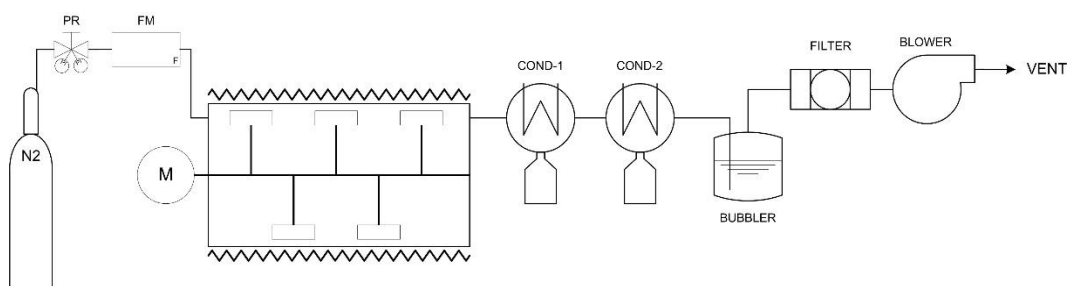


Figure 40: Simplified scheme of the slow pyrolysis experimental apparatus; PR: Pressure reducer, FM: Flow meter, COND: Condenser, M: Electric motor.



Figure 41: Picture of the RE-CORD pyrolysis apparatus.

For the slow pyrolysis experiment, 1047 g of dried digestate were put into the reactor (Figure 42), which was then sealed and purged with nitrogen. The inert gas flow (300 mbar , 10 l min^{-1}) was maintained throughout the test as well as the stirring system. After 10 min of purging, the heating was activated and the reactor reached the reaction temperature of $500 \text{ }^\circ\text{C}$ in nearly 70 min. This condition was held for 1 hour and then the reactor was let to cool down naturally, taking nearly 18 hours to reach ambient temperature. Subsequently the pyrochar was collected from the reactor (Figure 43), weighed and stored for analyses. Solids from the liquid products were recovered too by means of vacuum filtration through a Whatman glass microfiber filter ($1 \text{ } \mu\text{m}$, see Figure 44, Figure 45), oven-dried at $90 \text{ }^\circ\text{C}$ for at least 24 hours and their weight added to the pyrochar from the reactor to evaluate the total solid yield. Table 5 reports the distribution of the amount of solids collected from the liquid products, with respect to the total recovered pyrochar.



Figure 42: Batch-wise feeding of the dried digestate inside the pyrolysis reactor.



Figure 43: Pyrochar inside the slow pyrolysis reactor.



Figure 44: From left to right: condenser 1, condenser 2 and bubbler at the end of the slow pyrolysis experiment.



Figure 45: Vacuum filtration for solids recovery from slow pyrolysis liquid products.

Table 5: Distribution of recovered pyrochar.

Part	Recovered fraction [% w/w]
<i>Reactor</i>	95.4
<i>Condenser 1</i>	4.4
<i>Condenser 2</i>	0.07
<i>Bubbler</i>	0.11

Hydrothermal carbonization

Four operating conditions were investigated: 200 and 250 °C for the reaction temperature and 0.5 and 3 hours for the residence time. Initial reactor pressure was adjusted nearly to 5 bar higher than saturation pressure at reaction condition, that is 20 and 45 bar for experiments carried out at 200 and 250 °C respectively, so to avoid partial water boiling. This approach was adopted in order to ensure water to be always in liquid state and the differences in pressure between the experiments impart very low contribution to water properties at the investigated temperatures, so they can reasonably be neglected, assuming the same reaction condition.

The length of the reactor was 200 mm. Mean heating rate was not controlled and it ranged from 33.5 to 43.0 °C min⁻¹. In order to increase the repeatability of the HTC experiments, the digestate was dried at 75 °C for 48 hours and milled in a RETSCH SM 300 knife mill equipped with a 4 mm sieve (Figure 46). In each experiment, 2 g of dried and milled digestate were mixed with 20 g of ultrapure water (0.055 µS cm⁻¹) inside the reactor (10 % w/w dry biomass-to-water mass ratio).



Figure 46: Oven-dried and knife-milled (4 mm) digestate for HTC experiments.

A leakage test was performed by argon pressurization at 80 bar and air was then removed by five purging cycles with nitrogen at 5 bar. After these preliminary operations, the reactor was pressurized with argon at the chosen initial pressure, then immersed into the hot fluidized bed and agitated by the shaking device. When the reactor temperature reached the set point, computing of the residence time started. Once the time was elapsed, the reactor was immersed in a water bath for rapid cooling and the pressure released. The reactor was then disconnected from the bench (Figure 47) and its content collected for analyses.



Figure 47: Inner view of the reactor soon after its disconnection from the MRTB.

The experiments were carried out three times, apart from the one performed at 3 hours and 250 °C, which was replicated four times in order to collect enough material for the analyses.

The content of the reactor was collected and centrifuged at 4100 rpm for 30 min in order to separate the liquid fraction, which was stored at -4 °C prior to the analysis. The centrifuge vial and the reactor were rinsed with ultrapure water ($0.055 \mu\text{S cm}^{-1}$) and filtrated under vacuum over a Whatman glass microfiber filter (1 μm) with the aid of additional water. After the filtration process, the hydrochar and the filter were placed in oven at 90 °C until constant weight. In addition, also the reactor was oven-dried at 90 °C in order to take into account the unrecovered hydrochar for solid yield evaluation. The entire HTC products collection procedure is resumed in Figure 48.

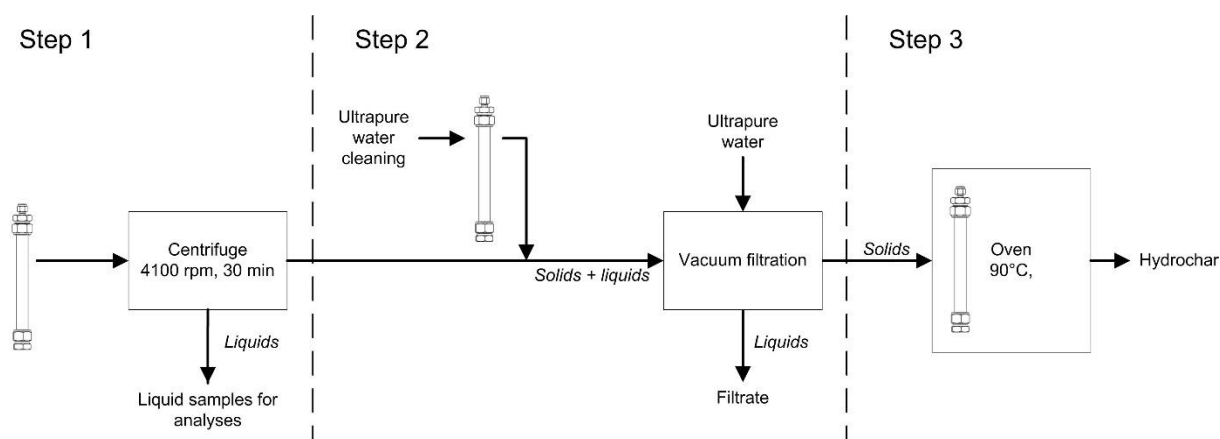


Figure 48: Procedure for collection of HTC products.

In order to ensure a minimum impact on hydrochar and aqueous phase composition, ultrapure water was chosen in place of a solvent for facilitating material collection. It is known, indeed, that solvents with different polarity affect yields and composition of hydrothermal liquefaction products in different ways [121,122], including hydrochar and aqueous phase, making the choice of the solvent critical for yields and properties comparison between different studies. Moreover, the use of solvents is discouraged in large-scale applications, due to health, environmental and economic issues. In Figure 49, a typical diluted liquid product after filtration is reported.

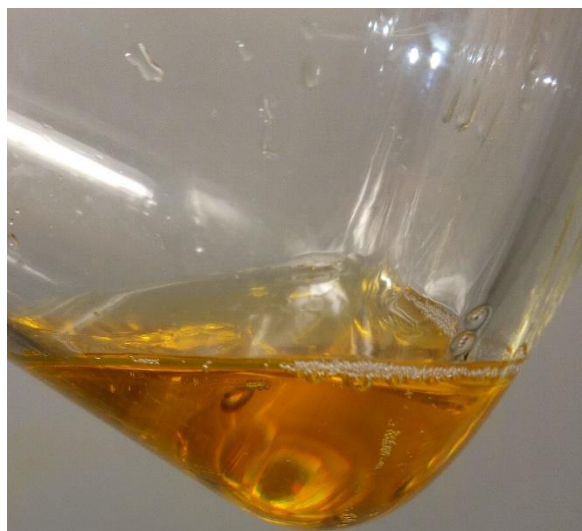


Figure 49: Typical aspect of diluted HTC liquid after filtration.

4.1.3 Analytical methods and chemicals

Analysis of solids

Prior to feedstock characterization, the digestate was dried at 75 °C for 48 hours and milled in a knife mill (RETSCH SM 300) equipped with a 4 mm-sieve. The drying process was carried out at low temperature in order to minimize the devolatilization of the organic matrix.

It was possible to determine moisture content, volatile matter, fixed carbon, inorganic carbon, pH, granulometry and the polycyclic aromatic hydrocarbon (PAH) content only for the pyrochar, due to the low amount of hydrochar produced.

Moisture, ash content and volatile matter were determined in a Leco TGA 701 instrument in ceramic crucibles. Moisture was measured according to UNI EN 13040 by heating the samples at 105 °C until a constant weight was achieved. Ash content were determined according to UNI EN 14775 by heating the sample under constant air flow up to 550 °C and holding there till constant weight. Volatile matter was measured according to UNI EN 15148 by heating the sample up to 900 °C under nitrogen flow and holding there for 7 minutes. Fixed carbon was calculated by difference from the results of proximate analysis.

The content of carbon, hydrogen, nitrogen (CHN) was determined through a Leco TruSpec according to UNI EN 15104, while the sulphur content was analyzed by means of a TruSpec S Add-On Module, according to ASTM D4239. In particular, samples of about 60-100 mg were burned at high temperature in presence of catalysts and converted to carbon dioxide, water vapor, nitrogen and sulphur dioxide. The oxygen content was evaluated by difference, considering C, H, N, S and ash content.

The inorganic carbon content was measured using the methods for fertilizers analysis (Dietrich-Fruhling calcimeter) according to the current Italian decree n.7276, addition n.13 of the 31st May 2006 [123] and the organic carbon was calculated as the carbon content less the inorganic carbon, according to national [124] and international standard on soil fertilizers [125,126].

The concentrations of Ca, K, Mg, Mn, Na, and Si were analyzed in an Agilent MP4200 ICP-OES using a nitrogen plasma. Before the ICP analysis, samples were mineralized with 3 ml of hydrogen peroxide and 5 ml of nitric acid in a Milestone Start D microwave digestion system in order to obtain clear acidic solutions.

Higher heating value (HHV) of digestate and pyrochar was measured according to UNI EN 14918 by means of a Leco AC500 isoperibol calorimeter. About 1 g of each sample was weighed with a precision of 0.1 mg in a crucible, then the crucible and a nickel ignition wire were placed into the calorimeter. The equipment was

closed and pressurized to 30 bar with high purity oxygen (99.999 %). After a suitable period required for reaching thermal equilibrium, the ignition was automatically started and temperature measured with an accuracy of 0.0001 °C. Lower heating values (LHV) were calculated according to the mentioned norm. HHV of hydrochar was evaluated with Channiwala and Parikh equation [127].

Brunauer–Emmett–Teller (BET) analysis was performed in the same equipment and with the same procedure reported in the previous chapter. The average pore diameter was calculated according to:

$$\text{Average pore diameter} = 4 \cdot \frac{\text{Total pore volume}}{\text{BET area}} \quad \text{Eq. 2}$$

Granulometry was determined with a 0.5 mm sieve, according to UNI EN 15428.

The determination of pH in the solid samples was performed according DIN ISO 10390. In particular, a spoon (5 ml) of milled and sieved (2 mm) char sample was added to a calcium chloride solution 0.01 mol l⁻¹, about 5 times the volume of the test portion, and mixed for 60 min ± 10 min using a mechanical shaker. The pH of the suspension was measured in a Metrohm 827 pHmeter at room temperature immediately after or during the stirring.

The PAHs extraction from pyrochar was performed following DIN CEN/TS 16181. Briefly, about 10 g of sample were extracted with toluene (Sigma Aldrich, ACS reagent HPLC grade) by a Soxhlet apparatus, the solvent extract was then concentrated and injected in a HPLC apparatus (Shimadzu) equipped with a diode array detector and previously calibrated with 16 US EPA PAHs standards after a 5 points calibration curve.

Analysis of HTC aqueous phase

In order to analyze the aqueous samples in GC apparatuses, a prior solvent extraction was performed. In particular, 2 ml of sample (collected after centrifugation and before filtration) was extracted with 3 ml of dichloromethane (DCM) under sonication and, then, a 10 min centrifugation at 4100 rpm was performed (Figure 50). The DCM soluble phase was then evaporated under nitrogen flow, dissolved and concentrated in isopropanol, and then injected in the GC-MS and FID apparatuses (GC 2010 Shimadzu) both equipped with a Zebron ZB-5HT INFERNO (Phenomenex) column (length 30 m, internal diameter 0.25 mm, film diameter 0.25 µm). The analysis was performed with a column flow of 2.02 ml min⁻¹ of helium for GC-MS, 3.17 ml min⁻¹ in GC-FID with an initial temperature of 40 °C (holding time 10 min), increased to 200 °C (heating rate 8 °C min⁻¹, holding time 10 min) and then to 280 °C (heating rate 10 °C min⁻¹, holding time 30 min).

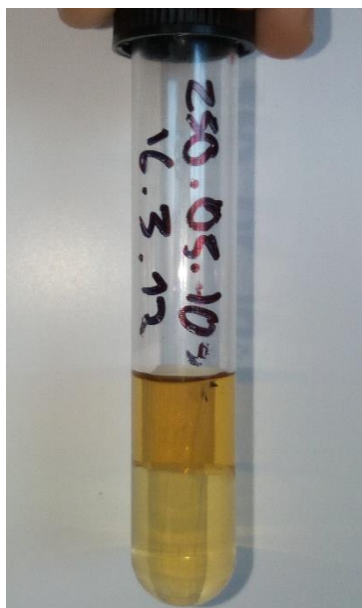


Figure 50: Extraction of HTC aqueous phase. The DCM-soluble organics are concentrated in the bottom fraction.

The GC-MS apparatus was used to determine the qualitative composition of the sample by comparing the acquired spectra against those of NIST 11 library; the GC-FID apparatus was used instead for the quantitative determination of identified compounds after a 3 to 4 calibration points with pure molecular standards and using *o*-terphenyl as internal standard. A simple scheme of the adopted methodology is shown in Figure 51.

The aqueous samples were also injected in a HPLC apparatus (UFLC Shimadzu) equipped with a refractive index detector, a Hi-Plex H column (Agilent) 300x7.7 mm, operating with 0.005 M sulfuric acid as mobile phase, following the NREL 42623 guidelines [128].

The inorganic elemental concentration was measured following the same procedure adopted for solid samples.

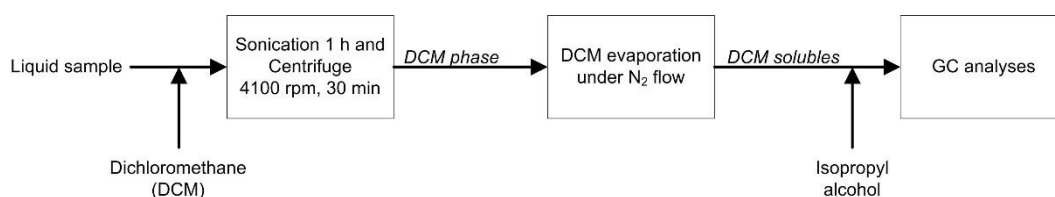


Figure 51: Methodology for gas-chromatographic analyses.

Chemicals

All solvents and reagents required for this work were purchased from Carlo Erba and Sigma Aldrich: they were used as received without any further purification. All chemicals were ACS reagent grade except for acetonitrile, water and toluene (HPLC grade), nitric acid (trace analysis), and hydrogen peroxide (for microanalysis). Ultrapure water ($0.055 \mu\text{S cm}^{-1}$) was collected from TKA Microlab ultrapure water system. Analytical standards for GC and HPLC were $\geq 98\%$ purity.

Chemical standards for instrument calibrations were purchased from Leco for HHV and CHNS analysis, BAM and Quantanalitica for BET analysis and Sigma-Aldrich for ICP analysis. All gases were purchased from Rivoira. Argon, air, nitrogen and oxygen were provided with a 99.999 % purity, helium with a 99.9995 % purity.

4.2 Results and discussion

4.2.1 Digestate characterization

The as-received digestate sample had a relatively high water content (76.2 % w/w w.b.) and in order to analyze its characteristics, it was dried and milled to a mesh size of 4 mm and smaller. Its properties are shown in Table 6.

Table 6: Characteristics of the digestate.

Parameter	u.m.	Value
<i>Moisture content</i>	% w/w (w.b.)	76.2
<i>Ash content</i>	% w/w (d.b.)	9.3
<i>Volatile matter</i>	% w/w (d.b.)	68.9
<i>Fixed carbon</i>	% w/w (d.b.)	21.8
<i>Higher heating value</i>	MJ kg ⁻¹ (d.b.)	19.2
<i>Lower heating value</i>	MJ kg ⁻¹ (d.b.)	17.9
<i>pH</i>	-	7.7
<i>Carbon</i>	% w/w (d.b.)	46.7
<i>Hydrogen</i>	% w/w (d.b.)	5.5
<i>Nitrogen</i>	% w/w (d.b.)	1.2
<i>Sulphur</i>	% w/w (d.b.)	0.5
<i>Oxygen</i>	% w/w (d.b.)	36.9
<i>Specific area</i>	m ² g ⁻¹	3.7
<i>Total pore volume</i>	cm ³ g ⁻¹	1.1 10 ⁻²
<i>Average pore diameter</i>	nm	11.6

4.2.1 HTC experimental results

Table 7 reports the average operating results of the HTC experiments. By considering the free inner volume of the reactor, the difference between the final and initial pressure gives an indication of gas formation. It can be noted that the average heating rate (HR) was far higher than the one obtained with conventional autoclaves, which, in general, ranges between 5 and 15 °C min⁻¹. The maximum heating rate was nearly 43 °C min⁻¹. In Figure 52 a temperature-pressure diagram of an experiment carried out at 250 °C - 3 h is reported.

Table 7: Average experimental results of the digestate HTC tests.

HTC test condition	Average heating rate [°C min ⁻¹]	Average reaction temperature [°C]	Pressure difference [bar]
200 °C - 0.5 h	33.96	201.27	0.99
200 °C - 3 h	33.46	201.21	0.67
250 °C - 0.5 h	42.97	251.49	1.41
250 °C - 3 h	40.86	250.80	2.63

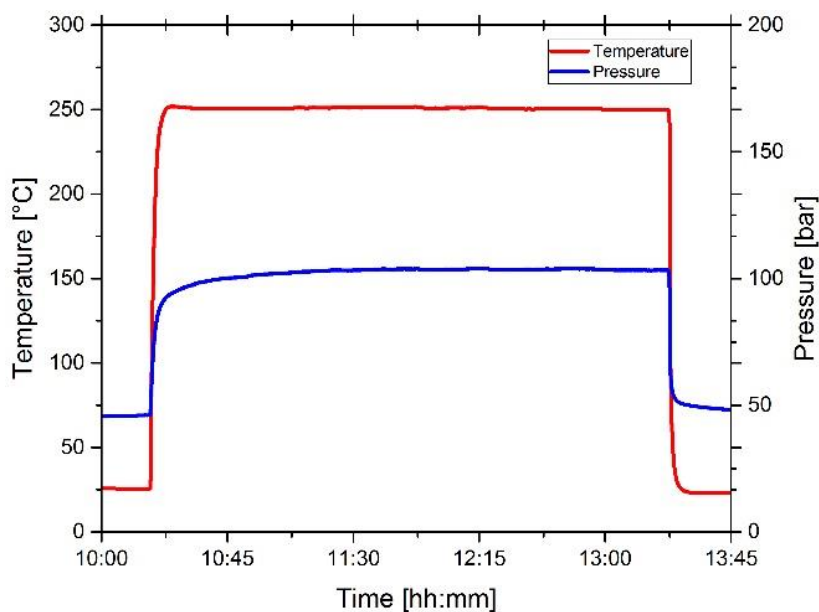


Figure 52: Operating diagram of a typical experiment carried out at 250 °C - 3 h.

4.2.2 Solid yields of slow pyrolysis and hydrothermal carbonization

The preliminary thermogravimetric test at 900 °C, which was performed in order to evaluate the minimum solid residue obtainable by SP, yielded 27.8 % w/w (d.b.) of solid. The slow pyrolysis led to a comparable char yield, 33.1 % w/w (d.b.), while the average hydrochar yields from the HTC experiments were higher, ranging from 51.0 % to 72.6 % w/w (d.b.). By increasing both reaction temperature and time, the hydrochar yield decreased, as reported in Figure 53. The observed behavior is in agreement with other published results reporting on the hydrothermal carbonization of digestate [16,129].

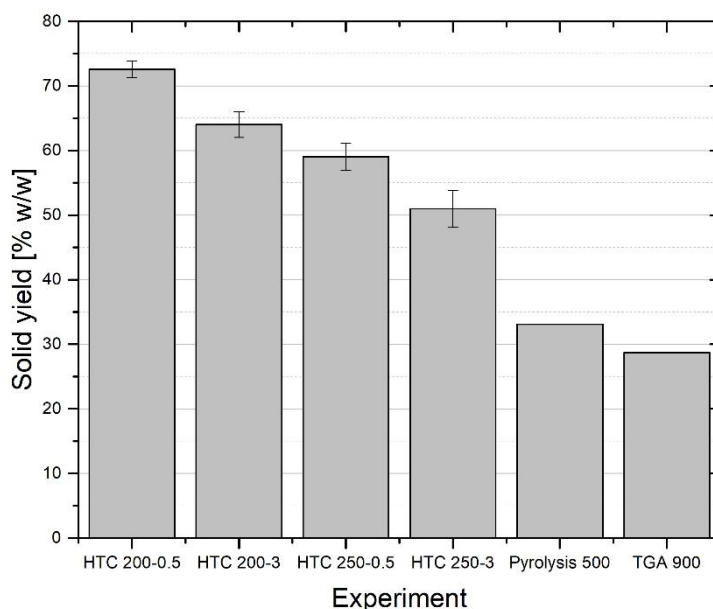


Figure 53: Comparison between the solid yields from the experiments. Error bars represent absolute standard deviation.

4.2.3 Solid product characterization

The two samples of char were similar in particle size, but differed in appearance: the pyrochar was dark grey, while the hydrochar was brownish, indicating that only mild carbonization occurred in this case (Figure 54). This statement is supported by the comparison of the solid yields of the two processes and by their O/C and

H/C molar ratio, shown in the van Krevelen diagram of Figure 57, which will be discussed later. Similarly, Figure 55 shows the difference in color of two hydrochars produced at different operating conditions.



Figure 54: Pyrochar (left) and hydrochar [250 °C-3 h] (right).

In Table 8, the mass percentage (dry basis) of carbon, hydrogen and nitrogen of the hydrochar samples is shown. As expected, the carbon content increased with reaction temperature and holding time, while the hydrogen content showed only a slight decrease. Nitrogen exhibited a minimum for the sample obtained at 200 °C-3 h and then increased up to 1.69 % w/w (d.b.). This behavior is also reflected in the hydrochar aspect: in Figure 55, a char produced at 200 °C is compared with the one produced at 250 °C; the sample produced at lower temperature better resembles the original feedstock.



Figure 55: Comparison between hydrochar samples obtained at 3 h and different temperature: left 200 °C, right 250 °C.

Table 8: Carbon, hydrogen and nitrogen mass percentage on dry basis of the hydrochar samples (absolute standard deviation is reported in brackets).

HTC test condition	Carbon	Hydrogen	Nitrogen
200 °C - 0.5h	49.69 (0.31)	5.90 (0.09)	1.03 (0.07)
200 °C - 3h	51.69 (0.40)	5.79 (0.07)	0.99 (0.01)
250 °C - 0.5h	55.24 (0.34)	5.72 (0.07)	1.25 (0.05)
250 °C - 3h	62.85 (0.25)	5.55 (0.03)	1.69 (0.07)

The hydrochar produced at the most severe condition, i.e. the sample with the highest carbon content, is the one chosen for the comparison with pyrochar and from now on it will be retained as the reference HTC sample for the sake of comparison with pyrochar. In Figure 56 the elemental composition of digestate, hydrochar and pyrochar are compared: the carbon content increased with respect to the feedstock due to the carbonization process, but the two char samples showed similar values. The hydrochar exhibited a practically unchanged hydrogen content, which is nearly halved in the pyrochar. Nitrogen showed only a minor increase, while the oxygen content experienced a sharp decrease, due to decarboxylation, being minimum for the pyrochar. Compared to digestate, the ash content increased from 9.3 to 12.3 % w/w (d.b.) in the hydrochar case and doubled the latter value in the pyrochar, reaching 24.6 % w/w (d.b.). In any case, sulphur content was less than 0.5 % w/w (d.b.).

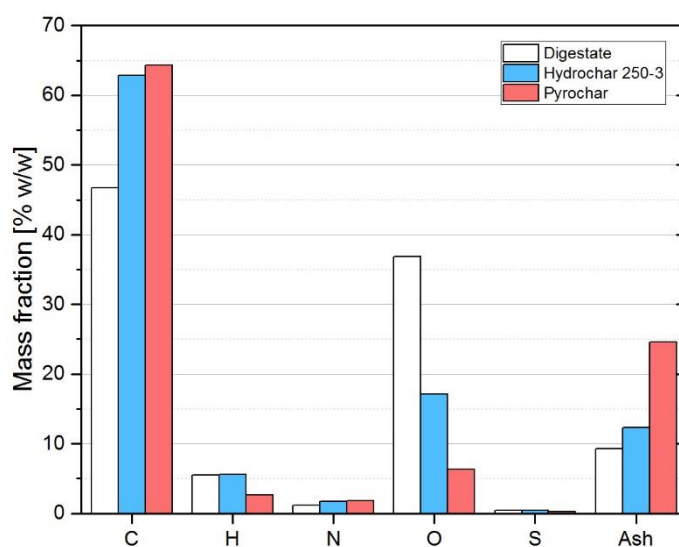


Figure 56: Comparison of elemental composition of digestate, hydrochar (250 °C-3 h) and pyrochar.

In Table 9, the full characterization of hydrochar (250 °C - 3 h) and pyrochar is reported. Due to variation in ash content and elemental composition, the higher heating value of the char samples increased with respect to the original feedstock, however the two values were quite similar; specifically, the hydrochar exhibited a 37 % increase, while the pyrochar a 28 % increase. This difference is mainly related to the fact that the hydrochar had nearly a double amount of hydrogen and a half amount of ash.

The analysis of particle size distribution was carried out with a 0.5 mm sieve only for the pyrochar, showing a high amount of fine particles (greater than 71 % w/w on dry basis). The powder-form of the char can negatively affect its management in terms of product handling and transport and impact on users' health and safety.

From the results of the BET analysis, appears that both char samples are characterized by a very low specific surface: 4.92 m² g⁻¹ for the hydrochar and 23.10 m² g⁻¹ for the pyrochar; these values are in line with the results from other works. Mumme et al. [119] performed HTC of cellulose and digestate of maize silage at 190, 230 and 270 °C, measuring a maximum BET area of 12 m² g⁻¹ for digestate converted at 190 °C and reported a decreasing trend for increasing reaction severity. Correa et al. [16] carried out BET analysis on hydrochar from biogas digestate at different reaction conditions and obtained a value of 8 m² g⁻¹ when processing at 250 °C for 3 hours. A direct comparison between the specific area of hydrochar and pyrochar from digestate was reported by Garlapalli et al. [116]: they found a higher surface for char from slow pyrolysis performed at 800 °C (161.60 m² g⁻¹) and a lower one for hydrochar obtained at 260 °C (2.93 m² g⁻¹). In addition, by pyrolyzing this latter hydrochar at 800 °C, they measured an intermediate value of BET area of

about 63.48 m² g⁻¹. In general, chars from slow pyrolysis exhibit higher specific area than hydrochars and the mechanism for which porosity is developed in the biomass matrix differs between the two conversion processes. During pyrolysis, the loss of volatile components is the main responsible for porosity growth, while in hydrothermal carbonization the morphological structure of hydrochars is strictly related to the typology of the original feedstock and two reaction mechanisms are commonly proposed. Biomass that can be easily solubilized in hot compressed water (e.g. cellulose) generally forms amorphous microspheres via polymerization of intermediate hydrolysis products [130], whereas more resistant feedstocks like lignin are preferably converted by means of solid-solid conversion, as proposed by Dinjus, Kruse and Tröger [131]. As suggested by Kang et al. for HTC of lignin [132], the biomass matrix which undergoes solid-solid reactions can adsorb on its surface the condensed intermediates in the liquid phase, resulting in a decrease of porosity. Another explanation of the low specific area of the hydrochar produced in the present study is that no solvent was used for facilitating char collection and therefore no tarry compounds were removed from the hydrochar pores.

Table 9: Comparison between hydrochar (250 °C-3 h) and pyrochar physico-chemical properties.

Parameter	u.m.	Hydrochar (250 °C - 3h)	Pyrochar
Moisture content	% w/w (w.b.)	n.m.	1.00
Ash content	% w/w (d.b.)	12.30	24.60
Volatile matter	% w/w (d.b.)	n.m.	16.80
Fixed carbon	% w/w (d.b.)	n.m.	58.60
Inorganic carbon	% w/w (d.b.)	n.m.	0.23
HHV	MJ kg ⁻¹ (d.b.)	26.47*	24.64
LHV	MJ kg ⁻¹ (d.b.)	25.15*	24.09
pH	-	n.m.	9.4
Carbon	% w/w (d.b.)	62.85	64.34
Hydrogen	% w/w (d.b.)	5.55	2.68
Nitrogen	% w/w (d.b.)	1.69	1.78
Sulphur	% w/w (d.b.)	0.43	0.22
Oxygen	% w/w (d.b.)	17.17	6.38
O/C	-	0.20	0.07
H/C	-	1.06	0.50
Granulometry (< 0.5 mm)	% w/w (d.b.)	n.m.	71.2
Specific area	m ² g ⁻¹	4.92	23.10
Total pore volume	cm ³ g ⁻¹	2.03 10 ⁻²	8.54 10 ⁻²
Average pore diameter	nm	16.50	14.80
Total PAHs content	mg kg ⁻¹ (d.b.)	n.m.	2.47

u.m.: unity of measure, n.m.: not measured, * evaluated with Channiwala and Parikh equation [127]

An interesting parallelism regarding pores blockage by condensed organic compounds in HTC and slow pyrolysis can be made considering the slow pyrolysis review made by Manyà [133]: when pyrolysis is performed under pressure, secondary char formation, i.e. polymerization of pyrolysis vapours, is enhanced because of an increase in vapours residence time and the deposition of the condensed particles onto the carbonaceous matrix eventually leads to a decrease in surface area due to pore clogging. Because vapours residence time is probably one of the main responsible for porosity decrease by secondary char together

with peak temperature, the typology of the pyrolysis reactor becomes a very important parameter affecting the surface area of the pyrochar.

In Figure 57 the O/C and H/C molar ratio of the digestate, pyrochar and hydrochar (250 °C - 3 h) are compared to some typologies of natural coal (data taken from [134]) in the van Krevelen diagram: hydrochar underwent a minor carbonization and is thus characterized by higher ratio values than pyrochar. In this case hydrochar is similar to subbituminous coal, while pyrochar is comparable to anthracite.

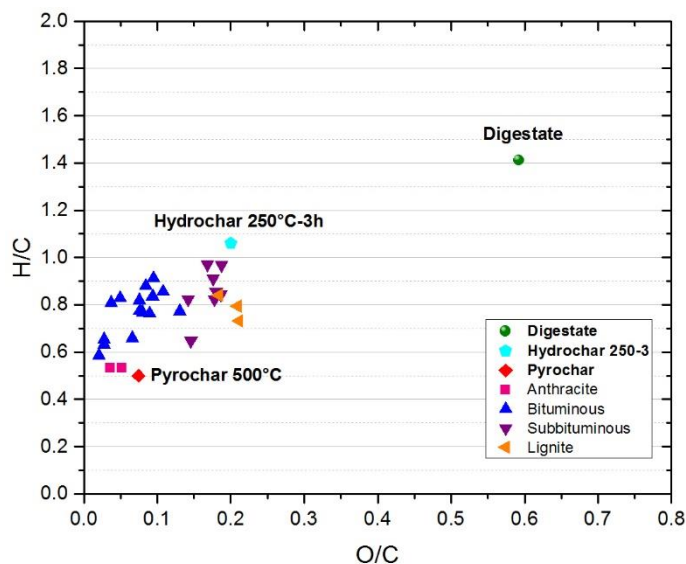
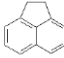
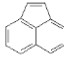
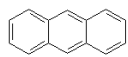
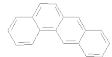

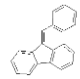
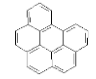
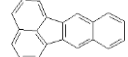
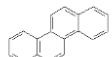
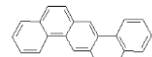
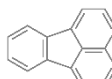
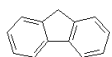
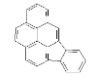
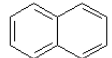
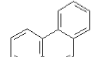
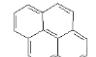


Figure 57: Van Krevelen diagram of digestate, hydrochar (250 °C-3h) and pyrochar compared to natural coals (coals data reproduced from [134]).

The total PAHs content of the pyrochar, 2.47 mg kg⁻¹ (d.b.), was considered as the sum of the concentration of the 16 PAHs defined by US EPA. In Table 10, the concentrations of the 16 PAHs are listed: the hydrocarbon with the highest concentration was pyrene, followed by chrysene, fluorene and naphthalene.

Table 10: PAHs concentration in the pyrochar sample. Values are on dry basis (absolute standard deviation is reported in brackets).

Polycyclic aromatic hydrocarbon	Concentration [mg kg ⁻¹]	Molecular weight [g mol ⁻¹]	Structure
<i>Acenaphthene</i>	0.07 (0.026)	154.2	
<i>Acenaphthylene</i>	<i>b.q.l.</i>	152.2	
<i>Anthracene</i>	0.04 (0.008)	178.2	
<i>Benz(a)anthracene</i>	<i>b.q.l.</i>	228.3	
<i>Benzo(a)pyrene</i>	<i>b.q.l.</i>	252.3	
<i>Benzo(b)fluoranthene</i>	<i>b.q.l.</i>	252.3	
<i>Benzo(ghi)perylene</i>	<i>b.q.l.</i>	276.3	
<i>Benzo(k)fluoranthene</i>	0.06 (0.006)	252.3	
<i>Chrysene</i>	0.53 (0.043)	228.3	
<i>Dibenz(a,h)anthracene</i>	0.02 (0.004)	278.4	
<i>Fluoranthene</i>	<i>b.q.l.</i>	202.3	
<i>Fluorene</i>	0.28 (0.071)	166.2	
<i>Indeno(1,2,3-cd)pyrene</i>	0.17 (0.029)	276.3	
<i>Naphthalene</i>	0.26 (0.008)	128.2	
<i>Phenanthrene</i>	0.16 (0.023)	178.2	
<i>Pyrene</i>	0.89 (0.035)	202.3	

b.q.l.: below quantification limit

Concerning the inorganic elements, it can be seen from Table 11 that the pyrochar was characterized by an increase in concentration of all inorganics, while, in the case of hydrochar, potassium, sodium and silicon exhibited a reduction with respect to the original feedstock. The reason behind this decrease in concentration can be attributed to leaching into the HTC process. When using this char as a solid fuel this will imply a better ash melting behavior during combustion.

Table 11: Inorganic elements concentration in mg kg⁻¹ (d.b.) in the digestate, hydrochar (250 °C-3 h) and pyrochar.

Element	Digestate	Hydrochar (250 °C - 3 h)	Pyrochar
Ca	8315	11480	21397
K	9656	364	28170
Mg	1224	1850	4877
Mn	70	125	204
Na	1962	73	5752
Si	812	718	2179

4.2.4 HTC aqueous phase characterization



Figure 58: Selected aqueous phase from the HTC experiments.

Significant concentrations of inorganic elements were found in the HTC aqueous phase; in Figure 59 their concentration is reported for representative samples obtained at the different reaction conditions. While an increasing trend was shown with increasing reaction severity for potassium, magnesium and sodium, the same cannot be said for calcium and silicon: the former exhibited nearly constant values, with a minimum at 200 °C-3 h (142 mg kg⁻¹), the latter showed a maximum at 250 °C-0.5 h (442 mg kg⁻¹). The most affecting parameter seems to be the reaction temperature. The most abundant element was potassium, with a concentration ranging from 805 to 1153 mg kg⁻¹.

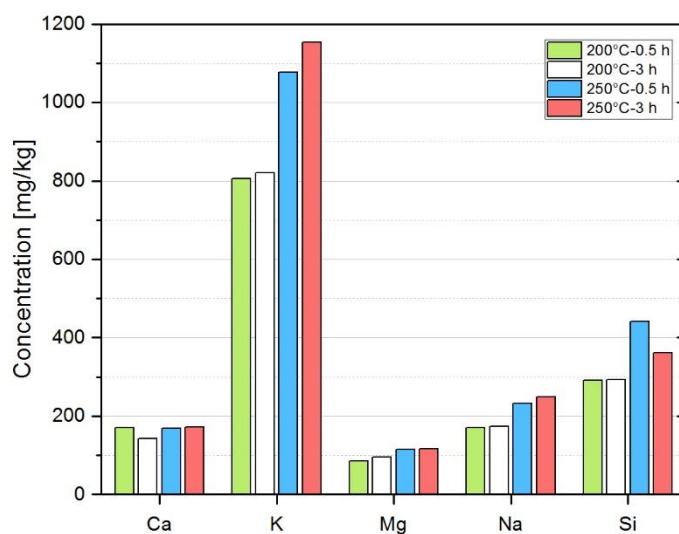


Figure 59: Concentration of inorganic elements in the HTC liquid phase.

All the organic molecules which were identified in the aqueous samples are listed in Table 42 in the appendix (to each detected compound the relative CAS number and chemical class and subclasses were assigned). The main chemical classes were aromatics and ketones: a great number of the molecules of the former class were oxygenated, mostly belonging to the groups of guaiacols, syringols and phenols, while the majority of the ketones possessed a cyclic structure. The only pure aromatic compounds identified were toluene and styrene and, in addition, some N-containing aromatics were detected, like pyridine, pyrimidine and 2-methylpyrazine, probably originating from the proteins contained in the digestate. Furanoid derivatives were also detected like 2,4-dimethylfuran, 5-HMF and furfural.

In Figure 60, four GC-MS chromatograms representative of each experimental condition are reported. It has to be pointed out that the intensity of the chromatogram area is not representative of concentration: GC-MS was used to assess a qualitative analysis, which was a necessary preliminary step in order to perform the quantitative analysis by means of HPLC and GC-FID. As can be seen from the chromatograms, compounds eluting in the lower-end of the retention times range (between 0 and 10 min), e.g. furfural, increased their peak areas at increasing residence time (from 0.5 to 3 h) at 200 °C, but their peak areas decreased or totally disappeared into the background noise, when the reaction temperature increased to 250 °C. An opposite behavior was shown for molecules that fell into the retention time range of 13 - 32 min, e.g. phenol, syringol and guaiacol, as their areas grew with temperature and residence time.

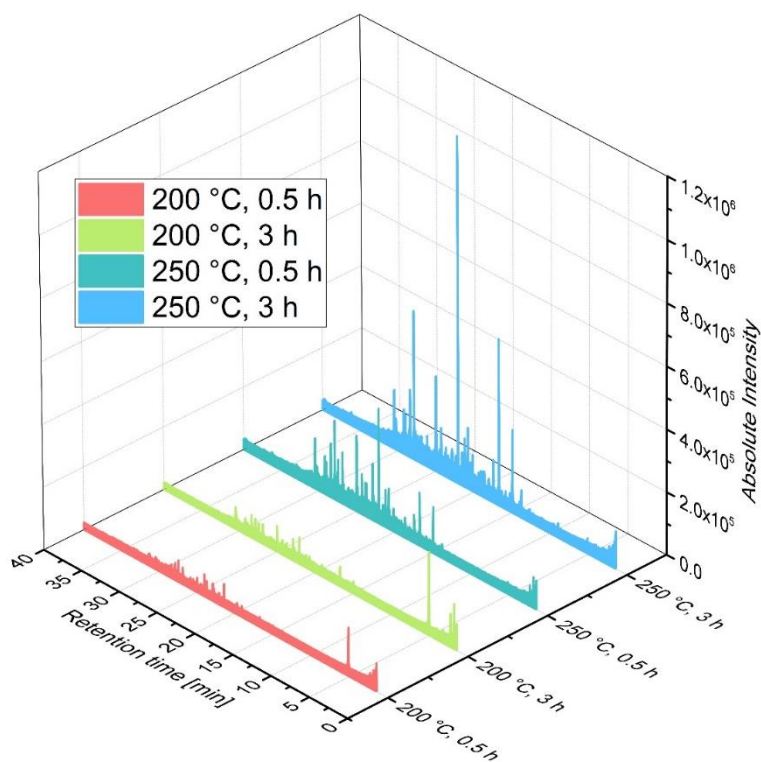


Figure 60: Chromatograms from GC-MS of HTC aqueous phase from the HTC of AD digestate.

In Table 12 the concentration of some of the identified compounds are reported: HPLC was carried out to quantify acetic acid, furfural and 5-HMF, while GC-FID was used for the other molecules. Acetic acid was the compound with the highest detected concentration, which increased with reaction temperature and time from 0.65 to 3.26 g l⁻¹. Hydrothermal carbonization is often described as an auto-catalytic process because the formation of organic acids in the aqueous phase, such as acetic acid, leads to a decrease in the pH-value, which favors hydrolysis and the overall carbonization reaction [36,39,65]. Conversely, an alkaline environment is known to enhance production of biocrude and suppression of char formation [135]. As

anticipated by the GC-MS analysis, furfural was detected only at 200 °C and its concentration increased with holding time, changing from 0.16 to 0.21 g l⁻¹, whereas 5-HMF concentration was below the HPLC quantification limit for all the aqueous samples (< 0.025 g l⁻¹).

Generally, in hydrothermal carbonization four parallel and recursive reaction steps are involved: hydrolysis, dehydration, polymerization and aromatization. When hexoses are considered as starting material, for example glucose, 5-HMF is formed from dehydration of fructose, which is the product of glucose isomerization; when the feedstock is a pentose, furfural is obtained instead [36]. The decrease in furfural content and the undetectable amount of 5-HMF can be explained by the fact that these two molecules are typically very reactive HTC intermediates: with more severe reaction conditions they convert, leading to the formation of long-lasting intermediates like acetic acid, phenols and cyclic ketones, whose concentration raised from below detection limit at 200 °C to 38.28 mg l⁻¹ at 250 °C-3 h; a similar behavior was shown also in other studies regarding HTC of digestate and sawdust [16,136]. In addition, the reduction of 5-HMF is known to be favored by potassium salts and, indeed, the HTC aqueous phase was rich in potassium, as shown by the ICP analysis: these salts catalyze the water-gas shift reaction, leading to the formation of hydrogen, which, in turn, hydrogenates the 5-HMF.

The other main molecules in the aqueous phase belonged to the group of guaiacol, syringol and phenol, which are derivatives of lignin; their concentration increased with reaction temperature and time, as for the ketones, but guaiacols and syringol concentrations were one order of magnitude above the other species. Syringol was favored for longer residence time at high temperature. To a lesser extent, the formation of phenolic compounds can be attributed also to carbohydrate decomposition, which is especially favored at high temperatures, in near-super-critical water, i.e. in hydrothermal gasification. However, the high amount of potassium in the aqueous phase could have further enhanced this reaction mechanism by acting as a catalyst [137].

Vanillin concentration increased with time at 200 °C and with temperature, being maximum at 250 °C - 0.5 h. Toluene concentration was very low if compared to the other compounds and increased at harsher reaction conditions (max 1.12 mg l⁻¹), but its quantification was uncertain due to its high standard deviation.

In Figure 61, the trend of the concentration of the compounds quantified by the GC-FID is shown; ketones, phenols and guaiacols were summed to make the chart more readable.

Table 12: Concentration, in mg l⁻¹, of major organic compounds in the HTC aqueous samples (absolute standard deviation is given in brackets).

Compound	200 °C - 0.5 h	200 °C - 3 h	250 °C - 0.5 h	250 °C - 3 h
Acetic acid	652 (48)	1721 (50)	2677 (309)	3259 (201)
Toluene	0.30 (0.06)	0.39 (0.15)	0.40 (0.19)	1.12 (0.91)
Furfural	164 (19)	207 (75)	<i>b.q.l.</i>	<i>b.q.l.</i>
5-(Hydroxymethyl) furfural	<i>b.q.l.</i>	<i>b.q.l.</i>	<i>b.q.l.</i>	<i>b.q.l.</i>
Phenol	<i>b.q.l.</i>	2.73 (0.55)	10.8 (2.9)	22.1 (6.6)
<i>m</i> -Ethylphenol	<i>b.q.l.</i>	<i>b.q.l.</i>	7.66 (1.04)	10.1 (2.4)
<i>o</i> -Ethylphenol	<i>b.q.l.</i>	1.23 (0.27)	<i>b.q.l.</i>	<i>b.q.l.</i>
<i>o</i> -Cresol	<i>b.q.l.</i>	<i>b.q.l.</i>	<i>b.q.l.</i>	2.34 (0.38)
<i>p</i> -Creosol	<i>b.q.l.</i>	<i>b.q.l.</i>	<i>b.q.l.</i>	0.73 (0.22)
3-Methoxycatechol	<i>b.q.l.</i>	<i>b.q.l.</i>	<i>b.q.l.</i>	10.2 (0.9)
<i>tert</i> -Butylpyrogallol	<i>b.q.l.</i>	<i>b.q.l.</i>	4.27 (0.55)	<i>b.q.l.</i>
<i>o</i> -Xylenol	<i>b.q.l.</i>	<i>b.q.l.</i>	1.90 (0.40)	<i>b.q.l.</i>
Guaiacol	2.4 (0.6)	9.3 (2.5)	38.7 (12.6)	95.5 (32.3)
Isoeugenol	4.95 (0.37)	<i>b.q.l.</i>	13.37 (1.86)	<i>b.q.l.</i>
Eugeonol	<i>b.q.l.</i>	4.93 (1.20)	3.77 (1.16)	0.89 (0.53)
Other guaiacols	17.2 (1.6)	16.7 (2.3)	59.1 (13.5)	30.1 (4.2)
Syringol	3.44 (0.45)	13.9 (4.2)	44.0 (5.1)	115 (16)
2-Methyl-2-cyclopentenone	<i>b.q.l.</i>	<i>b.q.l.</i>	5.03 (3.60)	27.8 (15.8)
3-Methyl-2-cyclopentenone	<i>b.q.l.</i>	<i>b.q.l.</i>	<i>b.q.l.</i>	10.5 (4.7)
1-Methyl-1-cyclopenten-3-one	<i>b.q.l.</i>	<i>b.q.l.</i>	2.50 (1.18)	<i>b.q.l.</i>
Vanillin	9.07 (1.07)	13.6 (2.7)	28.5 (4.0)	8.81 (1.18)

b.q.l.: below quantification limit.

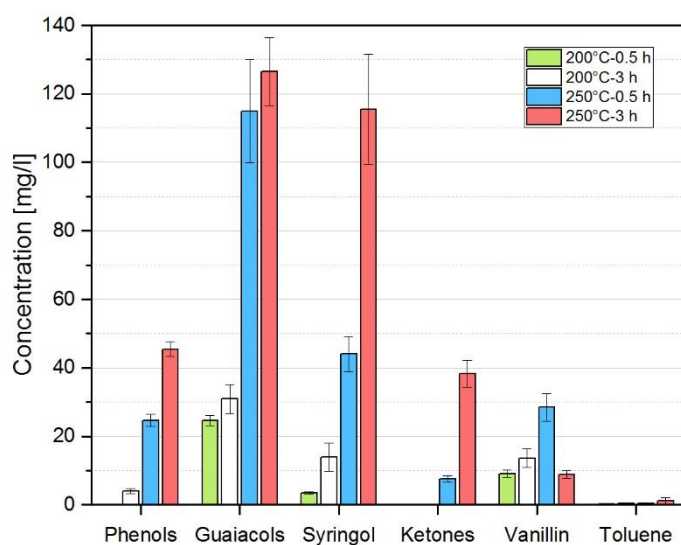


Figure 61: Concentration of organics in the HTC aqueous samples measured by GC-FID.

4.2.5 Comparison with EBC, IBI and Italian fertilization decree

A comparison between some of the characteristics of the two char samples and the threshold values of European and International standards for biochar as well as the Italian law for fertilizers was assessed in order to see if the samples obtained in this study would fit these limitations. In particular, two voluntary standards were chosen: the European Biochar Certificate (EBC) [125] and the International Biochar Initiative (IBI) [126]; the Italian decree for soil fertilizers (D.L. 29 APRILE 2010, N. 75 [124]) was modified in 2015, allowing biochar to be used in agriculture, was considered too.

IBI and the Italian decree define three classes of biochar quality, while EBC defines only two classes, premium and basic, related to the amount of contaminants. A lower limitation on the total carbon content is proposed only by IBI and, being this value greater than 60 % w/w (d.b.) for both hydrochar and pyrochar, they both fit into IBI high quality class 1. The low amount of inorganic carbon measured in the pyrochar (0.23 % w/w, d.b.) makes this sample conform to the EBC standard and to the high-quality class 1 of D.L. 29 APRILE 2010, N. 75. Threshold values for ash content are defined only in the Italian decree and, in the present case, both hydrochar and pyrochar fit into class 2, being their ash content between 10 and 40 % w/w (d.b.). As far as the H/C_{org} and the O/C_{org} molar ratio are concerned, the pyrochar sample satisfy all the requirements, while hydrochar, neglecting the inorganic fraction of the carbon content, exceeds the threshold values only because of its high hydrogen content. Regarding the PAHs, pyrochar fit into the premium class of EBC, having a concentration of polycyclic aromatic hydrocarbons lower than 4 ppm. In Table 13 and in Table 14 the comparison of the characteristics of the produced chars with threshold values of the above mentioned standards and law are reported. Concerning the concentration of inorganics, their concentration is higher in the pyrochar, as previously specified. A critical element is Cd, whose concentration in the digestate exceeded the limits, all the more so in the chars; Cu and Mo in the pyrochar exceeded only the EBC and the IBI thresholds, respectively.

Table 13: Char properties and threshold values from EBC, IBI and D.L. 29 APRILE 2010, N. 75.

Parameter	Hydrochar 250-3	Pyrochar	EBC	IBI	D.L. 29 APRILE 2010, N. 75
Carbon content [% w/w] d.b.	62.85	64.34	Not required	Class 1: ≥ 60 Class 2: ≥ 30 & < 60 Class 3: ≥ 10 & < 30	Not required
Total organic carbon [% w/w] d.b.	n.m.	64.11	≥ 50	Not required	Class 1: > 60 Class 2: > 30 & ≤ 60 Class 3: ≥ 20 & ≤ 30
Ash content [% w/w] d.b.	12.3	24.6	Declaration	Declaration	Class 1: < 10 Class 2: ≥ 10 & ≤ 40 Class 3: > 40 & ≤ 60
H/C _{org}	1.06*	0.50	≤ 0.7	≤ 0.7	≤ 0.7
O/C _{org}	0.20*	0.07	≤ 0.4	Not required	Not required
pH – Value	n.m.	9.4	Not required	Not required	4 - 12
Granulometry through 0.5 mm [% w/w] d.b.	n.m.	71.2	Declaration	Declaration	Declaration
Surface area [m ² g ⁻¹]	4.9	23.1	Declaration; better > 150 m ² g ⁻¹	Declaration	Declaration
PAHs [mg kg ⁻¹] d.b.	n.m.	2.47	Premium: < 4 Basic: > 4 & < 12	6 - 300	< 6

* Evaluated with total carbon

Table 14: Char concentration of inorganics and threshold values from EBC, IBI and D.L. 29 APRILE 2010, N. 75. Values are expressed in mg kg⁻¹ (d.b.).

Element	Digestate	Hydrochar 250-3	Pyrochar	EBC	IBI	D.L. 29 APRILE 2010, N. 75
<i>Cd</i>	2.9	8.7	21	<i>Basic: < 1.5</i> <i>Premium: < 1</i>	1.4 - 39	< 1.5
<i>Cr</i>	3.1	< 0.1	63	<i>Basic: < 90</i> <i>Premium: < 80</i>	64 - 1200	< 0.5 (hexavalent)
<i>Co</i>	< 0.1	< 0.1	<0.1	<i>Not required</i>	40 - 150	<i>Not required</i>
<i>Cu</i>	7.2	21	143	<i>Basic: < 100</i> <i>Premium: < 100</i>	63 - 1500	< 230
<i>Pb</i>	< 0.1	< 0.1	< 0.1	<i>Basic: < 150</i> <i>Premium: < 120</i>	70 - 500	< 140
<i>Mo</i>	7.6	<0.1	22	<i>Not required</i>	5 - 20	<i>Not required</i>
<i>Zn</i>	41	<0.1	< 0.1	<i>Basic: < 400</i> <i>Premium: < 400</i>	200-7000	< 500

5. Experimental campaign on lignin-rich residue from 2nd generation ethanol

The content of this chapter was partially published in:

E. Miliotti, L. Bettucci, G. Lotti, S. Dell’Orco, A. M. Rizzo, D. Chiamonti, Hydrothermal carbonization and activation of lignin-rich ethanol co-product, European Biomass Conference and Exhibition Proceedings, Volume 2018, Issue 26thEUBCE, Copenhagen, Denmark, 2018: pp. 969–972, [138].

In the present experimental campaign, lignin-rich residue (LRR) from a real demo plant was used as feedstock for thermochemical conversion. As reported in the aim of the study, the majority of experiments published in literature are generally conducted with lignin from the pulp and paper industry or with high purity model compounds.

5.1 Materials and methods

In Figure 62, a scheme referring to the experimental campaign workflow with LRR it is represented.

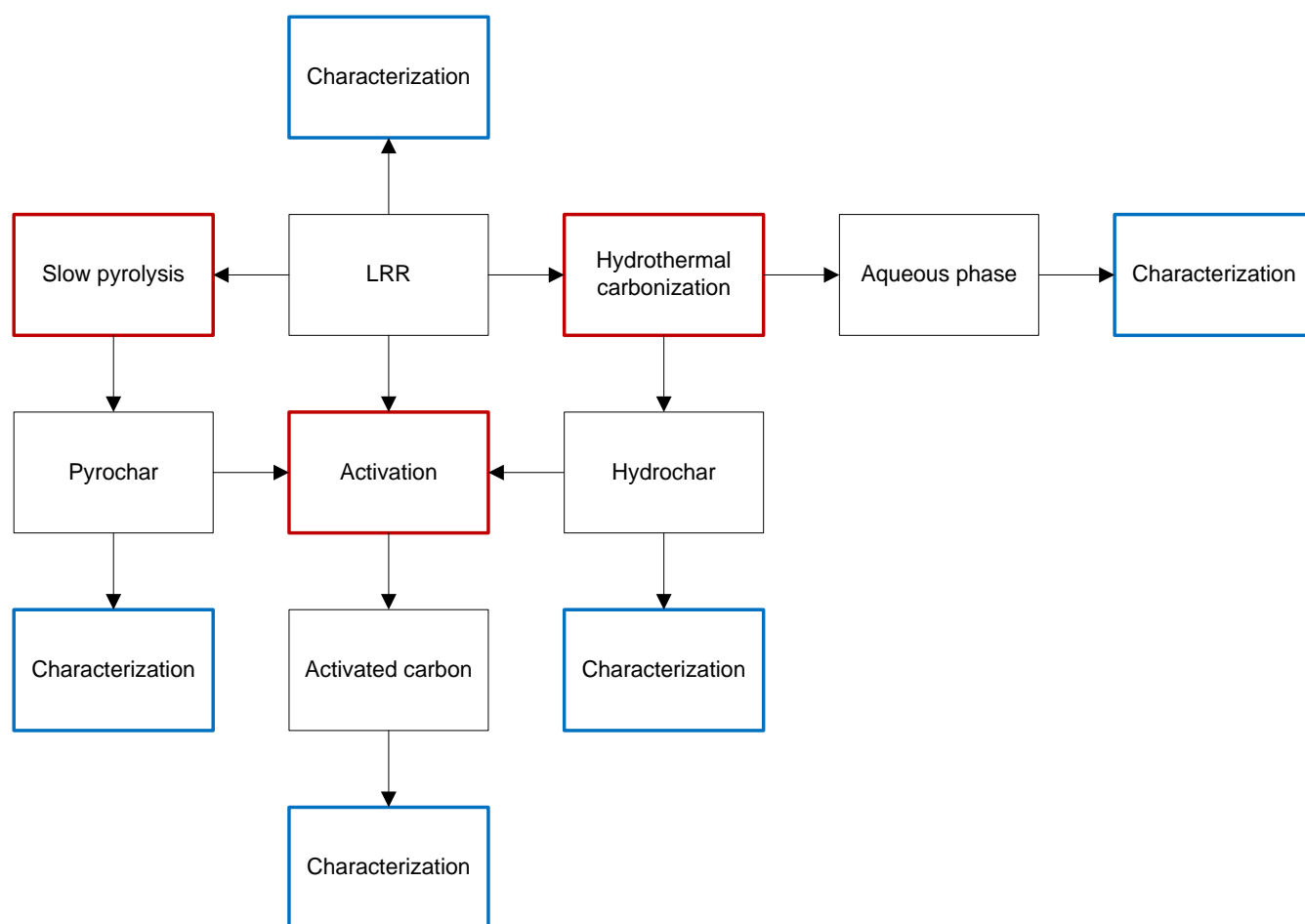


Figure 62: Workflow of the experimental campaign on lignin-rich residue.

5.1.1 Feedstock

The lignin-rich residue was produced in a 2nd generation ethanol demo plant where poplar was used as raw feedstock. It was collected after ethanol distillation and separation. Table 17 reports the characteristics of this particular kind of feedstock. In analogy to the experiments carried out with the AD digestate, for storage

issues and repeatability of the experiments, the LRR was dried in oven for 48 hours at 75 °C, knife-milled and then sieved to 4 mm (Figure 63).



Figure 63: Lignin-rich residue as received (left) and after drying, milling and sieving (right).

5.1.2 Experimental equipment and procedure

The HTC experiments were carried out in the same test bench and with the same methodology described in the previous chapter and the physical activation experiments were carried out in the previously described tubular furnace. Prior to hydrochar activation, a series of physical and chemical activation experiments were carried out with the LRR not being hydrothermally pretreated, in order to determine the best activation condition for the hydrochars in terms of a trade-off between apparent surface area and activated carbon yield. This preliminary step was necessary in order to reduce the number of the HTC experiments, but it had been also useful in order to assess the worthy of the HTC process as a pretreatment for activated carbon production and compare its effect with slow pyrolysis pretreatment.

5.1.2.1 Hydrothermal carbonization

The HTC experiments were carried out with the double-reactor configuration (right side of Figure 29), in each of which 7 g of dried and milled feedstock were dispersed in ultrapure water ($0.055 \mu\text{S cm}^{-1}$) to attain a 30 % w/w (d.b.) biomass-to-water mass ratio; an initial pressure of 20 bar was set using argon. Investigated temperatures and residence times were 200, 270 °C and 2, 4 hours, respectively. Pressure was autogenous. In order to have a higher amount of material available for the following activation, the experiments were replicated from 3 to 6 times and the length of the reactors was increased up to 300 mm. The operating conditions are resumed in Table 15.

Table 15: Experimental conditions of LRR hydrothermal carbonizations experiments.

Operating condition	HTC
<i>Pretreatment</i>	<i>Drying, milling ($\leq 4\text{mm}$)</i>
<i>LRR input (d.b.)</i>	<i>7 g</i>
<i>Temperature</i>	<i>200-270 °C</i>
<i>Time</i>	<i>2 - 4 h</i>
<i>Biomass/Water mass ratio (d.b.)</i>	<i>30 % w/w</i>

5.1.2.2 Physical activation

Physical activation experiments were carried out in the previously described horizontal tubular furnace, with CO₂ as activating agent. A two-step activation was performed: the feedstock was firstly “carbonized” and

then subjected to activation. In order to select the activation condition for the hydrochars, the LRR was carbonized by slow pyrolysis (SP) in a LECO thermogravimetric analyzer (Figure 64, the same described in the previous chapter and used for proximate analyses) at 550 °C for 2 h under a constant N₂ flow (10 l min⁻¹) at a heating rate of 5 °C min⁻¹. Then, the so-obtained pyrochar was physically activated at 700 °C and 800 °C with the following procedure: nitrogen was flushed in the activation reactor until temperature reached the setpoint; the gas flow (250 ml min⁻¹) was then switched to CO₂ and temperature was held for 2 h. The same procedure was used for hydrochar activation.

The hydrochars used for physical activation were the one produced at the four operating conditions (200 °C - 2 h; 200 °C - 4 h; 270 °C - 2 h; 270 °C - 4 h). Physical activation was carried out at a constant temperature of 700 °C; the average heating rate from ambient temperature was between 3 and 4 °C min⁻¹.

The so-produced activated carbons were denoted *physically-activated carbon*, namely PAC.



Figure 64: LECO 701 thermogravimetric analyzer used for SP and chemical activation experiments.

5.1.2.3 Chemical activation

Chemical activation was performed in the same LECO TGA 701 analyzer under nitrogen flow. The precursor used for this activation were the hydrochars and the LRR without the carbonization pretreatment (single-step activation). The selected activating agent was KOH; impregnation was carried out in a stirred aqueous solution, which was maintained at 60 °C for 6 h (Figure 65). The impregnated samples were then oven-dried overnight. As far as the LRR activation without carbonization pretreatment is concerned (six experiments), three activation temperatures and two KOH:LRR mass ratios (d.b.) were investigated: 600, 700 and 800 °C and 1:1 and 2:1, respectively. Activation time (at constant activation temperature) was 1 h, nitrogen flow rate 10 l min⁻¹ and heating rate 5 °C min⁻¹. After chemical activation, the samples were washed with HCl (1 M), in order to remove the KOH and other K-containing compounds, and then with ultrapure water until neutral pH. The best result in terms of apparent surface area and yield was obtained at 600 °C and mass ratio of 1:1; this condition was then chosen for the chemical activation of the hydrochars.

The so-produced activated carbons were denoted *chemically-activated carbon*, namely CAC.



Figure 65: Impregnation of the LRR with KOH at two different mass ratios: 1:1 (left) and 2:1 (right).

5.1.3 Analytical methods and chemicals

Where not specified, the same equations, analytical methods, chemicals and instrumentation reported in the previous chapter were used also for this study.

The activation yield and the total yield were evaluated as:

$$\text{Activation yield} = \frac{\text{dry weight of activated carbon}}{\text{dry weight of char}} \cdot 100 \quad \text{Eq. 3}$$

$$\text{Total yield} = \frac{\text{dry weight of activated carbon}}{\text{dry weight of LRR}} \cdot 100 \quad \text{Eq. 4}$$

The lignin content of the LRR was evaluated by a combination of three NREL procedures (Figure 66):

- The LRR was subjected to Soxhlet extraction with water and then ethanol in order to obtain the water-soluble and ethanol-soluble extractives (NREL procedure TP-510-42619 [139])
- The remaining solid residue was subjected to acidic hydrolysis for the evaluation of the acid soluble, acid insoluble lignin and structural sugars (cellulose and hemicellulose) by UV-VIS spectrophotometer and HPLC (NREL procedure TP-510-42618 [140])
- The ash content of the acid insoluble lignin was measured in order to determine the correct value of the latter (NREL procedure TP-510-42622 [141])



Figure 66: Water-soluble extractives (left), ethanol-soluble extractive (center) and lignin (right) obtained for the evaluation of the lignin content from the LRR.

For the evaluation of the BET area and the other morphological parameters (adsorption-desorption isotherms, total pore volume, micropore volume, pore size distribution), particular attention was taken in considering the pressure range for a proper evaluation of microporosity, according to Rouquerol et al. [142] and, in general, following the IUPAC guidelines reported in [143]. Micropore and external surface area were evaluated with the t-plot method and the pore size distribution with the DFT (density functional theory) model, assuming slit/cylinder pores. The total pore volume was determined at a pressure ratio of 0.95. Pores smaller than 2 nm were considered micropores, while mesoporosity was considered in the range of 2 - 50 nm [28].

The GC-MS of the aqueous phase was conducted on the fraction extracted with diethyl ether (DEE, Figure 67). Differently from the previous experimental campaign, DEE was used in place of DCM because it was seen that the former solvent was able to extract a lower amount of heavy GC-undetectable compounds, leading to a better resolution in the GC apparatus. However, the extraction with DEE is affected by the solvent extraction efficiency and therefore the concentration of some organics can be underestimated. This efficiency was evaluated for phenol, guaiacol and syringol, creating three aqueous solutions at different concentrations. The efficiency was not highly reliable, being compound and concentration-dependent, as can be seen in Table 16. The extraction step was necessary for keeping the GC column water-free and preventing its damage. Although GC-MS is affected by this issue, it has the advantage of identifying the hundreds of compounds dissolved in the sample and, by obtaining this information, it was possible to calibrate the HPLC with the most abundant ones, achieving a better and more trustful characterization of the aqueous phase. In this study, the GC-FID was not used and quantification was done only by GC-MS and HPLC.

Table 16: Results from the evaluation of the DEE extraction efficiency from the aqueous phase.

Concentration	Compound	Average efficiency	Absolute standard deviation
<i>High concentration</i>	<i>Phenol</i>	<i>75.0 %</i>	<i>7.6 %</i>
	<i>Guaiacol</i>	<i>77.9 %</i>	<i>5.9 %</i>
	<i>Syringol</i>	<i>85.2 %</i>	<i>6.7 %</i>
<i>Low concentration</i>	<i>Phenol</i>	<i>93.6 %</i>	<i>6.9 %</i>
	<i>Guaiacol</i>	<i>74.5 %</i>	<i>2.9 %</i>
	<i>Syringol</i>	<i>85.9 %</i>	<i>8.6 %</i>
<i>Single compound</i>	<i>Phenol</i>	<i>90.9 %</i>	<i>10.9 %</i>



Figure 67: Extraction of an aqueous phase sample; the DEE-soluble organics are concentrated in the top-phase.

5.2 Results and discussion

5.2.1 LRR characterization

Table 17 reports the properties of the lignin-rich residue; as it can be seen its moisture content is very high, approaching 70 % w/w (w.b.). The ash content is relatively low because of the initial feedstock, which is poplar and not straw. It is important to notice that the lignin content represents only a little more than the half of the whole dry mass fraction; unreacted and partially reacted carbohydrates and residual enzymes mainly compose the remaining part.

Table 17: Properties of the lignin-rich residue from poplar fermentation.

Parameter	u.m.	Value
Moisture	% w/w (w.b.)	69.7
Ash	% w/w (d.b.)	3.0
Volatile matter	% w/w (d.b.)	69.2
Fixed Carbon	% w/w (d.b.)	27.3
Higher Heating Value	MJ kg ⁻¹ (d.b.)	22.8
Carbon	% w/w (d.b.)	55.1
Hydrogen	% w/w (d.b.)	5.9
Nitrogen	% w/w (d.b.)	1.2
Sulphur	% w/w (d.b.)	0.2
Oxygen	% w/w (d.b.)	34.6
Lignin content	% w/w (d.b.)	57.0

The detailed results from the analysis of the lignin content are reported in Table 18: the majority of the lignin contained in the feedstock was *acid insoluble* (97.4 %). After the Soxhlet extraction of the extractives, the residual lignin, cellulose and hemicellulose were approximately ash-free; the low amount of ashes from the LRR were concentrated in the extractives due to leaching during the extraction process. A very low amount of cellulose and hemicellulose (structural sugars) was detected, indicating that these compounds were effectively converted into ethanol during poplar fermentation. The mass balance was very well closed (99.71%).

Table 18: Results from the lignin content evaluation.

Parameter	Value [% w/w] (d.b.)
<i>Water extractives*</i>	15.88
<i>Ethanol extractives*</i>	24.89
Total extractives	40.77
<i>Acid insoluble lignin</i>	55.45
<i>Acid soluble lignin</i>	1.50
<i>Lignin ashes</i>	<i>b.q.l.</i>
Total lignin	56.95
Structural sugars	2.00
Total	99.71

* Ash contribution included; b.q.l.: below quantification limit

5.2.2 HTC experimental parameters

Similarly to the HTC of AD digestate, Table 19 reports the average experimental results resulted from the LRR HTC experiments. The average heating rates were slightly lower because in this case a double-configuration of longer reactors was used, leading to a greater thermal inertia. In Figure 68 a temperature-pressure diagram of an experiment carried out at 200 °C - 2 h is reported. Again, pressure difference, which increased with reaction temperature, is an indicator of gas production.

Table 19: Average experimental results of the LRR HTC tests.

HTC test condition	Average heating rate [°C min⁻¹]	Average reaction temperature [°C]	Pressure difference [bar]
200 °C - 2 h	21.21	200.67	0.71
200 °C - 4 h	22.36	200.41	1.40
270 °C - 2 h	26.53	269.67	8.60
270 °C - 4 h	33.53	268.83	8.50

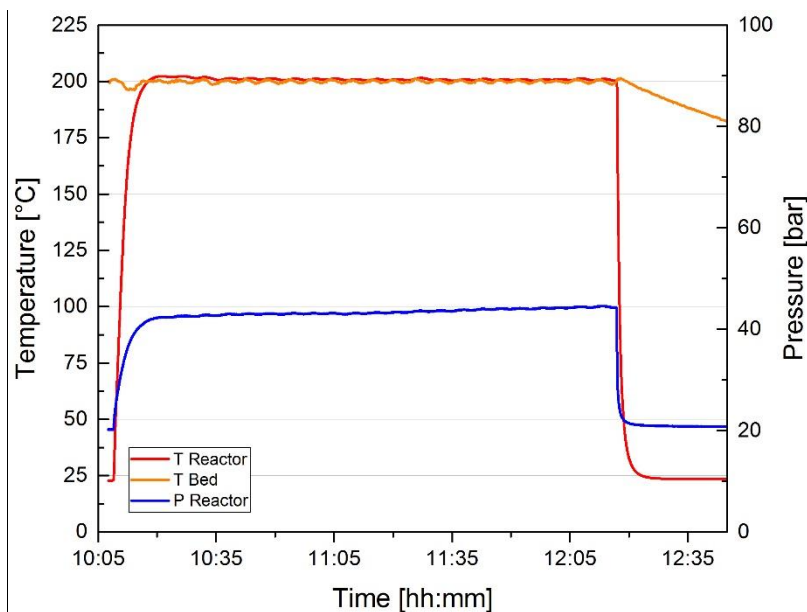


Figure 68: Operating diagram of a typical experiment carried out at 200 °C - 2 h.

5.2.3 Preliminary LRR activation

In order to select the appropriate activation conditions for hydrochars activation and so to reduce the amount of hydrochar needed for further activation (i.e. the number of HTC experiments), two physical and six chemical activation experiments were carried out. In the physical activation experiments, the LRR was firstly subjected to slow pyrolysis (two-step activation), while in the chemical ones it was activated without carbonization (one-step activation). The detailed results in terms of morphological parameters are reported in the appendix.

Physical activation

The pyrochar from the slow pyrolysis of the LRR had an apparent surface area (BET area) of 370.4 m² g⁻¹ and its solid yield was 27.8 % w/w (d.b.; absolute standard deviation 0.49 %). The results are reported in Table 20. At higher activation temperature a lower amount of activated carbon was produced, but with higher quality in terms of surface area, exceeding 1000 m² g⁻¹. Although the best trade-off between total yield and BET area was obtained when the activation temperature was 800 °C, 700 °C was chosen for the hydrochars activation. This decision was taken because the apparent surface area obtained at 700 °C is still a very good value, comparable with commercial activated carbons, and therefore the priority was shifted to maximization of the yield.

Table 20: Results from the preliminary physical activation of LRR.

Temperature [°C]	Activation yield [% w/w] (d.b.)	Total yield [% w/w] (d.b.)	BET area [m ² g ⁻¹]
700 °C	81.3	22.6	600.4
800 °C	59.2	16.5	1078.2

Chemical activation

The LRR was chemically activated in a single step, after its impregnation with the activating agent (KOH); the results are shown in Table 21. At a 1:1 mass ratio, an increase in the activation temperature led to a decreasing yield and to an increasing BET area, the latter reaching a maximum of 1484 m² g⁻¹. At 2:1 mass ratio the BET maximum value is obtained at 700 °C (1188 m² g⁻¹), which is lower if compared to the surface

area achieved at the same temperature but at a lower mass ratio ($1437 \text{ m}^2 \text{ g}^{-1}$). It is possible that the higher amount of KOH had led to an excessive opening of the pores, producing a lower value of BET area. As the best trade-off between yield and surface area was produced at $600 \text{ }^\circ\text{C}$ and 1:1, this condition was chosen for the following chemical activation of the hydrochars.

Table 21: Results from the preliminary chemical activation of LRR.

Temperature [°C]	KOH:LRR (d.b.)	Activation yield [% w/w] (d.b.)	BET area [$\text{m}^2 \text{ g}^{-1}$]
600	1:1	29.8	675.0
600	2:1	15.7	989.0
700	1:1	8.1	1437.0
700	2:1	10.7	1188.0
800	1:1	0.2	1484.4
800	2:1	3.6	558.0

During chemical activation, the samples inside the ceramic crucibles experienced the so-called *muffin effect*, rising as muffins do during baking (left picture of Figure 69). This behavior is attributed to the typical swelling of lignin under pyrolytic conditions, as it was reported by many authors [17,144].



Figure 69: Chemically activated carbons from LRR; as removed from the TGA (left, the *muffin effect* is clearly visible) and after washing and drying (right).

5.2.4 Solid yields

In Figure 70 and in Figure 71 the carbonization, activation and total yields (d.b.) are reported for the physical and the chemical activation experiments, respectively. With the term *carbonization yield* is intended the yield of the pretreatment process (i.e. HTC or pyrolysis).

As found in the conversion of AD digestate, by increasing the severity of the carbonization process, the char yield decreased, ranging in this case from 86.0 to 56.7 % w/w (d.b.) for HTC and down to 27.8 % w/w (d.b.) for SP; these values agree with literature [17,29,145]. In general, the higher the reaction severity the lower the yield and the higher the sample carbonization. Indeed, the activation yield increased with the severity of the pretreatment, indicating a more thermochemically stable material. Due to these contrasting trends, the total yield was approximately constant, being between 23.6 and 30.5 % w/w (d.b.).

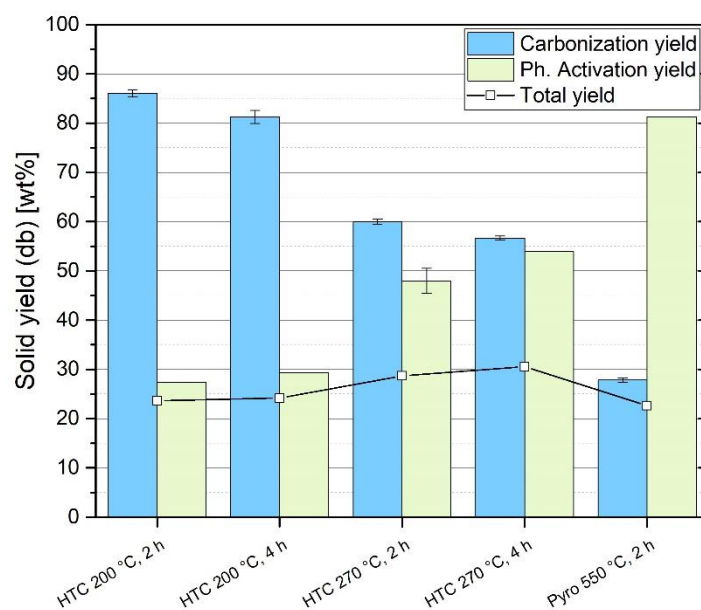


Figure 70: Solid yields from the physical activation experiments (the error bar represents the absolute standard deviation).

In the case of chemical activation (Figure 71), the minimum value of the activation yield was not reached at the less severe HTC condition, but at 200 °C - 4 h (30.8 % w/w, d.b.). However, a trend similar to the physical process was obtained, being the total yield between 25.4 and 33.1 % w/w (d.b.).

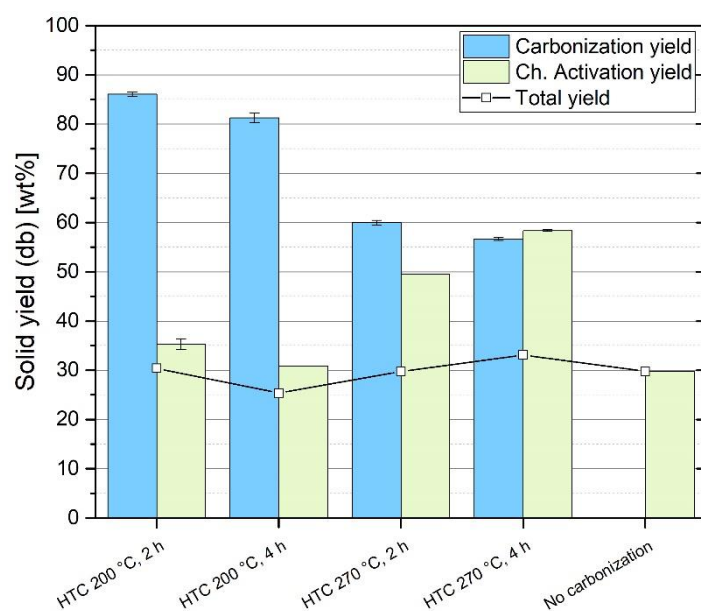


Figure 71: Solid yields from the chemical activation experiments (the error bar represents the absolute standard deviation).

5.2.5 Char characterization

Table 22 reports the results of the elemental analysis of the chars (hydrochars and pyrochar). An increase in reaction severity led to an increase in the carbon content, leading, so, to a more stable compound. During low-temperature HTC the hydrochar elements' concentrations were approximately unchanged with respect to the feedstock; only when the reaction temperature was 270 °C, a steep increase of the carbon content was obtained (71.1 % w/w, d.b.), which was similar to the one obtained with pyrolysis (75.0 % w/w, d.b.). During HTC, the hydrogen concentration remained roughly unaffected, whereas in the pyrochar it was more than halved. In agreement with the elemental analysis, also a visual observation of the samples (Figure 72)

revealed that the hydrochar obtained at 200 °C was less converted, being its aspect very similar to the LRR, while the hydrochar produced at 270 °C and the pyrochar had the characteristic char-black color.

Table 22: Results from the elemental analysis of the chars.

HTC test condition	Carbon % w/w (d.b.)	Hydrogen % w/w (d.b.)	Nitrogen % w/w (d.b.)	Oxygen* % w/w (d.b.)	H/C	O/C
Feedstock	55.1	5.9	1.2	37.8	1.28	0.51
200 °C - 2 h	57.8	5.9	1.1	35.2	1.23	0.46
200 °C - 4 h	58.5	5.9	1.3	34.4	1.20	0.44
270 °C - 2 h	<i>n.m.</i>	<i>n.m.</i>	<i>n.m.</i>	<i>n.m.</i>	<i>n.m.</i>	<i>n.m.</i>
270 °C - 4 h	71.1	5.6	1.6	21.7	0.95	0.23
550 °C - 2 h	75.0	2.6	1.9	20.5	0.42	0.21

n.m.: not measured, * evaluated by difference without considering the S and the ash content



Figure 72: Char samples obtained after the carbonization pretreatment.

5.2.6 Activated carbon characterization

The characterization of the activated carbons produced via physical and chemical activation was carried out with the BET analyzer Quantachrome NOVA 2200E by means of N₂ adsorption-desorption at 77 K.

Figure 73 shows the adsorption isotherms of the produced carbons. A visual inspection of these curves provides information on the carbon porous structure. Comparing the shape of these isotherms to the ones reported in Figure 74 it is possible to assess that the PAC isotherms can be classified as type I, which indicates that the PAC are mainly composed of micropores, while the CAC isotherms are a combination of type I and II; this latter behavior is an indication of wider pores [143].

Another information that can be obtained from these curves, is that, in general, the adsorbed volume decreased with the HTC reaction severity. This is true for the PAC, where the AC pretreated at the mildest HTC condition achieved the highest volume. The AC that was pretreated by pyrolysis showed an isotherm curve similar to the one pretreated by HTC at 200 °C - 4 h. In the case of chemical activation, the best sample was the one that was activated without carbonization. Among the HTC-pretreated samples, the best was the one processed at 200 °C - 4 h.

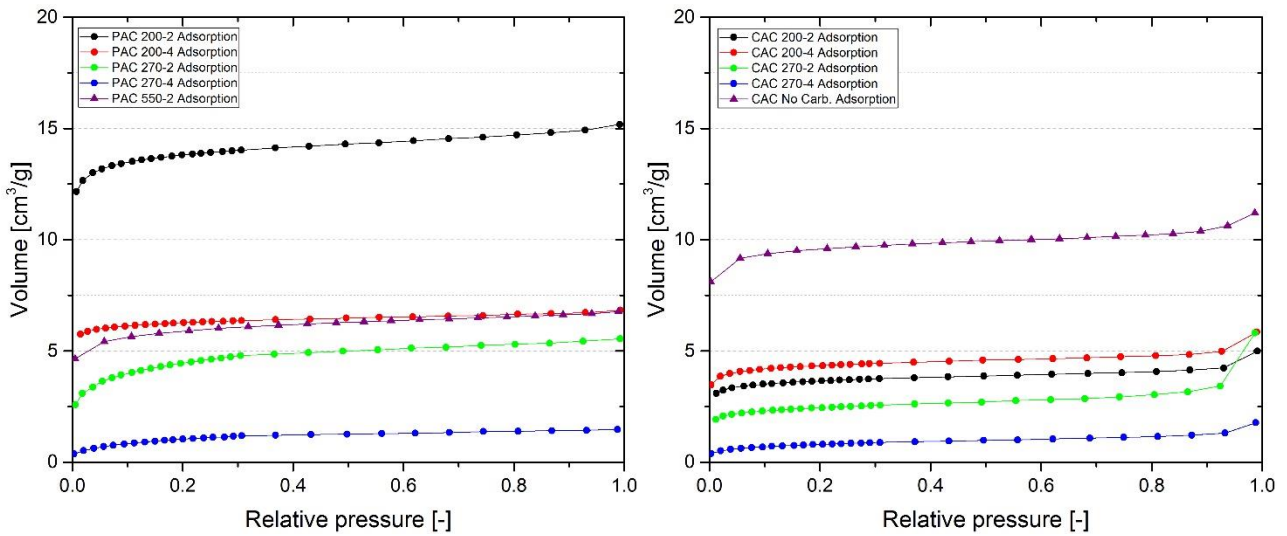


Figure 73: Adsorption isotherms (N_2 , 77 K) of the physically (left) and chemically (right) activated carbons.

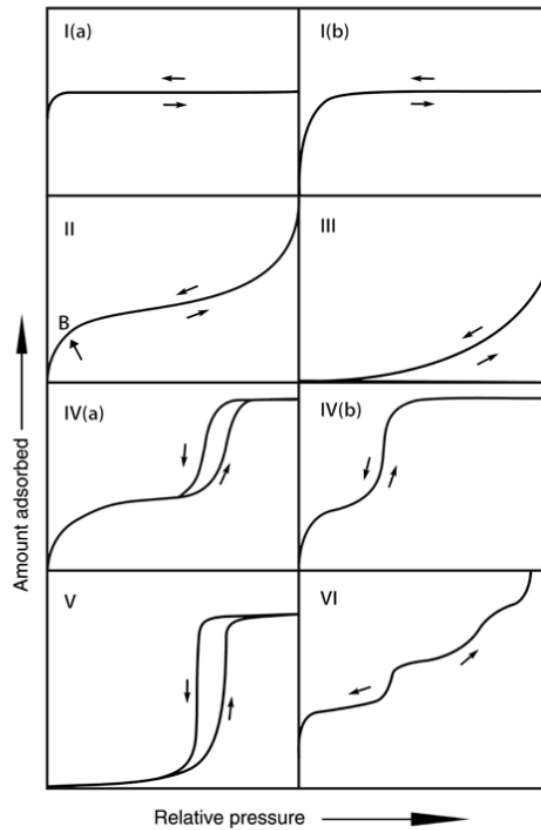


Figure 74: Isotherms classification [143].

A more comprehensible comparison between the adsorption-desorption isotherms of the best PAC and CAC with and without the HTC pretreatment is reported in Figure 75. The shape of the hysteresis loop gives an additional insight on the pore structure: all the samples exhibited a type H4 loop (see Figure 76 for comparison), indicating a combination of micro and mesoporosity.

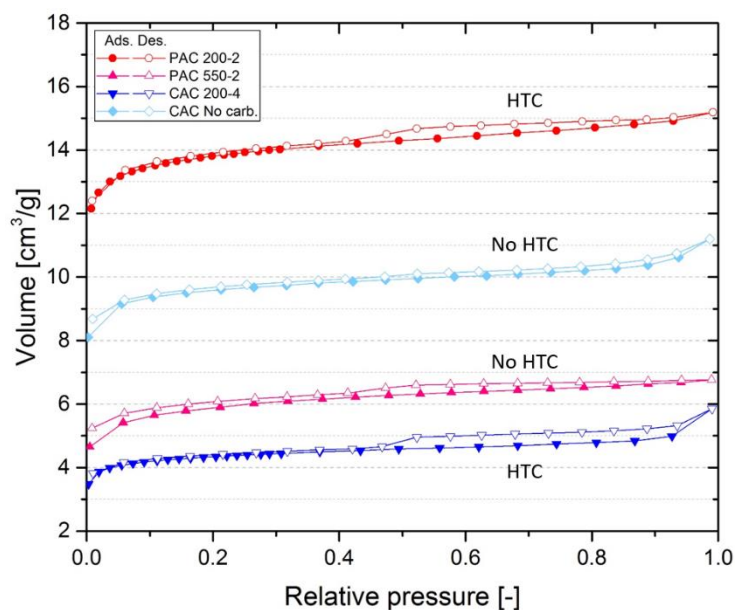


Figure 75: Comparison between the adsorption-desorption isotherms (N_2 , 77 K) of selected activated carbon samples.

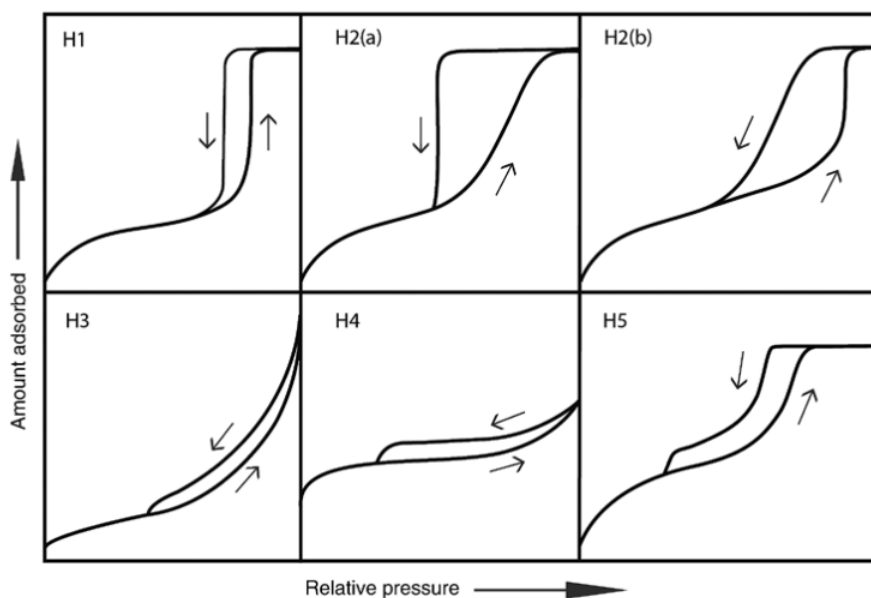


Figure 76: Classification of hysteresis loops [143].

In Figure 77, the BET apparent surface area is reported. Similarly to the results obtained in the HTC of AD digestate, the feedstock and the hydrochars had a practically null specific surface (from 3 to 9 $m^2 g^{-1}$). Considering the produced AC, a drastic decrease in specific surface occurs as the HTC temperature reaches 270 °C and, in general, these results are in agreement with the trends of the adsorption isotherms. The highest value of BET surface area was achieved by chemical activation without carbonization, reaching 675 $m^2 g^{-1}$.

This finding was unexpected because, in general, studies dealing with the activation of hydrochar report an increase of the AC BET area with the HTC process severity [16,19]. Purnomo, Castello and Fiori [19] produced granular activated carbons from grape seeds via HTC and further chemical activation with KOH. At HTC and activation operating conditions similar to the ones reported in the present study, they obtained very similar BET values (around 600 $m^2 g^{-1}$), but, as they increased HTC severity, AC of better quality were produced, reaching 1018 $m^2 g^{-1}$ when the HTC temperature was 250 °C. Likewise, Correa et al. [16] performed chemical

KOH activation of hydrochar from AD digestate and reported an increase in BET area from 930 to 1351 m² g⁻¹ when HTC conditions shifted from 190 °C - 6 h (pH 7) to 250 °C – 6 h (pH 5); however, the maximum total yield they obtained was below 8 % w/w. To the author’s knowledge, it is the first time that lignin-rich residue from a lignocellulosic ethanol plant was converted by HTC and subsequently activated; therefore, it is probable that the particular combination of lignin and complex enzymes or carbohydrates had led to results which contrast with literature.

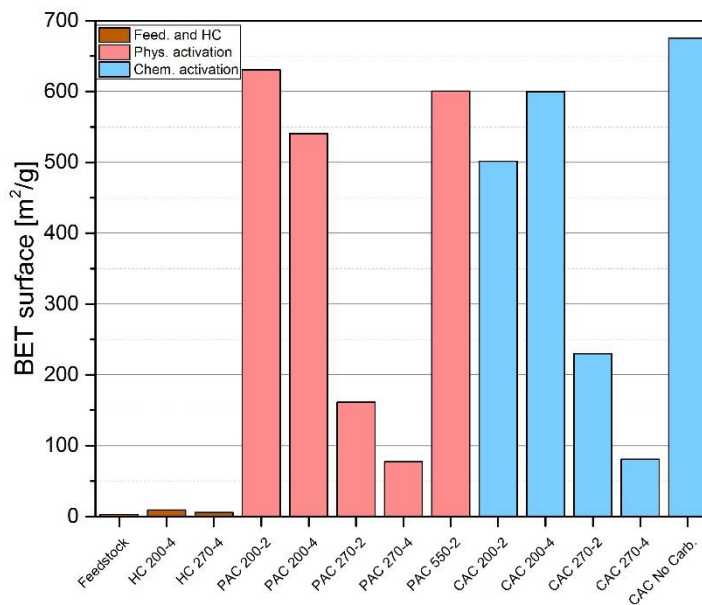


Figure 77: BET area of feedstock, hydrochars, PAC and CAC (with PAC 500-2 it is denoted the activated carbon subjected to the pyrolysis pretreatment).

The total pore volume (Figure 78) followed a similar trend too, being maximal for the CAC produced at 200 °C - 4 h (0.32 cm³ g⁻¹).

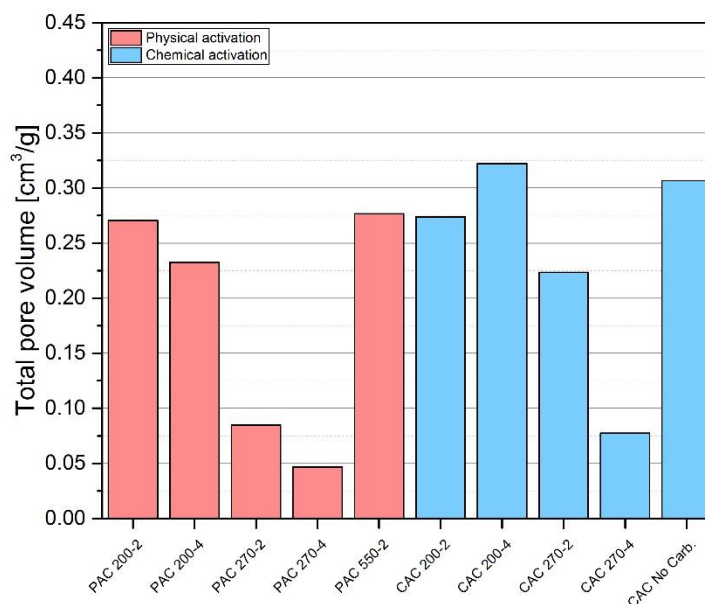


Figure 78: Total pore volume of the produced activated carbons.

The results from the t-plot method confirmed the shape of the adsorption isotherms (Figure 79): the PAC produced at a low HTC temperature had a micropore contribution to the total pore volume greater than 85

%. In the case of CAC, the activated carbon with higher microporosity was the one produced without the HTC pretreatment.

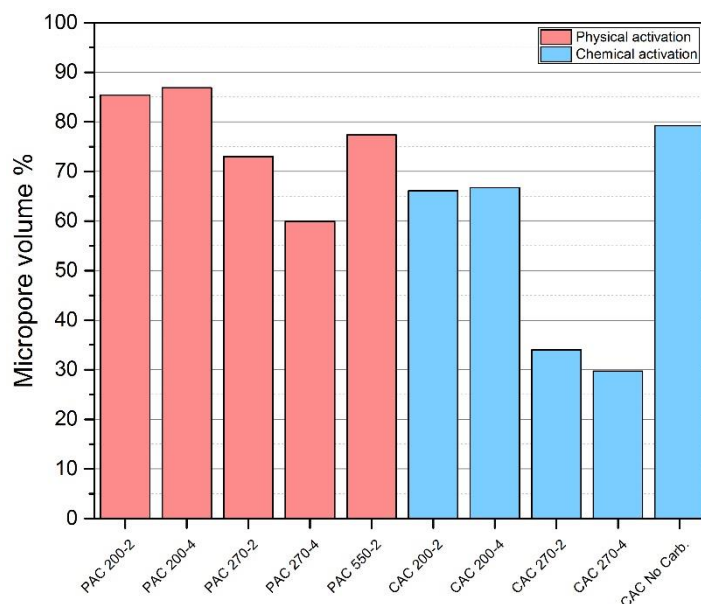


Figure 79: Percentage of the micropore volume in the produced activated carbons.

The pore size distribution of the produced activated carbons was evaluated by DFT; the results, together with the cumulative pore volume, are reported in Figure 80 and Figure 81 for PAC and CAC, respectively. In the figures, it is shown a comparison between the best and worst AC (in terms of BET area) produced with the HTC pretreatment (left) and between the best AC with and without HTC pretreatment (right).

In the case of physical activation, PAC 200 - 2 exhibited a high microporosity, with a mesoporosity concentrated below 6 nm (mainly 5.5 nm), where the cumulative pore volume experienced a sudden increase. On the contrary, PAC 270 - 4 was less microporous, having a mesoporosity developed from 2 to 8 nm. The AC produced with the SP pretreatment had still good microporosity, but a mesoporosity from 2 up to 15 nm, as can be seen from the increasing curve of the cumulative volume.

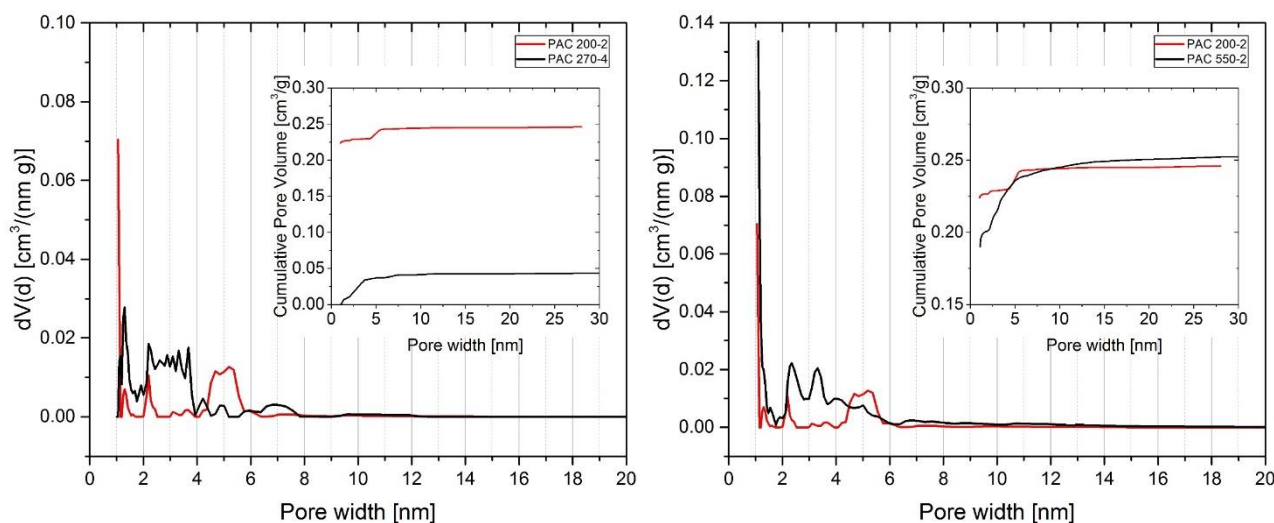


Figure 80: Pore size distribution of selected physically-activated carbons.

The CAC pretreated at 200 °C - 4 h exhibited a very concentrated mesoporosity (around 5.5 nm), while the mesoporosity of the CAC 270 -4 was extended above 20 nm. Without the carbonization pretreatment a result similar to the CAC 200 – 2 is obtained, but with a better-developed microporosity.

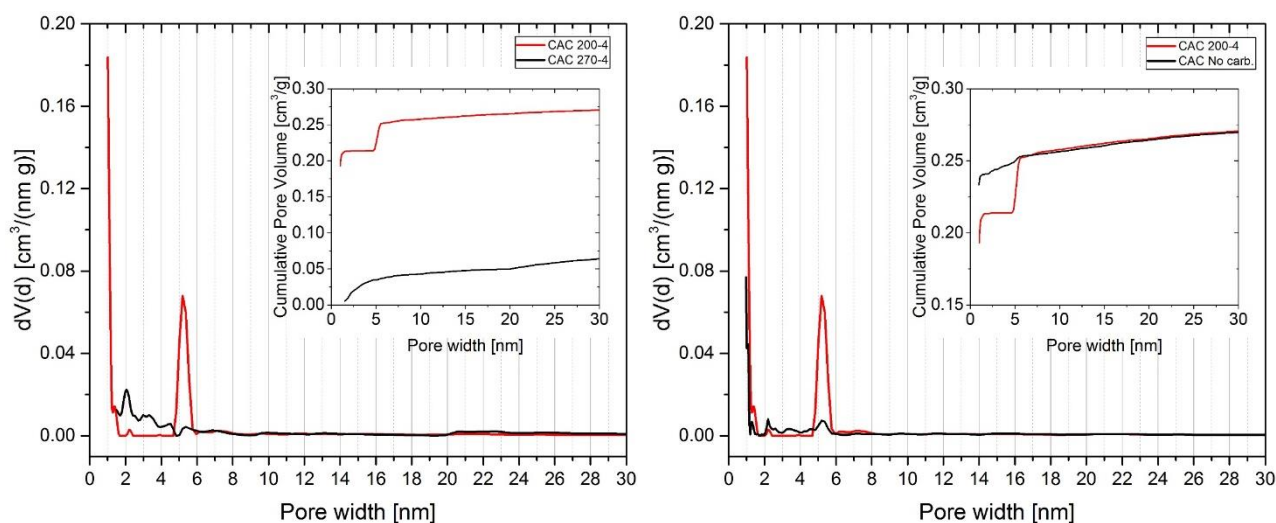


Figure 81: Pore size distribution of selected chemically-activated carbons.

In general, the higher HTC pretreatment severity, the lower the resulting AC quality, in terms of BET surface area and microporosity, for both physical and chemical activation. Considering the particular kind of feedstock and activation conditions, by comparing the characteristics of the hydrochar-activated samples with pyrolysis pretreatment, it can be concluded that for physical activation the HTC pretreatment is deleterious for AC quality and that pyrolysis leads to results that are similar to that of mild hydrothermal carbonization, producing a good quality AC. Similarly, the HTC step should be avoided also for chemical activation.

5.2.7 HTC aqueous phase characterization

The aqueous phase from hydrothermal carbonization was characterized by GC-MS and HPLC. Again, the characterization of this fraction is fundamental in order to assess its possible utilization and management. Like in the characterization of the aqueous phase from the HTC of AD digestate, in general, by increasing the reaction severity the concentration of organics dissolved in this phase increased, as it can be seen from Figure 82, Figure 83 and Figure 84 (error bar represents the absolute standard deviation).

At higher temperatures, it is shown a drastic increase of the concentration of oxygenated aromatics, such as species belonging to the families of phenol, guaiacol and syringol, and of complex ketones; these compounds are derivatives of lignin degradation. Only syringaldehyde concentration increased with time, but became unquantifiable at 270 °C. This behavior indicates that at low temperatures the reaction mechanisms are dominated by hydrolysis, while, when the temperature is increased to 270 °C, a more complex network of free radical reactions takes place.

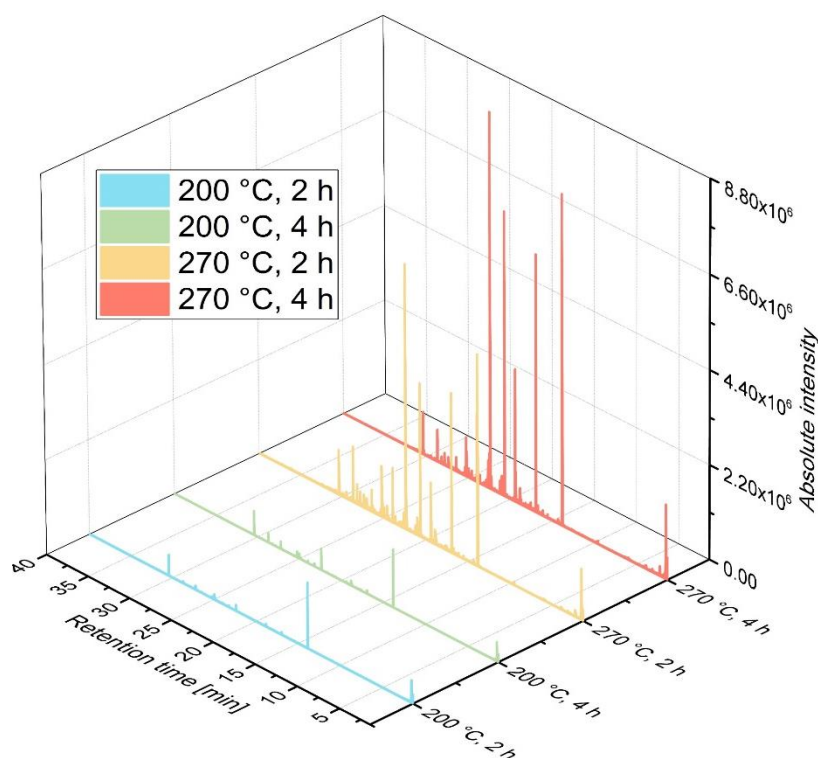


Figure 82: Chromatograms from GC-MS of HTC aqueous phase from the HTC of LRR.

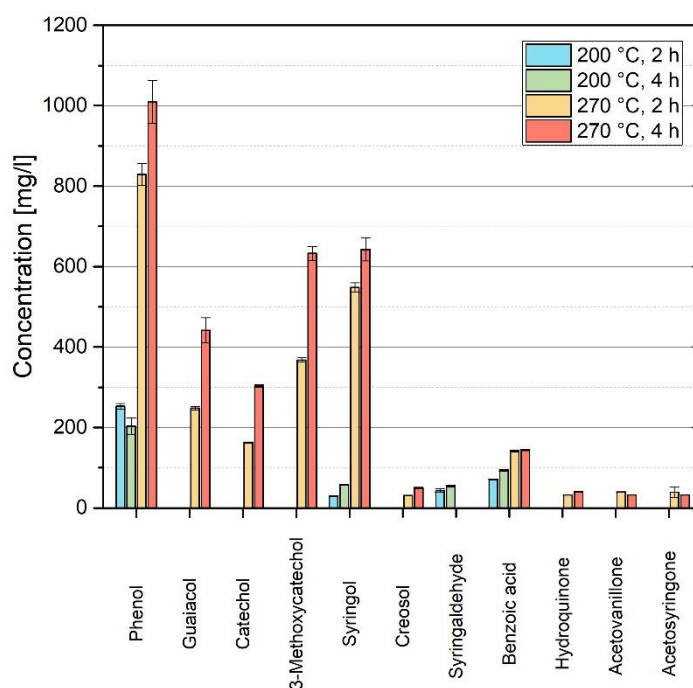


Figure 83: Results from the GC-MS of the aqueous phase from the HTC of LRR.

From the results of HPLC, it can be seen that the aqueous phase was rich in carboxylic acids, mainly lactic and acetic, which, in general, increased in concentration with severity. Also low concentrations of glycerol, ethanol and 5-HMF were detected. In particular, this latter compound, deriving from the degradation of unfermented cellulose is a highly reactive intermediate, which could have been converted into carboxylic acids. More specifically, as proposed by Castello, Kruse and Fiori [146], 5-HMF is formed by the dehydration of fructose, which is produced by the isomerization of glucose. At hydrothermal conditions, 5-HMF can be

degraded into formic acid. Fructose can also lead to the formation of glyceraldehyde, which can consequently produce glycolic acid or pyruvaldehyde, which in turn forms acetic acid.

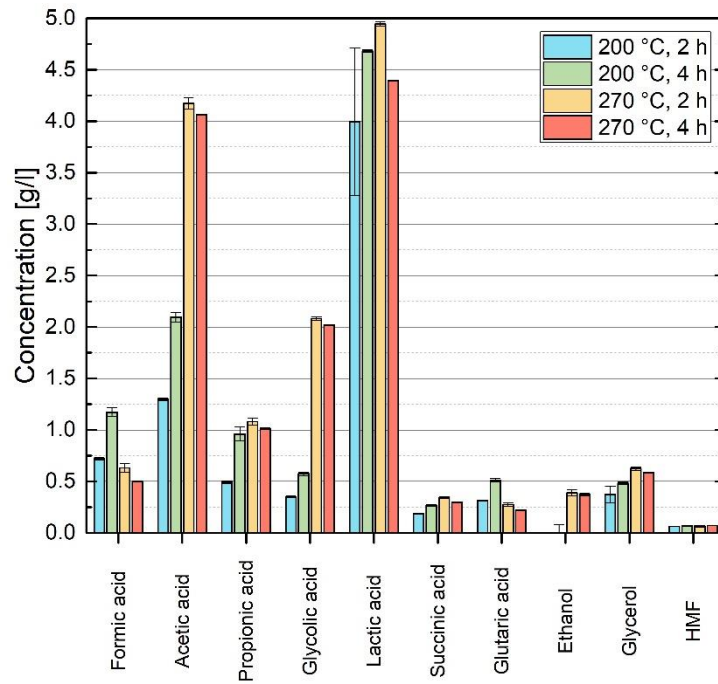


Figure 84: Results from the HPLC of the aqueous phase from the HTC of LRR.

6. Process integration and preliminary scale-up design

6.1 Process integration between anaerobic digestion and hydrothermal carbonization or slow pyrolysis

In this paragraph, three options of AD integration for digestate carbonization are proposed. Because the technological level of the carbonization process (HTC or SP) is inferior to that of AD, a lower amount of annual operating hours was considered. In particular, by referring to the AVA-CO₂ HTC plant [88], the value of 7200 h y⁻¹ was assumed for the bottom plant in the three cases. This difference in the operating hours leads to the adoptions of “buffer tanks” in order to ensure a continuous flow of material between the two plants.

6.1.1 Reference AD plant

As a reference for a typical Italian AD plant (mesophilic, wet digester), it was considered a plant producing 999 kW of power and 1049 kW of heat [147]. The digester is mainly fed with corn silage (65 % w/w, w.b. of moisture), producing almost 3886 kNm³ y⁻¹ of biogas and nearly 17 kt y⁻¹ of digestate (7.3 % w/w of solid content, the same inside the digester). The plant uses a Jenbacher J416 CHP engine [148], whose electric and thermal efficiencies were evaluated by considering the annual energy production and the effective hours of functioning at full load, resulting in 41.3 % and 43.4 % respectively. Power loss for grid connection and AD auxiliary power demand were near to 10 % of the gross produced power, while the heat demand of the digester was considered 35 % of the heat produced by the CHP engine [149,150]. The digester and the CHP were assumed to have the same operating hours. The composition of the biogas is the following:

- 51.8 % v/v (d.b.) of CH₄
- 48.2 % v/v (d.b.) of CO₂
- H₂O (saturated) [151–154]

In general, it is common practice to condense water from the saturated biogas [150,155] and to recycle it into the reactor [156]. From the mass balance, it is shown that the AD plant needs an integration of water for attaining 7.3 % w/w of solid inside the digester, which can be provided by the recycle of the liquid fraction of the digestate after its separation from the solid content [150,156–158]. In case the liquid digestate is spread in the fields for fertilization or is treated in a wastewater treatment plant (WWT), fresh new water is needed [7,147]. In order to evaluate the chemical power of the corn silage, its LHV was considered 17 MJ kg⁻¹ (d.b.) [159], while, as far as the digestate is concerned, this value was taken from the results of the characterization of digestate from the experimental campaign. In Figure 85 and in Table 23 and Table 24, the mass and power values of the reference AD plant are reported.

Table 23: Mass flow of the reference AD plant.

Stream	Value [kg h ⁻¹]
<i>Corns silage (wet)</i>	2212
<i>Make-up water</i>	449
<i>Biogas (wet)</i>	648
<i>Biogas (dry)</i>	618
<i>Digestate (wet)</i>	2042
<i>Digestate (dry)</i>	150

Table 24: Power values of the reference AD plant.

Power	Value [kW]
Gross CHP power	999
Power losses + AD demand	92
Net CHP power	907
Gross CHP heat	1049
AD heat demand	367
Net CHP heat	682
Corn silage chemical power (dry)	3627
Biogas chemical power (dry)	2417
Digestate chemical power (dry)	748

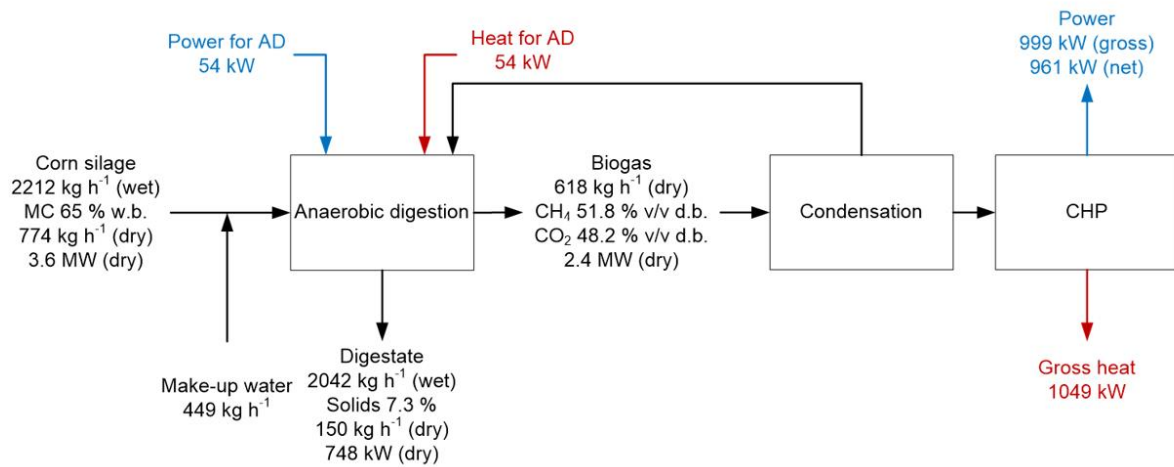


Figure 85: Scheme of the AD reference plant with mass and power values.

The plant's global efficiency can be evaluated by considering the ratio between the net power output and the power input; if the chemical power of the digestate is excluded, then the global efficiency of the AD reference case, defined as Eq. 5, is 44 %.

$$\eta_g = \frac{\text{Net CHP electric power} + \text{Net CHP thermal power}}{\text{Corn chemical power}} \quad \text{Eq. 5}$$

6.1.2 Integration with fixed bed autothermal slow pyrolysis

In this paragraph, it is proposed an integration of the AD reference with a fixed bed autothermal slow pyrolysis plant for digestate carbonization. The main characteristic of this kind of reactor is that, by injection of a small amount of oxidizing agent (air) for biomass partial oxidation, the pyrolysis process is thermally self-sustaining, avoiding the need of an external heat source [160]. In the proposed configuration, the pyrolysis process is thermally self-sustaining, avoiding the need of an external heat source [160]. In the proposed configuration, the pyrolysis process is thermally self-sustaining, avoiding the need of an external heat source [160]. In the proposed configuration, the pyrolysis process is thermally self-sustaining, avoiding the need of an external heat source [160]. In the proposed configuration, the pyrolysis process is thermally self-sustaining, avoiding the need of an external heat source [160].

compacting through milling and briquetting was investigated and confirmed with RE-CORD milling and briquetting machines; a detailed description of the experiment is reported in the appendix.

For the mass and energy values, it was taken as a reference the RE-CORD pilot carbonization unit [160]. According to the experimental results, the char LHV and its yield were assumed 24.1 MJ kg⁻¹ and 33 % w/w (d.b.), respectively. The required milling and briquetting power was evaluated with the digestate mass flow rate, initial and final average particle diameters, work index and grinder efficiency, according to [162–164].

In Figure 86 and in Table 25 and Table 26 the mass and power values of the AD + autothermal SP plant are reported. The imbalance in the mass flow of water is due to the adoption of the buffer tanks, which are needed in order to match the operation of the two plants, being their operating hours different.

In this case, the global efficiency, defined by Eq. 6, is 51%.

$$\eta_g = \frac{\text{Net electric power} + \text{Net thermal power} + \text{Char chemical power}}{\text{Corn chemical power}} \quad \text{Eq. 6}$$

Table 25: Mass flow of the AD and autothermal SP plant.

Stream	Value [kg h⁻¹]
<i>Corns silage (wet)</i>	2212
<i>Make-up water</i>	449
<i>Biogas (wet)</i>	648
<i>Biogas (dry)</i>	618
<i>Digestate (wet)</i>	2042
<i>Digestate (dry)</i>	150
<i>Char</i>	57
<i>Pyrogas</i>	115
<i>Excess water</i>	1095

Table 26: Power values of the AD and autothermal SP plant.

Power	Value [kW]
Gross CHP power	999
Power losses + AD demand	92
Power for dewatering	10
Power for milling and briquetting	13
Power for SP reactor (blower)	13
Net CHP power	871
Gross CHP heat	1049
AD heat demand	367
Heat for drying	293
Heat from pyrogas combustion	193
Net heat	582
Corn silage chemical power (dry)	3627
Biogas chemical power (dry)	2417
Digestate chemical power (dry)	748
Char chemical power (dry)	380

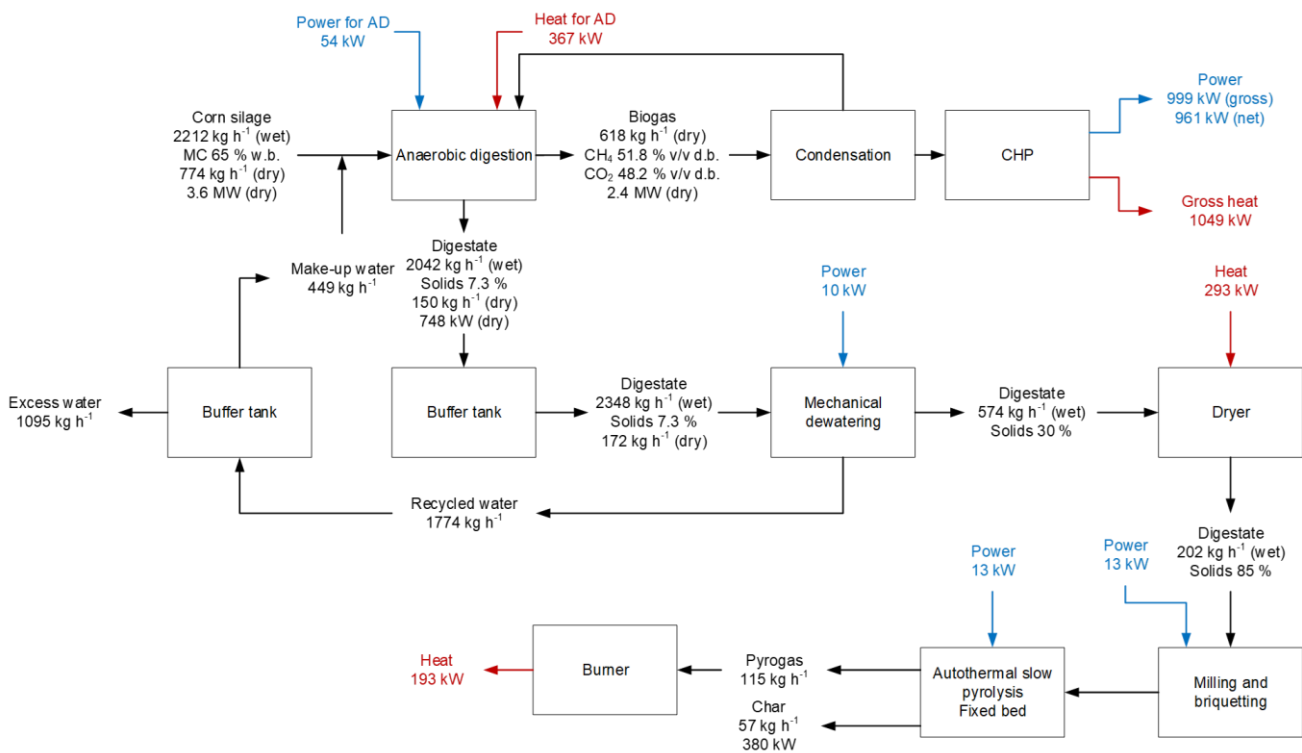


Figure 86: Scheme of the AD + autothermal SP plant with mass and power values.

6.1.3 Integration with rotary slow pyrolyzer

In this case, the anaerobic digester is integrated with a SP plant equipped with an allothermal rotary kiln reactor. The adoption of this kind of equipment leads to the advantage of avoiding the milling and briquetting step, as this reactor can accept also non-homogeneous biomass; on the contrary, no partial oxidation occurs inside the reactor and an external heat source is required. For the evaluation of this latter value, it was considered the dried digestate (with its remaining moisture) to be subjected to a temperature increase from 90 °C (dryer outlet) to the pyrolysis reaction temperature (500 °C). For the sake of simplification, the char

yield and heating value were assumed the same of the previous case and, therefore, the mass values are not changed, but changing autothermal to allothermal reaction condition and reactor configuration will produce char with different yield and properties. The specific heat of the digestate was approximated to that of corn [165]. The power demand of the rotary kiln was evaluated from [166].

The layout of the integration is shown in Figure 87, while the power values are reported in Table 27.

Table 27: Power values of the AD and rotary SP plant.

Power	Value [kW]
Gross CHP power	999
Power losses + AD demand	92
Power for dewatering	10
Power for SP reactor (rotation)	23
Net CHP power	873
Gross CHP heat	1049
AD heat demand	367
Heat for drying	293
Heat for pyrolysis	82
Heat from pyrogas combustion	193
Net heat	500
Corn silage chemical power (dry)	3627
Biogas chemical power (dry)	2417
Digestate chemical power (dry)	748
Char chemical power (dry)	380

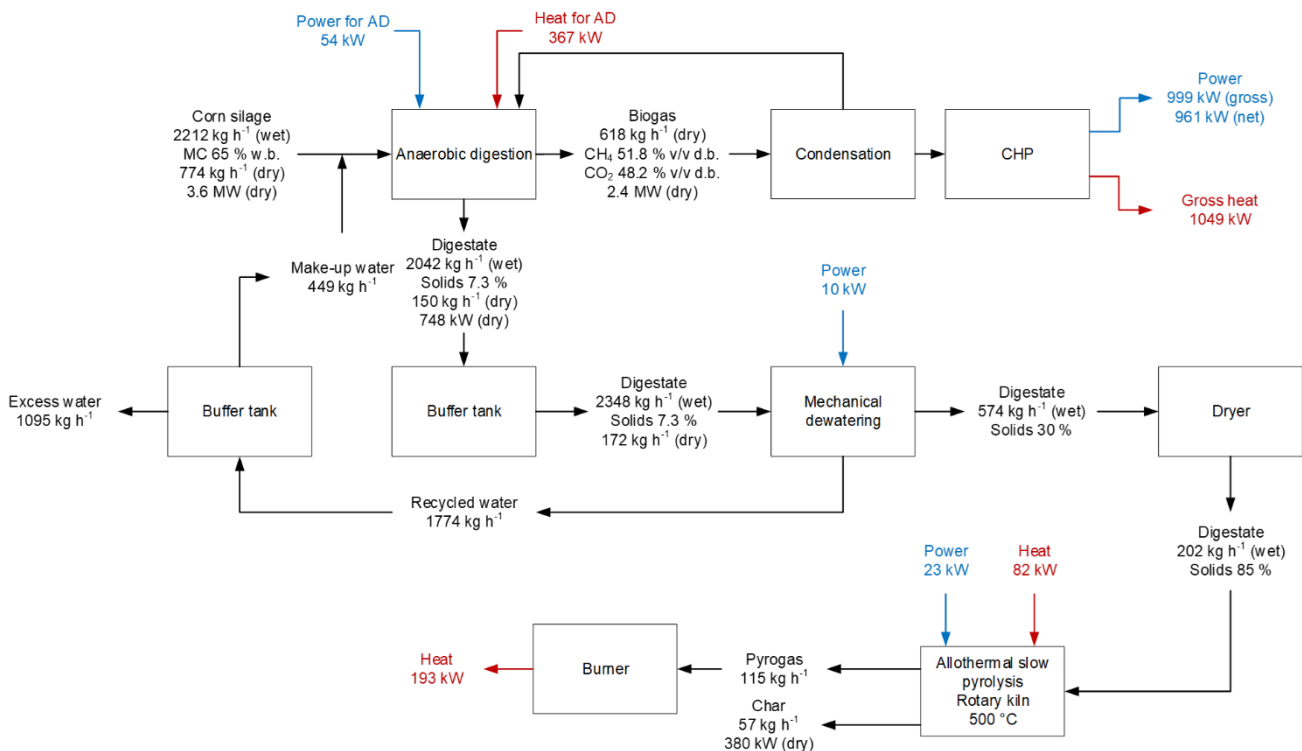


Figure 87: Scheme of the AD + rotary SP plant with mass and power values.

In this case, the global efficiency, again defined by Eq. 6, is slightly lower: 48%.

6.1.4 Integration with hydrothermal carbonization

In the present case, the digested slurry (solid content of 7.3 % w/w, w.b.) is directly pumped to the HTC reactor. A heat exchanger was considered to recover the heat of the reaction products for cold slurry preheating. Next, the slurry is depressurized in a back-pressure valve and the hydrochar is separated from the aqueous phase by a filter-press and then it is dried to a final moisture content of 10 % w/w (w.b.). Again, the process water is in part recycled to the AD as make-up water. In general, hydrochar is reported to be a hydrophobic material [38] and, therefore, after the dewatering step a lower water content (i.e. 50 % w/w) was considered.

The heat required for integrating the loss in the heat exchanger and in the HTC reactor was considered the 40 % of the heat needed for slurry heat-up to reaction temperature (200 °C) [164,167]. The same references were considered for the evaluation of the HTC power demand. In accordance with literature and with the experimental results, the yields of char, water-soluble organics and gas were considered 60, 35 and 5 % w/w (d.b.) [38,73,168]. The LHV of the char was assumed 25 MJ kg⁻¹.

In Figure 88 and in Table 28 and Table 29 the mass and power values of the AD + HTC plant are reported.

The global efficiency is the highest among all cases, reaching 52 %.

By considering all the taken assumptions, at the end of this simple mass and energy integration, it can be said that, in terms of global plant efficiency, the best option is the integration of anaerobic digestion with hydrothermal carbonization, followed by autothermal slow pyrolysis (Table 30).

Table 28: Mass flow of the AD and HTC plant.

Stream	Value [kg h⁻¹]
<i>Corns silage (wet)</i>	2212
<i>Make-up water</i>	449
<i>Biogas (wet)</i>	648
<i>Biogas (dry)</i>	618
<i>Digestate (wet)</i>	2042
<i>Digestate (dry)</i>	150
<i>Char</i>	103
<i>Water-soluble organics</i>	60
<i>Gas (CO₂)</i>	9
<i>Excess water</i>	1407

Table 29: Power values of the AD and HTC plant.

Power	Value [kW]
Gross CHP power	999
Power losses + AD demand	92
Power for HTC	1
Power for dewatering	6
Net CHP power	894
Gross CHP heat	1049
AD heat demand	367
Heat for HTC	230
Heat for drying	78
Net heat	374
Corn silage chemical power (dry)	3627
Biogas chemical power (dry)	2417
Digestate chemical power (dry)	748
Char chemical power (dry)	717

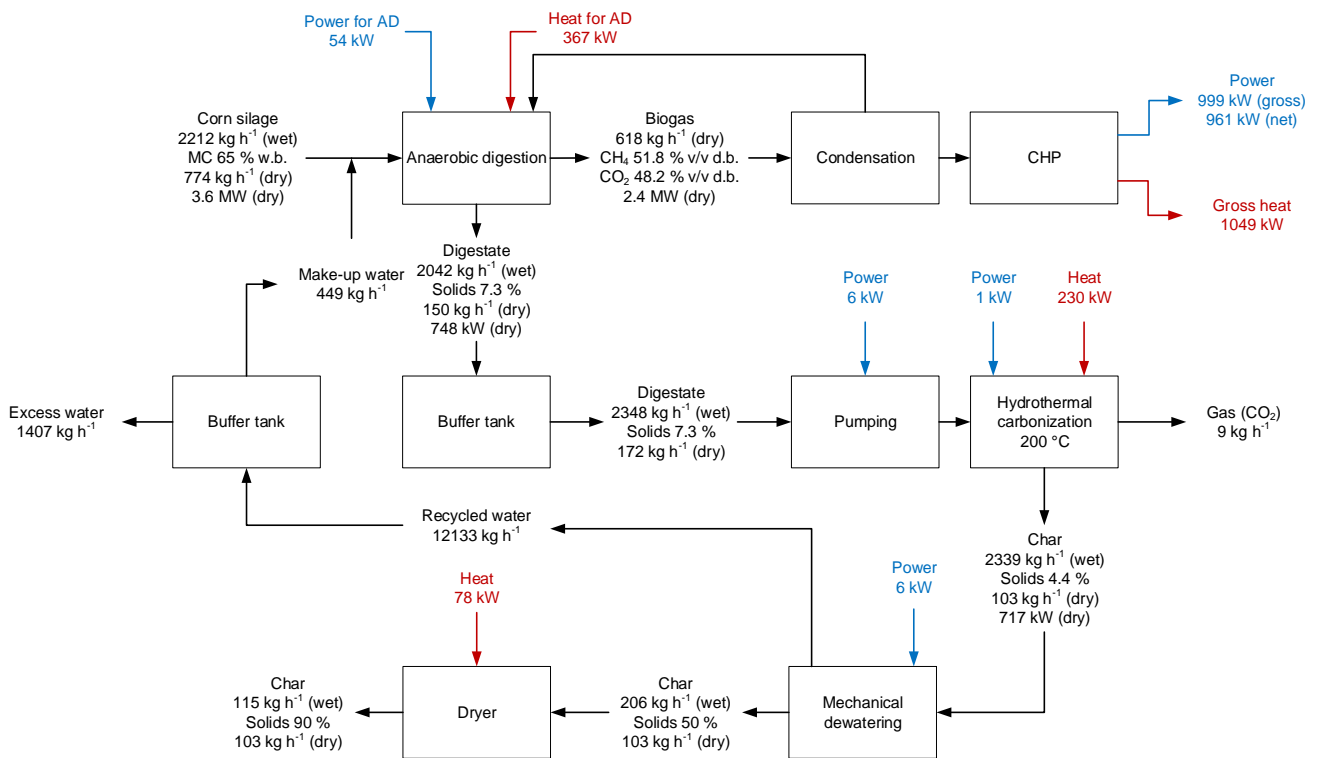


Figure 88: Scheme of the AD + HTC plant with mass and power values.

Table 30: Global efficiencies of the integration with AD.

Case	Global efficiency
AD reference	44 %
AD + autothermal SP	51 %
AD + allothermal SP	48 %
AD + HTC	55 %

Matching of heat flow

It has to be pointed out that anaerobic digestion plants cannot be easily regulated, because of their high inertia, which is intrinsic of a biochemical process. The contrary is true for continuous hydrothermal carbonization, which is characterized only by thermochemical reactions. Therefore, in the following section, only a steady state matching between the top-AD and the bottom-HTC plant will be presented.

The matching of heat flow consisted in the evaluation of heat exchange from the CHP fumes (high temperature) and cooling circuit (low temperature) to the digester, HTC reactor and char dryer. Different options and heat transfer fluids (steam, water, diathermic oil and a combination thereof) were evaluated, and the final solution was the one depicted in Figure 89. Here, diathermic oil (THERMINOL66 [169]) is used to transfer the CHP fumes' high-temperature heat to the HTC process and to heat the ambient air, which is sent to the char dryer. A water circuit is used for transferring the CHP low-temperature heat to the digester and to potential extra users. This layout was chosen for its simplicity and cost-effectiveness in terms of heat exchanger area.

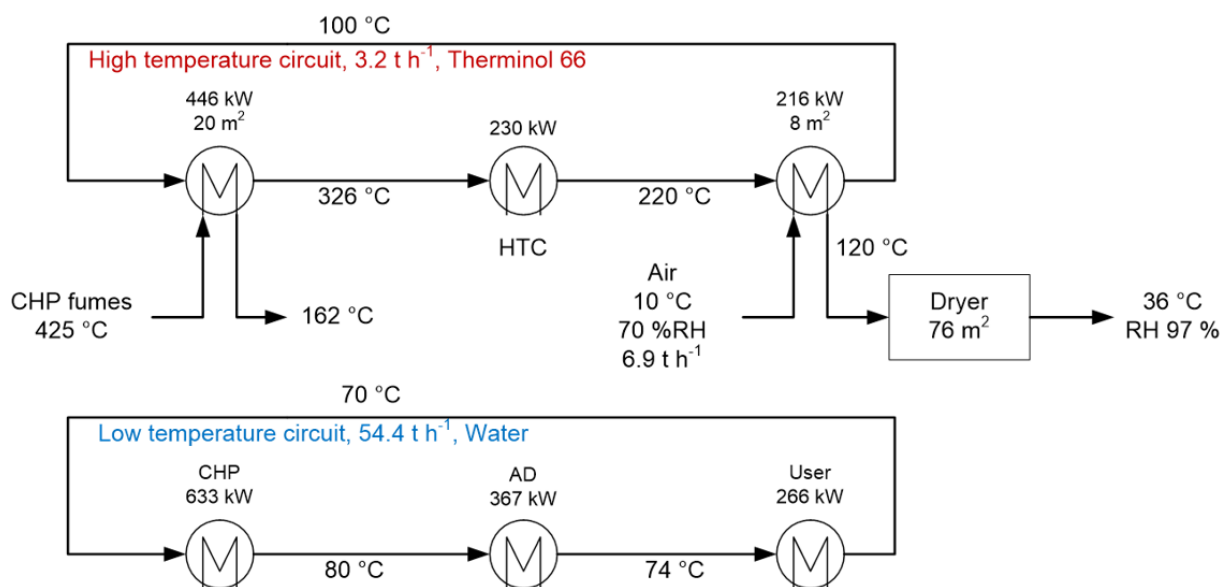


Figure 89: Scheme of the adopted solution for the heat flow matching.

Preliminary design of a continuous HTC plant

In this paragraph, the results from the preliminary design of the previously described continuous hydrothermal carbonization plant are reported. Temperature values were evaluated in the whole circuit, together with the heat exchangers' surface. The input values of the calculation are reported in Table 31. Isenthalpic transformations were considered for pressurization and depressurization.

In this layout a series of externally heated (diathermic oil, heat from CHP) CSTR reactors were considered. This solution was adopted because of its simplicity and flexibility. By using actuated valves, the access to the reactors can be bypassed, easily modifying the slurry residence time. The single CSTR reactor was preliminary designed according to [170]: each reactor has an inner volume of approximately 3 m³ (ellipsoidal heads because of pressure, 1.4 m diameter, 2.4 m height), where only the 80 % of which is filled with the digested slurry; the mean residence time is evaluated to be 1 h. The reactor's volume is relatively high, but similar values were also adopted in other studies [88,164]. Each reactor has a stirrer for optimal mixing of the reagents and temperature homogeneity. CSTR reactors do not ensure a well-defined residence time, but, by considering multiple in-series reactors, this problem is reduced, being the whole reactors set more similar to

a single plug flow reactor (in the theoretical case of using an infinite number of CSTRs). At the outlet of each reactor an actuated valve for flow control and a check valve were considered, while on the top, a pressure relief valve was adopted in order to decrease pressure build-up due to gas formation. Reaction temperature was 200 °C. A high-pressure piston pump pressurizes the digested slurry, so to avoid water vaporization during heating and reaction, to the reaction pressure (≥ 22 bar), which is maintained in the reactors by means of a back-pressure regulating valve, which is located prior to the dewatering step.

The inner diameter of the pipes was evaluated by determining the condition in which the settling of the slurry particles is avoided. The different temperatures, pressures and solid loads, characteristic of each zone of the plant were considered and the digested slurry was assumed as a non-Newtonian fluid with 8 mm particles [171]. The logic behind this evaluation is the following: the diameter of the pipes should guarantee a stream velocity higher than the so-called settling velocity and at the same time ensure low pressure drops in the circuit. Various empirical correlations were evaluated (Metcalf and Eddy [171], Newin [172], Couper [173], Flygt [174]) and a commercial inner diameter of 35 mm was determined.

In Figure 90, the layout of the HTC plant with calculated values is shown.

Table 31: Input values used for the calculation of the HTC plant.

Position	Temperature [°C]	Pressure [bar]
Slurry inlet	20	1
Reactor	200	≥ 22
After cooler	80	-
After BPR valve	80	1
Diathermic oil to preheater	215	-

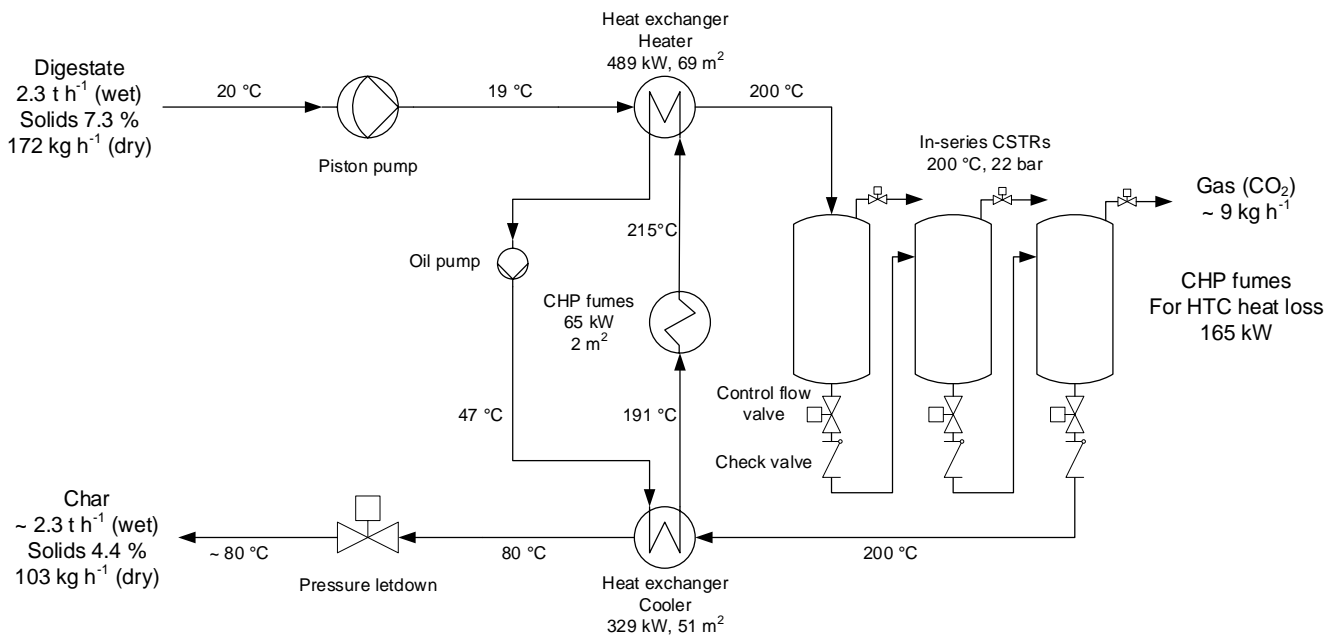


Figure 90: Layout of the continuous HTC plant.

6.1.5 Preliminary Economic analysis

In this paragraph, a preliminary and very simplified economic analysis of the three integration cases is reported. This analysis does not claim to be exhaustive, but can be useful in order to assess a first economic comparison.

For the sake of simplicity, annual operating hours of the top and bottom plant were assumed 8000 h y⁻¹. Fixed costs were considered as sum of the top and bottom plant cost. The AD fixed cost, in which are included also all installation costs, was assumed 4 M€ (a 30-plants survey was considered as reference [175]). The fixed cost of the HTC plant was scaled according to the 6/10 rule [176], from Lucian et al. [164], while the slow pyrolysis plant costs derived from a research made by RE-CORD. The installation costs of the bottom plant (civil works, etc.) were considered as 5 % of the plant cost. The fixed-bed autothermal slow pyrolysis plant is the cheapest, being very simple if compared, for example, to the rotary pyrolyzer, where the reactor seals, needed in order to prevent oxygen inclusion and ensure inert atmosphere, add further complexity. The whole amount of the capex was not assumed to be paid in the first year, but it is diluted by a 10 years' loan.

Annual costs are divided in biomass supply/production, natural gas purchase for fulfill the plant's heat demand, electric energy purchase, generic plant costs (employees, maintenance, general expenditures, etc.) and the loan payment. The cost of the biomass feedstock was obtained by considering an average value related to plants cultivated in fields of property [175]. The cost of natural gas was assumed 38.45 c€ m⁻³ [177], while that of electric energy, related to the annual consumption, was 10.21 c€ kWh⁻¹ [178]. The operative cost of the AD plant were scaled from [175], for the HTC plant from [164], while for the slow pyrolysis plants the 10 % of the capex was considered. In this evaluation the excess water is sent to a waste water treatment plant, with a cost of 13.7 € t⁻¹ [164]. The annual loan payment (10 years) was calculated by considering an 8 % interest.

Annual incomes are represented by selling of the net CHP electric energy (0.28 € kWh⁻¹ [179], considering the loss for grid connection), selling of thermal energy (conventional value 0.04 € kWh⁻¹), and selling of the char for agriculture (310 € t⁻¹). All these values, together with annual profits, are shown in Table 32. Eng. David Casini of RE-CORD provided the value of char after a market research done for the Agrochar project.

The net present value (NPV) of the three cases was also evaluated for a duration of 20 years and its trend is shown in Figure 91. After 10 years, the curve increases its slope because of the end of the annual loan payment.

It was also evaluated the profitability index (Table 33), defined as Eq. 7.

$$\textit{Profitability index} = \frac{NPV_{20}}{I_0} \quad \text{Eq. 7}$$

Where NPV₂₀ is the net present value at 20 years and I₀ is the total capex amount.

Table 32: Resume of the preliminary economic analysis (values are expressed in k€).

	Cost item	AD + HTC	AD + SP (autothermal)	AD + SP (allothermal)
	<i>CHP net Power [kW]</i>	961	961	961
	<i>Heat supply [kW]</i>	0	0	0
	<i>Power supply [kW]</i>	61	90	87
	<i>Net produced heat [kW]</i>	374	582	500
	<i>Char [t y⁻¹]</i>	824	456	456
<i>Capex</i>	<i>AD plant</i>	4000	4000	4000
	<i>Bottom plant</i>	580	400	550
	<i>Bottom installation</i>	29	20	28
<i>Total capex</i>		4609	4420	4578
<i>Opex</i>	<i>Corn supply</i>	730	730	730
	<i>Natural gas supply</i>	0	0	0
	<i>Power supply</i>	50	74	71
	<i>AD</i>	577	577	577
	<i>Bottom</i>	58	39	53
	<i>Waste water treatment</i>	154	120	120
	<i>Loan payment</i>	687	659	682
<i>Total opex</i>		2243	2198	2234
<i>Annual income</i>	<i>Power</i>	2153	2153	2153
	<i>Heat</i>	120	186	160
	<i>Char</i>	255	141	141
<i>Total income</i>		2528	2480	2454
<i>Total profit</i>		272	282	220

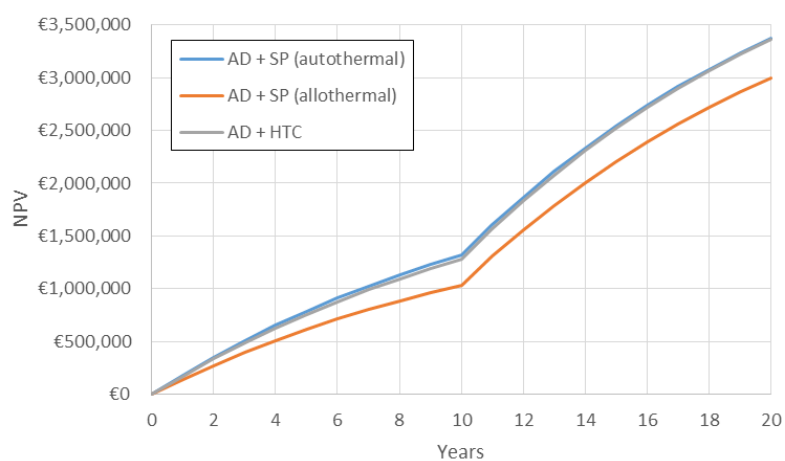


Figure 91: NPV trends for the three evaluated cases.

Table 33: Profitability index for the three evaluated cases.

Case	Profitability index
<i>AD + HTC</i>	0.73
<i>AD + SP (autothermal)</i>	0.76
<i>AD + SP (allothermal)</i>	0.66

From this preliminary economic analysis, it can be concluded that the integration of anaerobic digestion and a fixed bed autothermal slow pyrolysis plant is the more profitable option, even if all the cases exhibited similar results.

6.2 Physical activation of LRR at demo-scale: preliminary design and integration with 2nd generation ethanol and HTC or slow pyrolysis

In this paragraph, an integration between a demo-scale 2nd generation ethanol plant and a physical (steam) activation plant is proposed after the results obtained in the lab-scale experimental campaign with LRR from poplar fermentation. Detailed mass flow data and preliminary design calculation were carried out only for the integration with SP plant.

Steam was considered as activating agent in place of carbon dioxide. This choice is supported by the fact that steam, rather than CO₂, is a medium, which is extremely easier to obtain and to process in an industrial environment. It is true that the lignocellulosic ethanol process produces many kt y⁻¹ of carbon dioxide, but its recovery and concentration is technically very difficult, being heavily diluted.

6.2.1 Integration of HTC and physical activation with a demo-scale lignocellulosic ethanol plant

Figure 92 depicts the block diagram of process integration with hydrothermal carbonization. The wet LRR is processed in a HTC plant where it is eventually diluted with recycled water for decreasing the biomass-to-water mass ratio to an optimal value; after the thermochemical conversion the slurry is firstly mechanically dewatered and dried. The dried char is then conveyed to the activator. Process steam for the activation can be recovered from the dryer and/or produced in a boiler fired with the off-gas from the activation.

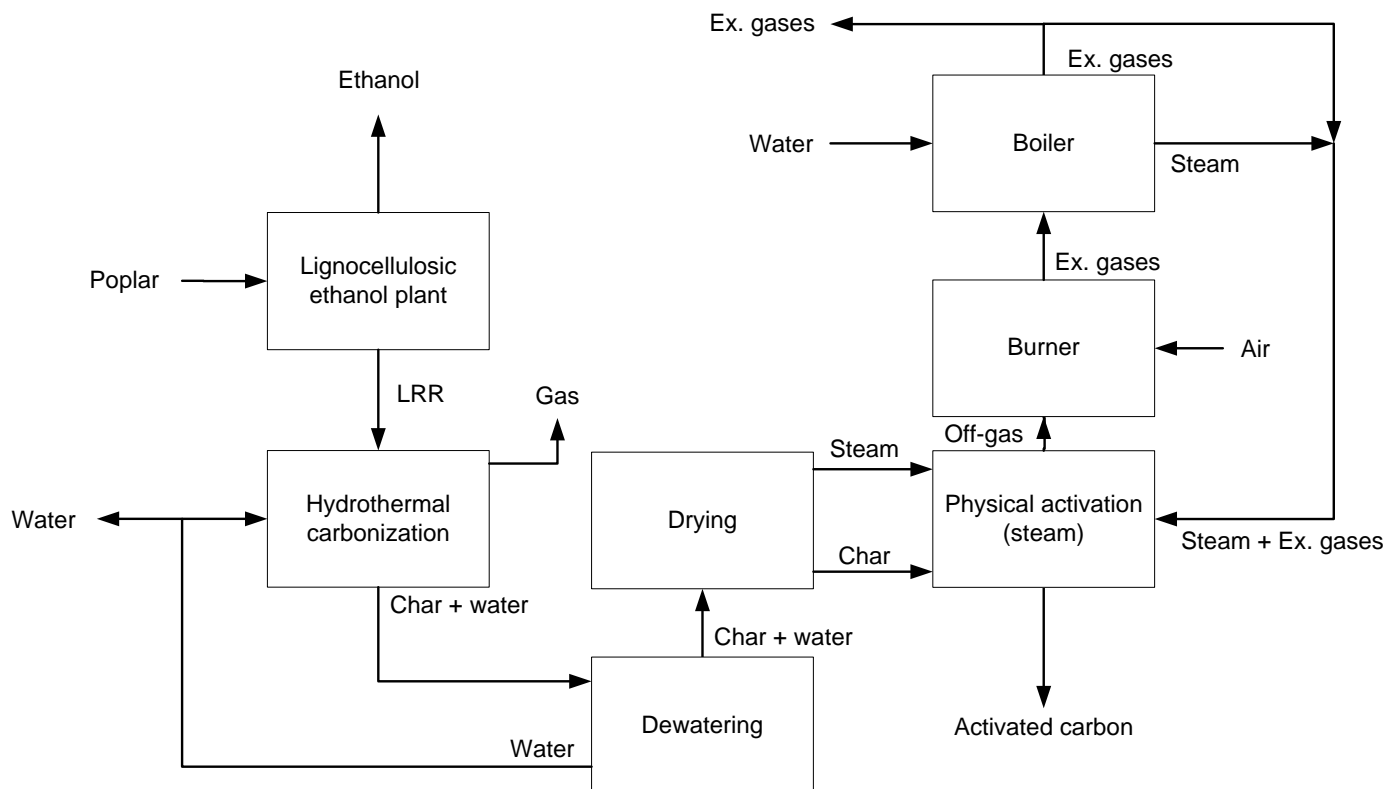


Figure 92: Block diagram representing the integration with HTC.

Mass balance

In Figure 93, it is reported a preliminary mass balance of the integrated plant; the hydrochar yield, carbon content and the AC yield values were taken from the experiment carried out at 200 °C - 2 h, as it produced an activated carbon with better morphological properties. A better explanation of each process step and the related assumptions that were taken are reported in the following paragraph, where this evaluation is performed in the case of integration with slow pyrolysis. As it can be seen, the energetic content of the off-gas from the activation plant (12.91 MJ kg⁻¹, corresponding to ~ 42 MW) is more than sufficient to fulfil the heat demand of the HTC plant, dryer and activation unit.

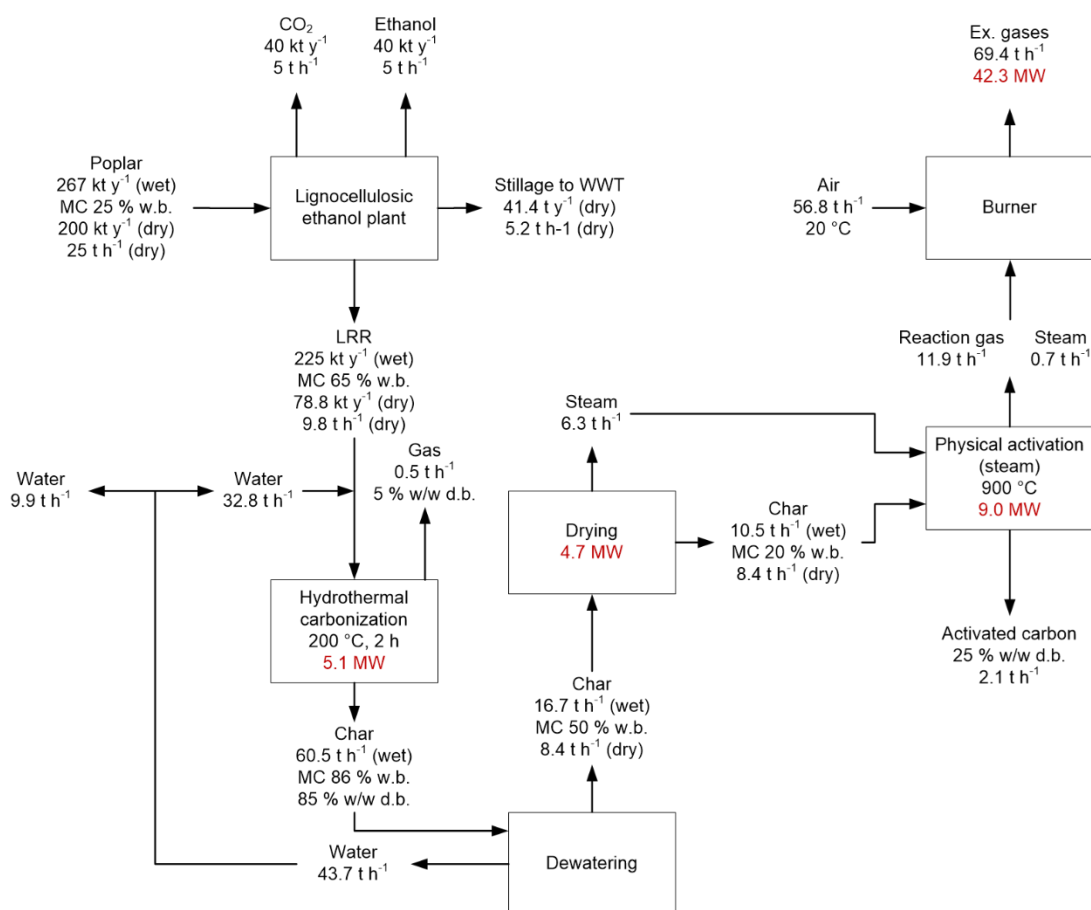


Figure 93: Scheme of the whole process integration with HTC with additional data.

6.2.2 Integration of slow pyrolysis and physical activation with a demo-scale lignocellulosic ethanol plant

Figure 94 depicts the block diagram of process integration with SP. After the LRR is separated and firstly dewatered in the ethanol plant, it is dried in order to reach a suitable moisture content for the following pyrolysis step. After carbonization, the pyrochar is finally activated with steam. The drying, the pyrolysis and the activation were considered to occur in rotary dryer/kilns, which, indeed, are the most common type for biomass applications and have low maintenance costs [180,181]; in addition, they are particularly suitable to process the LRR, whose lignin content swells and agglomerates during heating (as confirmed during the activation experiments), being their functioning less sensitive to particle size.

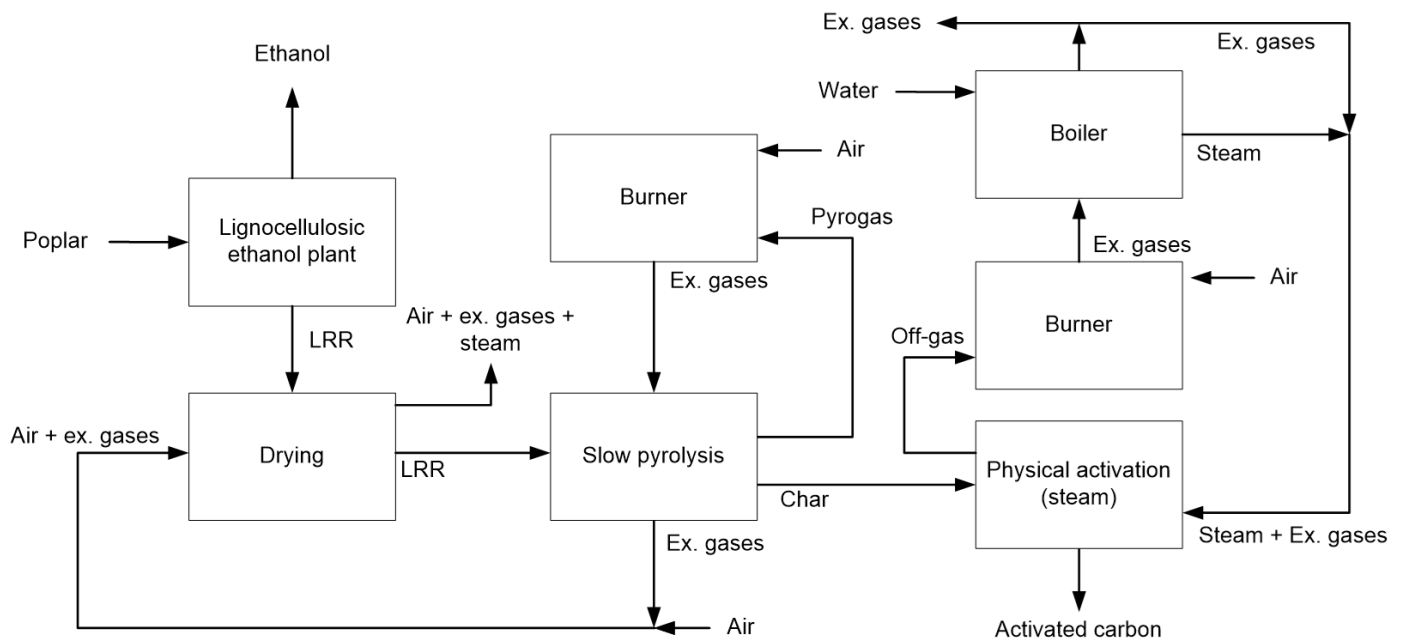


Figure 94: Block diagram representing the integration with slow pyrolysis.

Mass balance

The 2nd generation ethanol demo-plant that was considered (Figure 95) produces 40 kt of ethanol per year and carbon dioxide is produced in the same amount. The biomass input is of approximately 200 kt y⁻¹ (d.b.) at a moisture content of 25 % w/w (w.b.). Nearly 9.8 t h⁻¹ (d.b.) of lignin-rich residue is produced; its moisture content was assumed 65 % w/w (w.b) after the dewatering step. Nearly 41 kt y⁻¹ of stillage are also produced, which are sent to a waste water treatment plant. In Table 34, the mass flow values are resumed; 8000 h y⁻¹ were considered as annual hours of operation, due the big capacity of the plant.

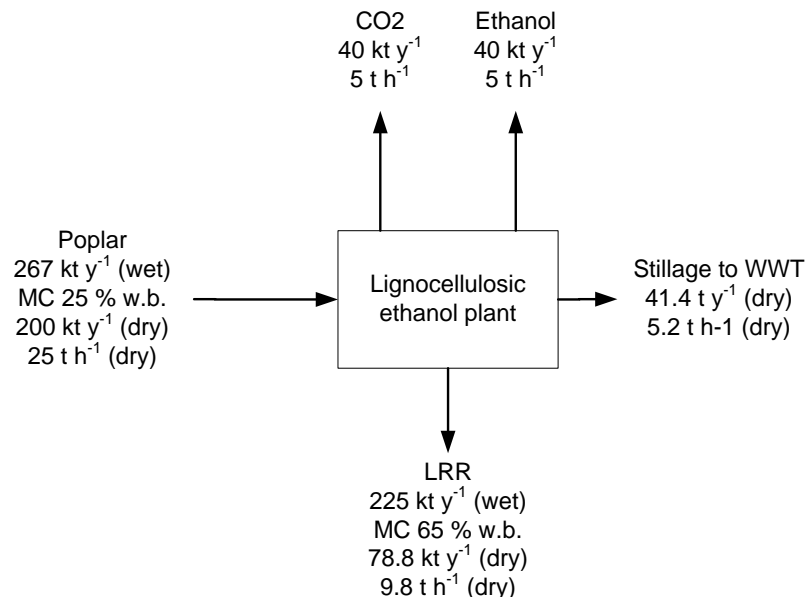


Figure 95: Mass flow of the lignocellulosic ethanol plant.

Table 34: Mass flow of the demo lignocellulosic ethanol plant.

Stream	Value [kt y ⁻¹]
<i>Poplar (wet)</i>	267
<i>Poplar (dry)</i>	200
<i>Ethanol</i>	40
<i>CO₂</i>	40
<i>LRR (wet)</i>	225
<i>LRR (dry)</i>	78.8
<i>Stillage to WWT</i>	41.4

Prior to the slow pyrolysis reactor, the LRR has to be dried to a moisture content of at least 20 % w/w (w.b.). In order to keep the size of the rotary dryer to acceptable values, a pre-drying step is needed to decrease the water content from 65 to 50 % w/w (w.b.). This step can be achieved by considering a more effective dewatering in the ethanol plant and/or by exploiting the waste heat from the combustion of the off-gas produced by the activator unit.

A direct rotary dryer with internal flights and co-current flow was considered for the drying unit (Figure 96). Although the co-current flow leads to a lower heat-transfer efficiency, its adoption is more frequent when heat-sensitive material has to be processed: a higher gas inlet temperature can be used because of rapid cooling during initial evaporation of moisture [182]. The showering action of the flights allows a better heat exchange between the solids and the drying gas; radial flights should be used for preventing agglomeration of the sticky LRR, especially at the inlet region of the dryer.

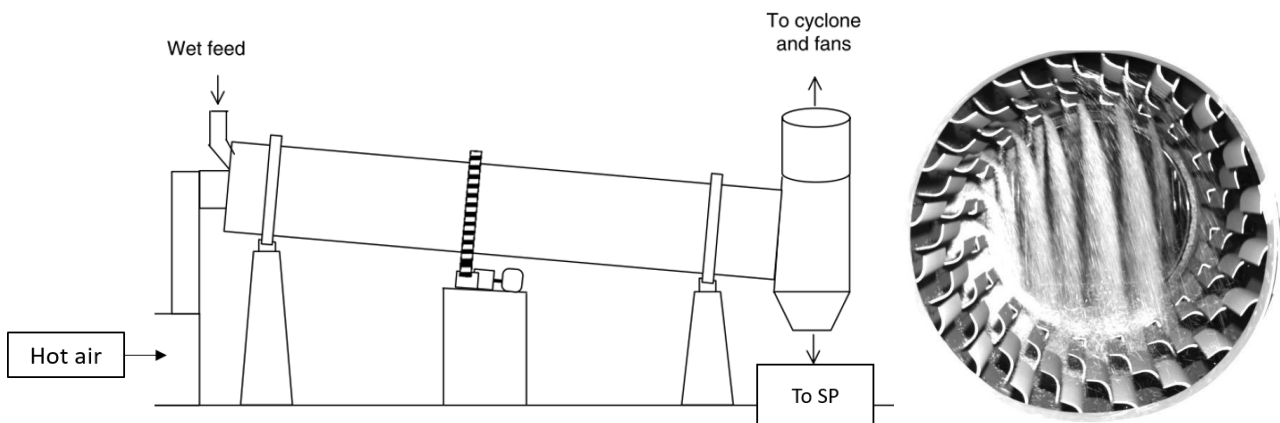


Figure 96: Simplified scheme of a co-current rotary dryer, modified from [183] and example of biomass showering due to inner flights.

Due to the very high amount of LRR that has to be processed, two parallel dryers were considered, as shown in Figure 97. The drying gas was a mixture of ambient air and flue gas from pyrogas combustion, which were mixed in a direct heat exchanger. In Table 35, the mass flow of the drying plant is reported.

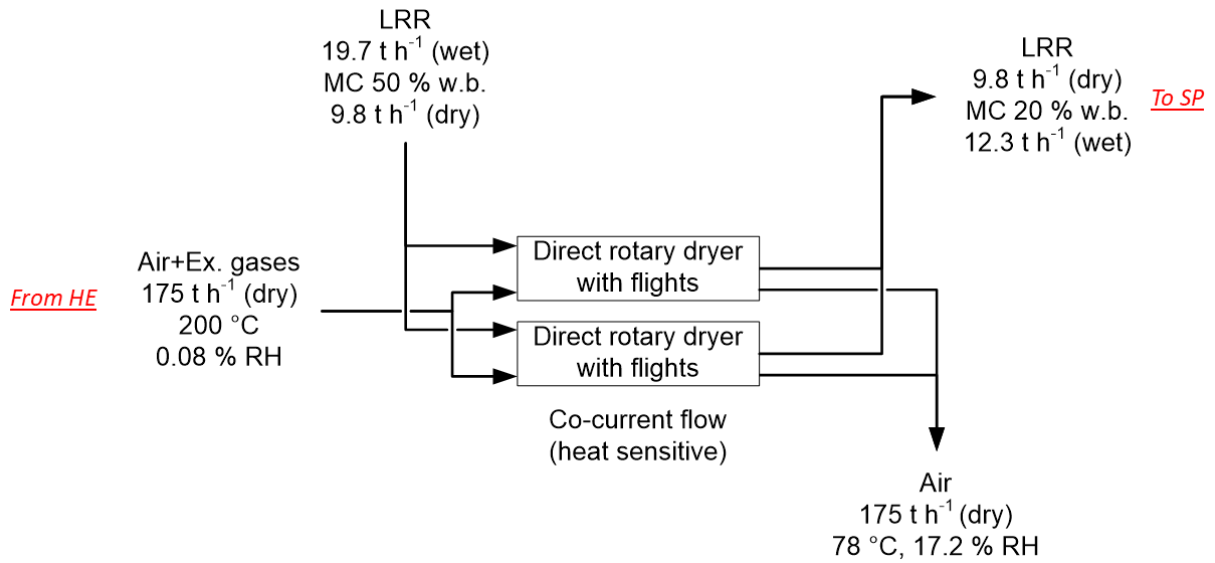


Figure 97: Mass flow scheme of the drying plant.

Table 35: Mass flow of the drying plant.

Stream	Value [t h ⁻¹]
<i>Input LRR (wet)</i>	<i>19.7</i>
<i>Input LRR (dry)</i>	<i>9.8</i>
<i>Evaporated water</i>	<i>7.4</i>
<i>Output LRR (wet)</i>	<i>12.3</i>
<i>Drying gas</i>	<i>175</i>

As far as the slow pyrolysis is concerned, an indirect rotary kiln without flights was considered. The kiln is heated by an external flow of hot gas produced by pyrogas combustion; the reason behind the choice of an indirect rotary kiln resides in the will to keep, as best as possible, an oxygen-free atmosphere inside the reactor. Because no flights were considered, the motion of the dried LRR depends on the rotational speed of the kiln. A regime of rolling was assumed (Figure 99), as, in this case, the mixing is maximized. Similarly to the drying plant, two parallel pyrolyzers were adopted. The Froude number, Eq. 8, where ω is the angular rotational velocity, R is the kiln radius and g the gravity acceleration, defines the bed motion (Figure 98).

$$Fr = \frac{\omega^2 R}{g} \quad \text{Eq. 8}$$

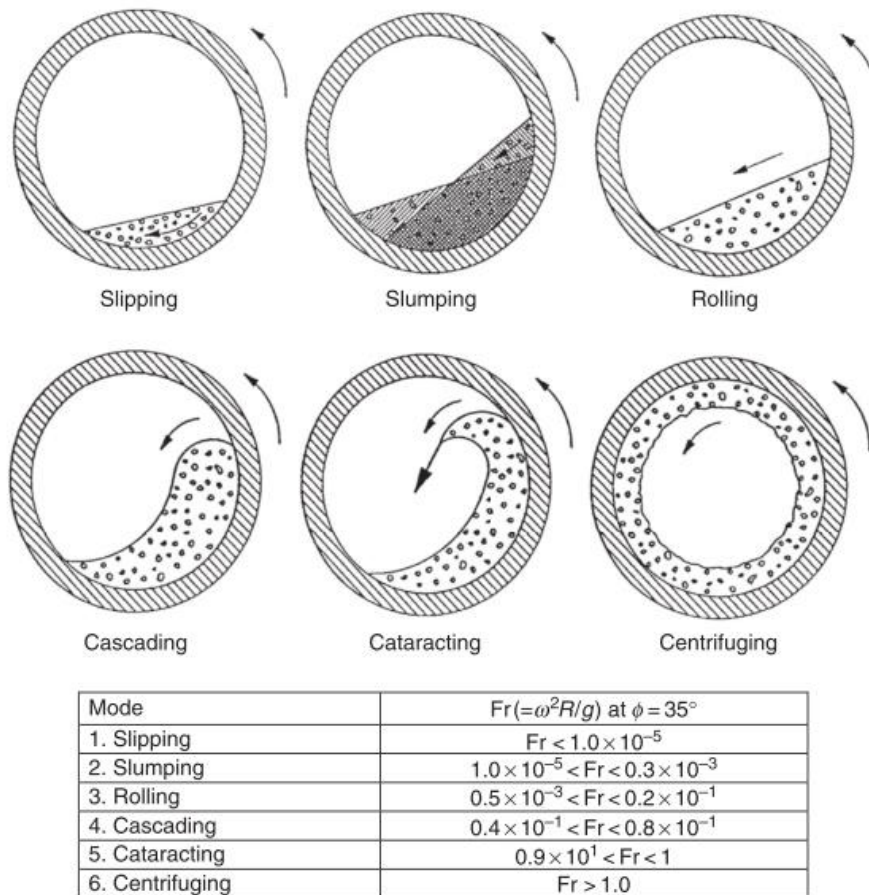


Figure 98: Rotary kiln bed motions and Froude number ranges (without flights) [33].

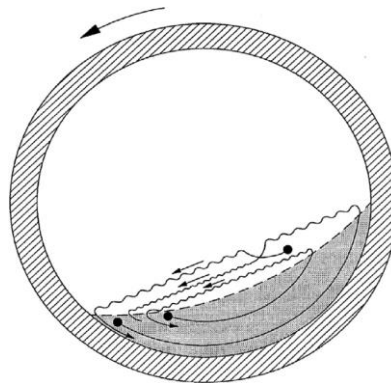


Figure 99: Particular of the rolling flow regime [33].

By considering the experimental campaign, a char yield of 30 % w/w (d.b.) was assumed and, by difference, a 70 % w/w (d.b.) of non-condensable gases and tars yield. Tars were considered to be maintained in gas phase: the pyrogas is burned and the corresponding flue gases are used for providing the heat for pyrolysis. After this heat exchange, these gases are mixed with ambient air and sent to the dryer (Figure 100). Table 36 resumes the mass flow.

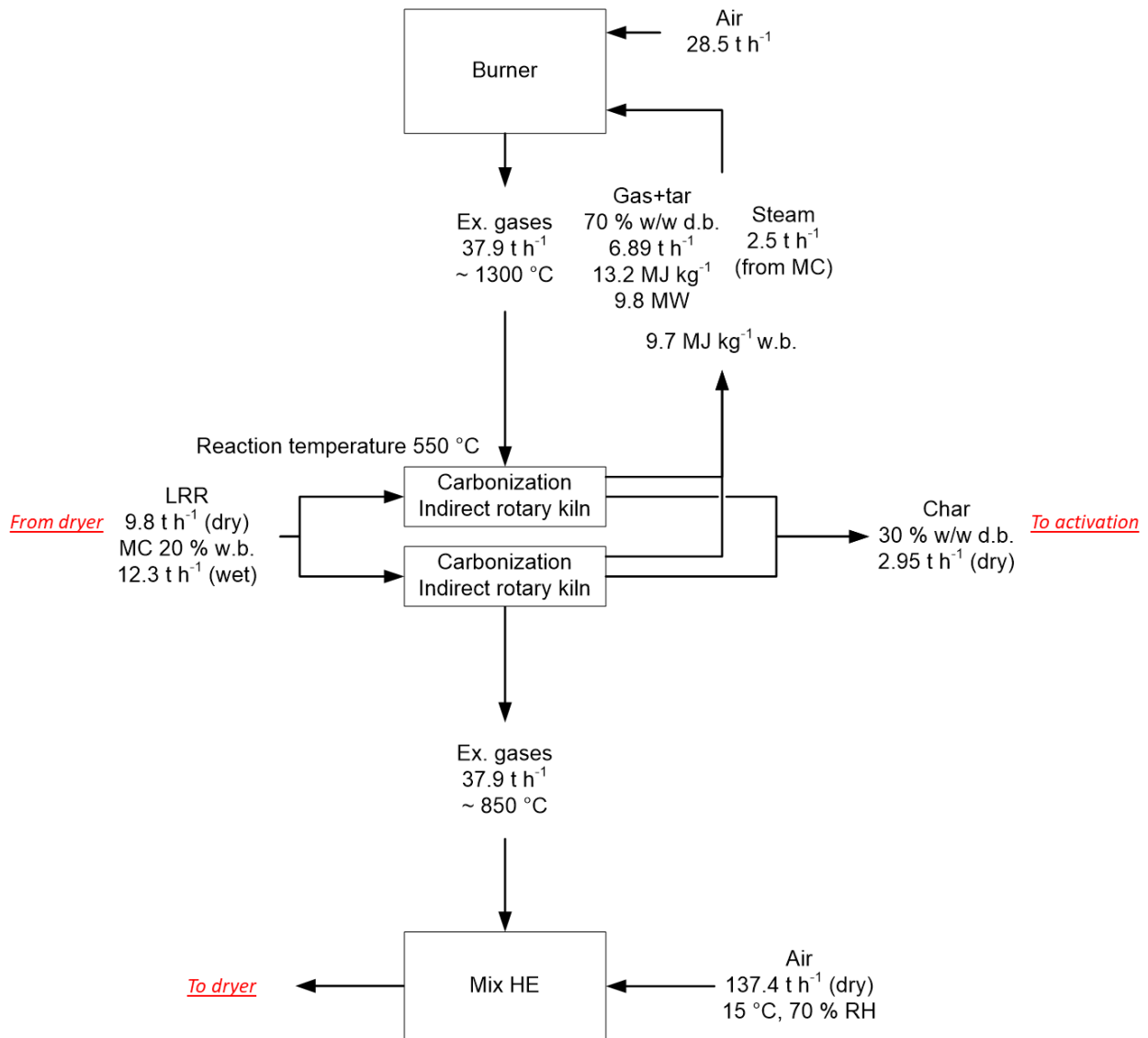


Figure 100: Mass flow scheme of the SP plant.

Table 36: Mass flow of the SP plant.

Stream	Value [t h ⁻¹]
Input LRR (wet)	12.3
Input LRR (dry)	9.8
Evaporated water	2.5
Char	2.9
Pyrogas (gas + tars)	6.9
Combustion air	28.5
Flue gas	37.9

For the activation plant, one direct, countercurrent rotary kiln without flights (rolling regime) was considered. The activation temperature (900 °C) is reached by means of injection of a mixture of steam and combustion gases; steam is produced by the combustion of the gases produced during activation (H₂, CO) from the activation process (Figure 101). Table 37 resumes the mass flow data of the activation plant.

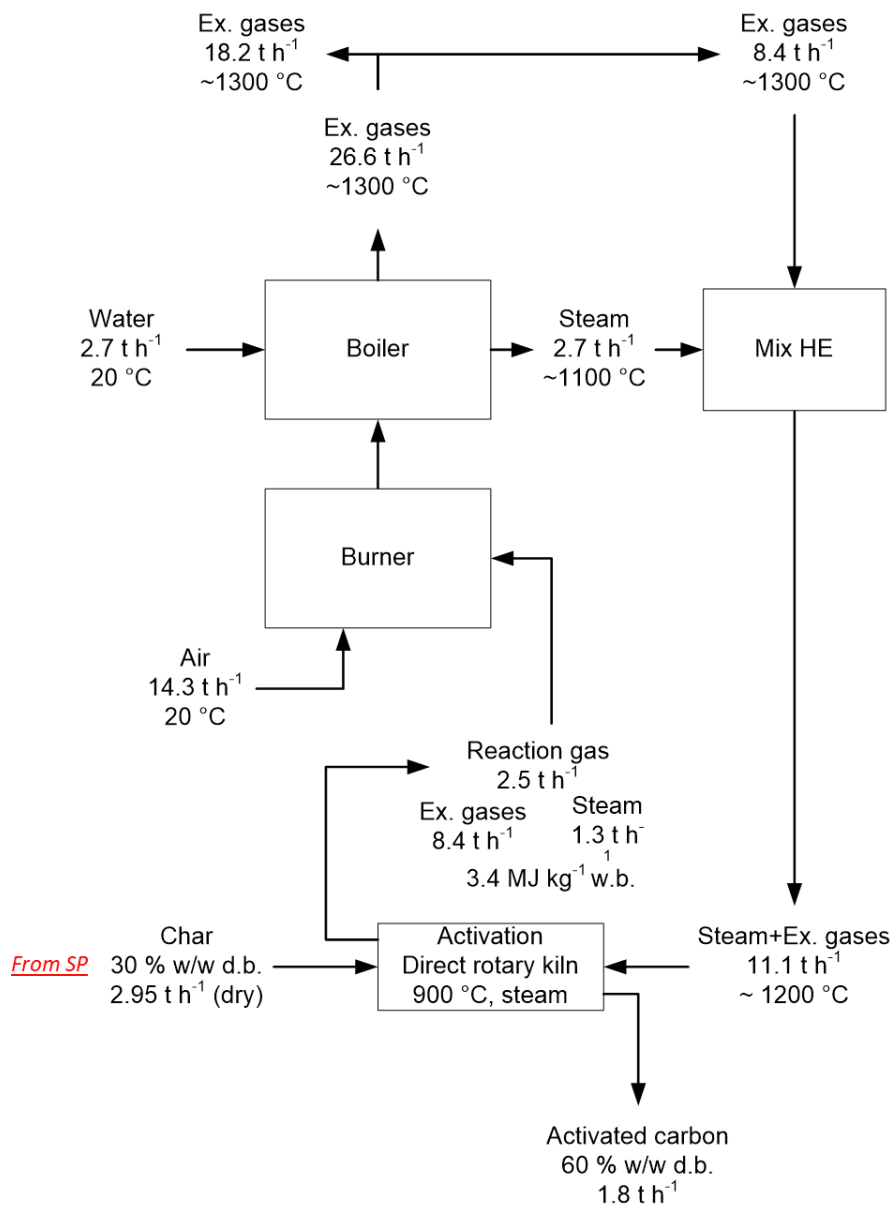


Figure 101: Mass flow scheme of the activation plant.

Table 37: Mass flow of the activation plant.

Stream	Value [t h ⁻¹]
<i>Input char</i>	2.9
<i>Activated carbon</i>	1.8
<i>Reaction gas</i>	2.5
<i>Steam for activation</i>	2.7
<i>Combustion air</i>	14.3
<i>Flue gas</i>	26.6
<i>Flue gas to pre-dryer</i>	18.2
<i>Flue gas in activator</i>	8.4

Figure 102 shows a scheme of the whole integration with mass flow data.

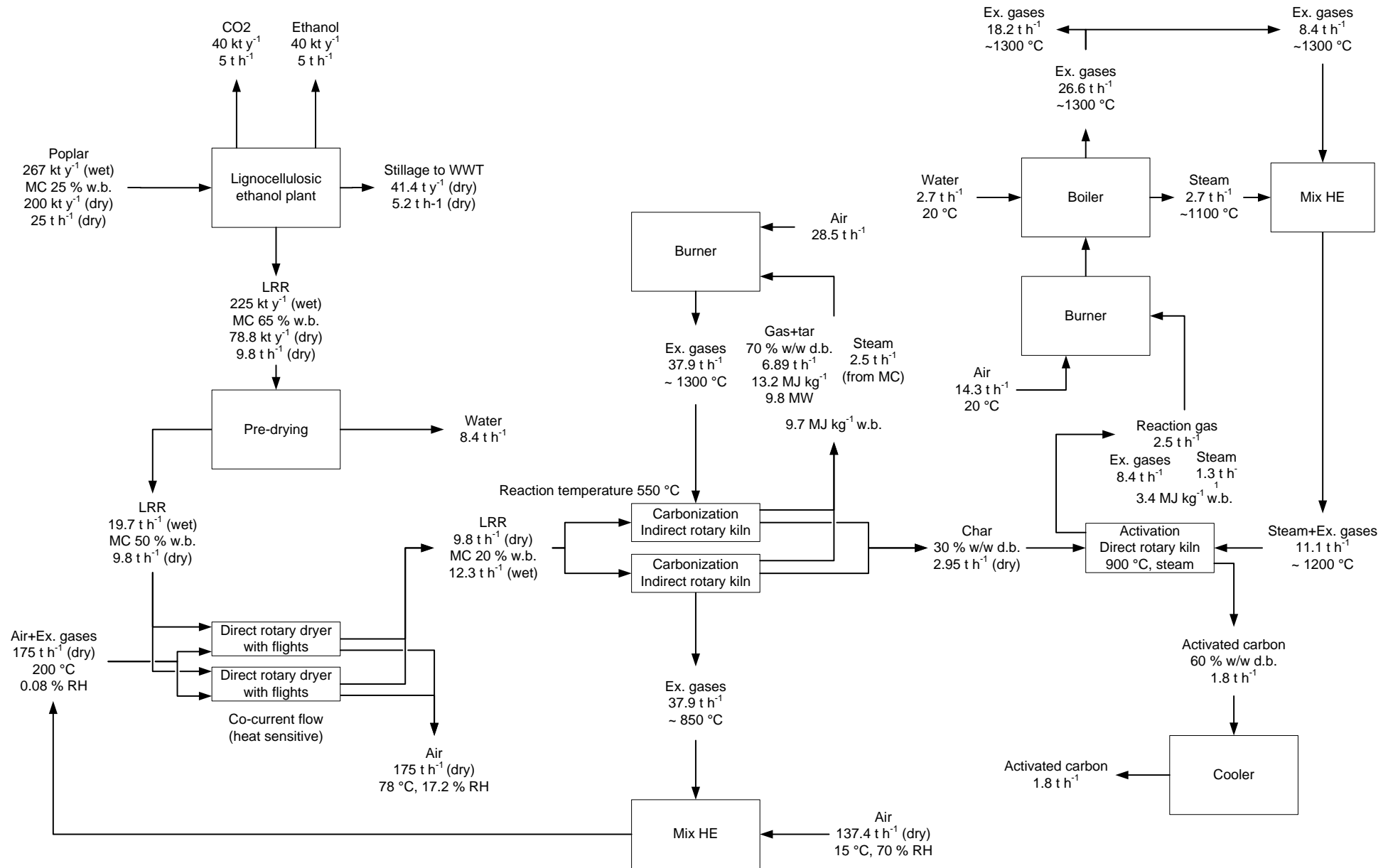


Figure 102: Scheme of the whole process integration with SP with additional data.

Results from the preliminary design of the rotary dryer/kilns

This section reports the assumptions that were taken for the evaluation of the previously shown mass balance and the results of the preliminary design of the rotary dryer/kilns. These results do not claim to be definitive, but just an insight on equipment dimensions on demo-scale, being used in this investigation only empirical correlations and not experimental proofs with LRR. The design of rotary dryer/kilns is indeed very complex and only on the basis of pilot-plant tests trustful results can be obtained [182]. Here is reported a design based on heat transfer, as this is the common practice [182].

Table 38 reports the data assumed for the evaluation of the rotary dryer.

Table 38: Assumed data taken for the rotary dryer evaluation.

Parameter	u.m.	Value	Ref.
LRR specific heat	kJ (kg K)^{-1}	1.2	[184]
Ambient air temperature	$^{\circ}\text{C}$	15	-
Ambient air relative humidity	-	70 %	-
Inlet hot gas temperature	$^{\circ}\text{C}$	200	-
Gas mass velocity	$\text{kg s}^{-1} \text{m}^{-2}$	1.6	[162,182]
Number of transfer units	-	1.5	[162,182]
Heat loss	-	10 %	[183]
Solids particle diameter	mm	1	

Because the LRR is particularly sensitive to heat due to its high lignin content, the drying gas inlet temperature should be kept at least below lignin glass transition temperature. Glass transition temperature of lignin can vary between different kinds of lignin samples, being affected by the lignin extraction method and by the composition of the original lignocellulosic feedstock; however its value ranges between 120 and 165 $^{\circ}\text{C}$ [184–189]. In rotary dryers, in general, the drying gas has an inlet temperature from 120 to 800 $^{\circ}\text{C}$, depending on the heating gas and on the nature of the material to be dried [162]. For the present case, an inlet temperature of 200 $^{\circ}\text{C}$ was chosen with a co-current configuration: in this way, even if gas temperature is higher than the lignin glass transition value, the initial sudden water evaporation cools the gas to an acceptable temperature.

Another important parameter that was assumed is the so-called gas mass velocity, G , involved in Eq. 9 for the evaluation of the global volumetric heat transfer coefficient, representing the gas flow rate per unit of dryer cross section area. Its value ranges between 400 and 5000 $\text{lb h}^{-1} \text{ft}^{-2}$ ($0.5 - 5 \text{ kg s}^{-1} \text{m}^{-2}$) [162,182]; in general, higher G values are preferred, but dusting and entrainment of the material limits this parameter [162,182]. It was assumed a value of 1200 $\text{lb h}^{-1} \text{ft}^{-2}$, corresponding to $1.6 \text{ kg s}^{-1} \text{m}^{-2}$, which can be considered an acceptable value for particles of 0.5 mm [182]; in the present evaluation, the diameter of particles was assumed 1 mm. The amount of dusting occurring during drying is a complex function of the material being dried, its physical state, the gas flow rate, the holdup in the dryer, the number of flights, the rate of rotation, and the constructive characteristics of the dryer itself; therefore this parameter can be predicted accurately only by experimental tests [182]. Eq. 9 represents the main recommended correlation adopted for the design of dryers manufactured in the United States [162,182].

$$Q = UaV\Delta T_{ml} = \frac{0.5G^{0.67}}{D}V\Delta T_{ml} = 0.125\pi DLG^{0.67}\Delta T_{ml} \quad \text{Eq. 9}$$

Where Q is the total heat transferred, D and L are respectively the diameter and the length of the dryer, G is the gas mass velocity and ΔT_{ml} the log mean of the drying-gas wet-bulb depression at the inlet end and exit end of the dryer.

The outlet gas temperature was evaluated by considering the number of transfer units, defined by Eq. 10 [162,182]:

$$N_t = \frac{\text{Inlet gas temperature} - \text{Outlet gas temperature}}{\Delta T_{ml}} \quad \text{Eq. 10}$$

Rotary dryers are most economically operate when N_t is between 1.5 and 2.5 [162,182]; a value of 1.5 was chosen. Steam and air properties were taken from EES software.

The diameter and the length of the two dryers resulted 4.5 and 32 m respectively, for a L/D value of 7.1. This value fits in the range which is commonly adopted for industrial dryers (from 2 to 20 [183], better from 4 and 10 [182]).

These big dimensions are not surprising: as reported by Boateng in his book on rotary kilns [33], kilns fed with slurry materials can reach length on the order of 150 - 180 m. In the cement industry these kilns are often not efficient, being replaced by long dry kilns (fed with dry material), but in certain applications, like in the pulp and paper or in the food industry they are necessary. In addition, in Perry's Chemical engineering handbook [182] it is reported that: "The first rotary kilns used in the United States were very small, 2 by 20 m. Sizes gradually increased and seemed to stop for a period at a maximum size of 4 by 150 m. A few much larger units have been installed for cement production". A triple-pass dryer would reduce the size of the unit, but its modeling and design are out of the scope of this thesis.

Table 39 reports the assumption adopted for the two pyrolyzers.

Table 39: Assumed data taken for the rotary kiln pyrolyzer evaluation.

Parameter	u.m.	Value	Ref.
Char yield	% w/w (d.b)	30	Exp. campaign
Non-condensable gas yield	% w/w (d.b)	20	[190]
Tar yield	% w/w (d.b)	35	[190]
Reaction water	% w/w (d.b)	15	[190]
Pyrolysis temperature	°C	550	-
Dried LRR inlet temperature	°C	30	-
LRR density	kg m ⁻³	500	Exp. campaign
Char density	kg m ⁻³	150	Exp. campaign
Kiln loading	-	15 %	[33,182]
Solids mean residence time	min	90	-
Ambient air temperature for combustion	°C	20	-
Solids particle diameter	mm	1	-
Pyrogas combustion efficiency	-	90 %	-
Kiln thickness	cm	15	-
Material angle in the kiln	°	48.5	-
Kiln longitudinal slope	°	1	[33]
Heat loss	-	50 %	[182]

The correlations for the material's axial motion and heat transfer reported in [33,191–193] were used for the determination of the approximate dimensions of the two pyrolyzers. The problem was constrained by the maintaining of the rolling regime ($Fr < 0.01$), while keeping an acceptable rotational speed (< 5 rpm). The

composition of pyrogas was scaled from the experiments of Fassinou et al. [194]; the specific heat of tar in vapor phase was approximated to that of methane. The value for heat loss was taken from [182], as for indirectly heated kiln the thermal efficiency is between 30 - 65 %. The air stoichiometric ratio for pyrogas combustion and pyrogas heating value were evaluated by considering pyrogas composition. The thermo-physical properties of the various chemical species in the pyrogas, as well as air and water properties, were taken from EES.

The diameter and the length of the two pyrolyzers resulted 4 and 54 m, respectively.

Table 40 reports the assumption adopted for the activator.

Table 40: Assumed data taken for the rotary kiln activator evaluation.

Parameter	u.m.	Value	Ref.
<i>Char carbon content</i>	% w/w (d.b)	75	<i>Exp. campaign</i>
<i>Activated carbon yield</i>	% w/w (d.b)	60	<i>Exp. campaign</i>
<i>Off-gas yield</i>	% w/w (d.b)	40	<i>By difference</i>
<i>Activating steam excess</i>	-	100 %	[195]
<i>Activation temperature</i>	°C	900	-
<i>Inlet char temperature</i>	°C	20	-
<i>Gas mass velocity</i>	kg s ⁻¹ m ⁻²	0.5	[162,182]
<i>Ambient air temperature for combustion</i>	°C	20	-
<i>Excess air for off-gas combustion</i>	-	30 %	[196]
<i>Ambient water temperature</i>	°C	20	-
<i>Minimum flue gas temperature</i>	°C	120	-
<i>Heat loss</i>	-	15 %	[182]

The activation reactor is internally heated by a countercurrent steam and flue gas flow. The inlet char temperature was conservatively considered as if cooled after the carbonization. From the experimental campaign resulted an activated carbon yield of approximately 80 % w/w (d.b.), but, in that case carbon dioxide was used as activating agent and reaction temperature was only 700 °C. In this case a yield of 60 % w/w (d.b.) was assumed because of the higher activation temperature and because steam is generally more active than CO₂ [28].

The main reaction involved in steam physical activation is the one reported in Eq. 11:



Many other reactions take place during activation, but, when steam is supplied in excess with respect to the stoichiometric value, it is acceptable to consider only the reaction reported in Eq. 11 [197]. Benson, Zaman and Olson [195] reported an optimal value of excess steam in North Dakota lignite activation of 73 %. In the present study this value was adjusted to 100 %, taking in consideration also heat transfer requirements, by ensuring the selected gas mass velocity G. This latter parameter determines the heat transfer coefficient by means of Eq. 12 [182]:

$$U = 23.7G^{0.67} \quad \text{Eq. 12}$$

This equation is different from Eq. 9, because it is specifically recommended for rotary kilns without flights with a separated combustion chamber, as in this case. Moreover it will yield a conservative design because it does not account for radiation [182].

Char specific heat at mean activation temperature was evaluated from Antal and Grønli [29]. The thermo-physical properties of the chemical species in the off-gas, as well as air and water properties, were taken from EES.

The diameter and the length of the kiln activator resulted 2.8 and 18 m respectively.

6.2.3 AC expected incomes

The current LRR management is co-combustion for heat and power production, but the activated carbon industry represents, indeed, a bigger opportunity for obtaining additional incomes to ethanol selling.

The selling price of activated carbons widely varies depending on its specific characteristics and can range from 1.0 k\$ t⁻¹ - 5.0 k\$ t⁻¹ up to 20 k\$ t⁻¹ for special applications [198]. By considering the lowest selling price, the annual incomes from the AC production for the SP and the HTC scenario were evaluated and reported in Table 41.

Table 41: Annual income from AC selling for the SP and HTC scenario.

Case	AC production [kt y ⁻¹]	Total income [M\$ y ⁻¹]
<i>Slow pyrolysis</i>	14.2	14.2
<i>Hydrothermal carbonization</i>	16.7	16.7

7. Conclusion

Anaerobic digestion digestate from a real farm plant was characterized and successfully converted via slow pyrolysis and hydrothermal carbonization and the produced char, together with the HTC aqueous phase, was analyzed in laboratory for comprehensive characterization. In particular, HTC experiments at different reaction conditions were carried out in a dedicated test bench, which was designed and built for this study. The findings from the experimental campaign on digestate followed literature results: higher yields are obtained with HTC, but at the expense of a lower carbon content. Hundreds of organic compounds were found in the HTC aqueous phase and their number and concentration increased with the HTC reaction severity; the most abundant one was acetic acid, but increasing amounts of oxygenated aromatics like phenol, guaiacol and syringol, as well as cyclic ketones and vanillin, were also found. Most of the char properties fit in the range proposed by European and International standards for biochar as well as by Italian law for fertilizers.

Lignin-rich residue from a demo lignocellulosic ethanol plant was characterized and successfully converted into char by slow pyrolysis and hydrothermal carbonization. LRR and the so-produced chars were chemically (with KOH) and physically (with CO₂) activated and the morphological properties of the obtained activated carbons were characterized and compared. An activation reactor and a ceramic tubular furnace were respectively built and adapted for these experiments. To the best of the author's knowledge, it was the first time that this feedstock was converted via slow pyrolysis and HTC and used for activated carbon production. The physical and the chemical activation processes gave very similar results: microporous AC were created and the maximum value of BET area was 630 m² g⁻¹. The physically activated carbons had a better-developed microporosity than the ones produced with KOH. The results from the experimental campaign differ from literature experiences: by increasing the HTC reaction severity, the quality of the resulting AC decreases, both for the chemical and the physical activation process. The HTC aqueous phase was analyzed: dissolved organics concentration increased with reaction severity and the most abundant compounds were carboxylic acids (lactic and acetic).

In the last chapter, a process integration between the investigated thermochemical technologies (slow pyrolysis, hydrothermal carbonization and activation) and the 1 MW anaerobic digestion plant or demo-scale lignocellulosic ethanol plant was proposed together with preliminary reactor design and economic analysis. By considering the anaerobic digestion case, the highest global efficiency was obtained with hydrothermal carbonization (55 %), while the best profitability index was achieved by integration with autothermal fixed bed slow pyrolysis (0.76). A detailed heat flow matching with the CHP of the anaerobic digestion plant was carried out for the integration with HTC. In the LRR case, rotary dryer and rotary kilns for slow pyrolysis and activation were considered and preliminarily sized.

8. Appendix

8.1 MRTB technical drawings

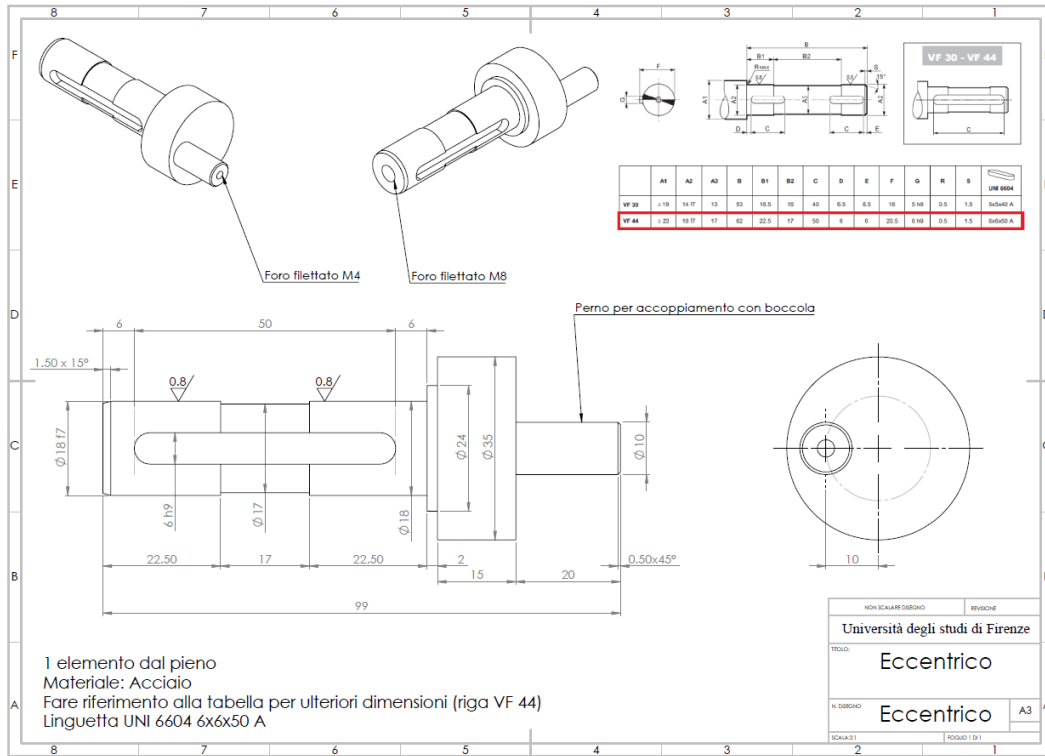


Figure 103: Pivot technical drawing.

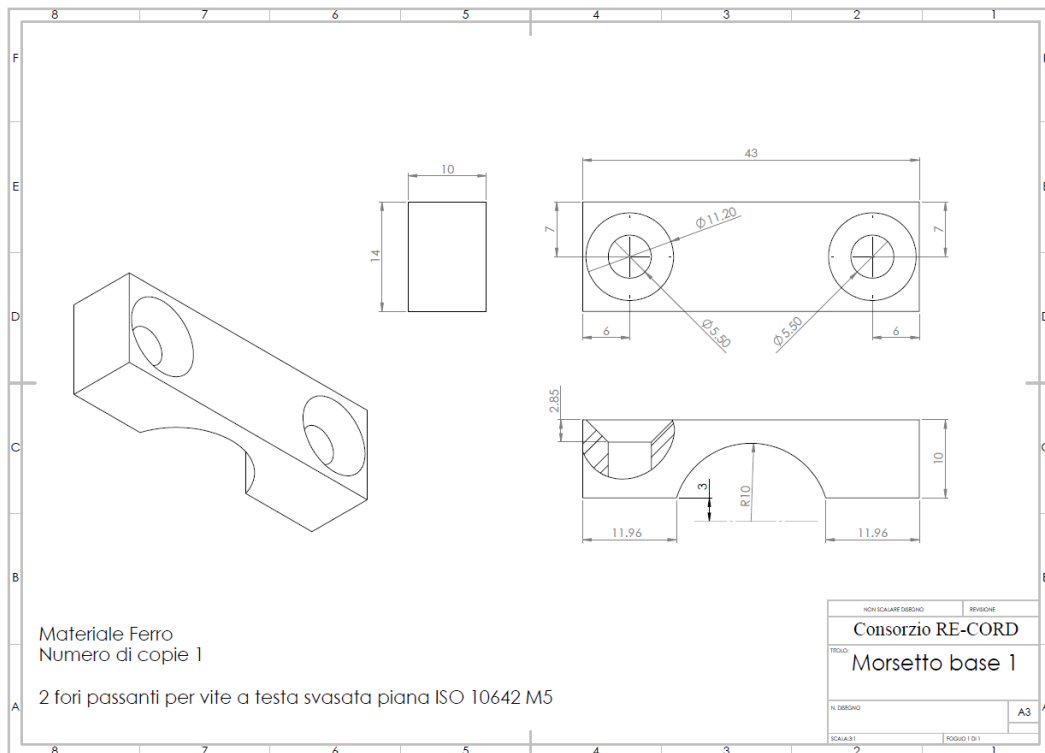


Figure 104: Clamp 1 technical drawing.

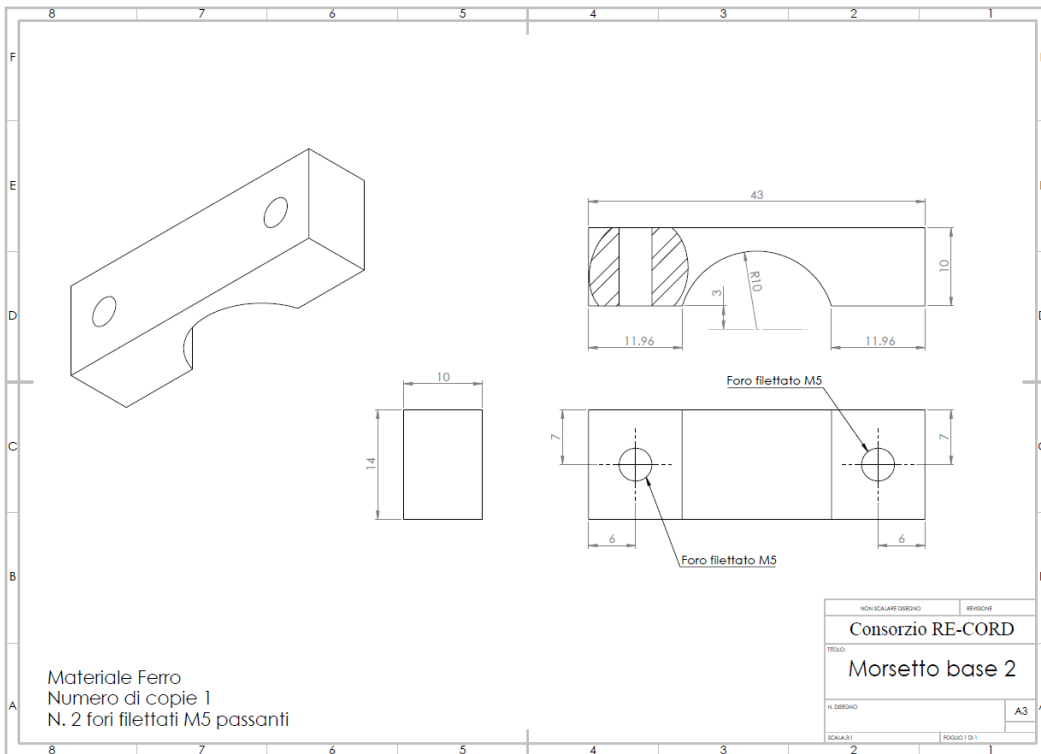


Figure 105: Clamp 2 technical drawing.

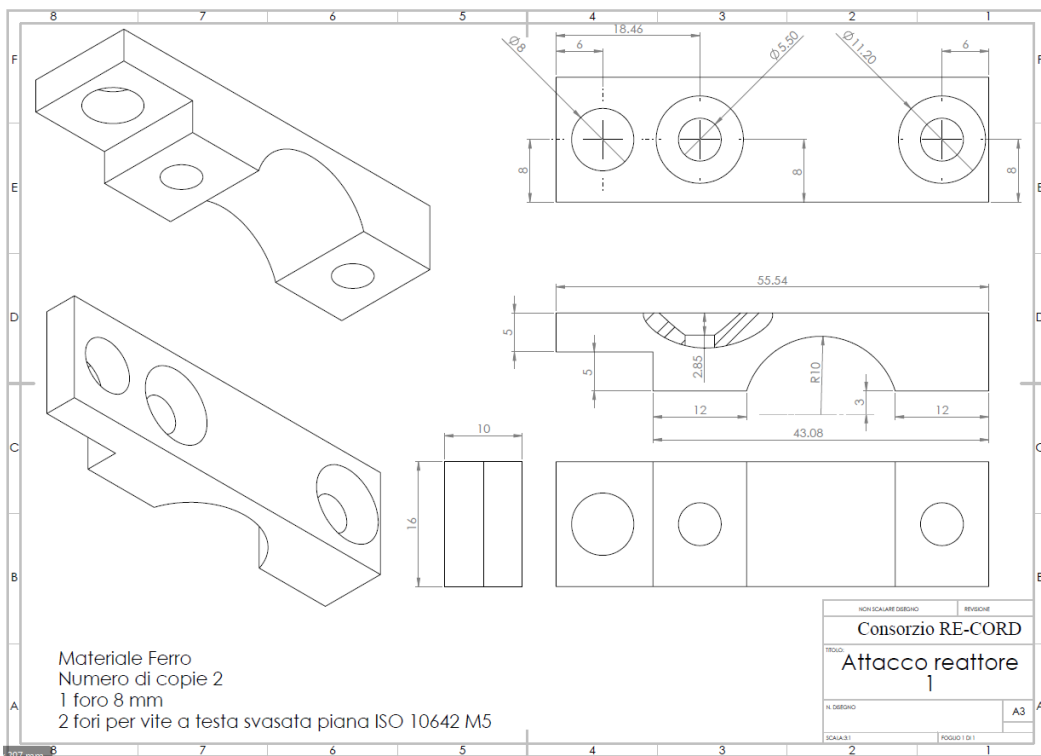


Figure 106: Clamp 3 technical drawing.

8.2 HTC of AD digestate

Table 42: List of compounds that were identified in the aqueous phase from HTC of AD digestate.

Compound name	CAS number	Compound class 1	Compound subclass 1	Compound subclass 2
<i>Isovaleraldehyde</i>	590-86-3	<i>Aldehyde</i>		
<i>1,2,4-Trimethoxybenzene</i>	135-77-3	<i>Aromatic</i>	<i>Oxygenated aromatic</i>	
<i>2,4-Dimethylfuran</i>	3710-43-8	<i>Aromatic</i>	<i>Oxygenated aromatic</i>	<i>Furan</i>
<i>2,5-Dimethoxy-4-methylbenzaldehyde</i>	4925-88-6	<i>Aromatic</i>	<i>Oxygenated aromatic</i>	
<i>2-Methylpyrazine</i>	109-08-0	<i>Aromatic</i>		<i>Heterocyclic Aromatic</i>
<i>2-Phenylpropanal</i>	93-53-8	<i>Aromatic</i>	<i>Oxygenated aromatic</i>	<i>Aromatics Aldehyde</i>
<i>3,4-Dimethoxyphenylacetone</i>	776-99-8	<i>Aromatic</i>	<i>Oxygenated aromatic</i>	<i>Aromatics Ketone</i>
<i>3-Methoxycatechol</i>	934-00-9	<i>Aromatic</i>	<i>Oxygenated aromatic</i>	<i>Phenol</i>
<i>4-Ethylguaiacol</i>	2785-89-9	<i>Aromatic</i>	<i>Oxygenated aromatic</i>	<i>Guaiacol</i>
<i>4-Propylguaiacol</i>	2785-87-7	<i>Aromatic</i>	<i>Oxygenated aromatic</i>	<i>Guaiacol</i>
<i>5-(Hydroxymethyl)furfural</i>	67-47-0	<i>Aromatic</i>	<i>Oxygenated aromatic</i>	<i>Furan</i>
<i>5-tert-Butylpyrogallol</i>	20481-17-8	<i>Aromatic</i>	<i>Oxygenated aromatic</i>	<i>Phenol</i>
<i>Acetosyringone</i>	2478-38-8	<i>Aromatic</i>	<i>Oxygenated aromatic</i>	<i>Aromatics Ketone</i>
<i>Acetovanillone</i>	498-02-2	<i>Aromatic</i>	<i>Oxygenated aromatic</i>	<i>Aromatics Ketone</i>
<i>Desaspidinol</i>	<i>n.a.</i>	<i>Aromatic</i>	<i>Oxygenated aromatic</i>	<i>Aromatics Ketone</i>
<i>Dihydromethyleugenol</i>	69780-73-0	<i>Aromatic</i>	<i>Oxygenated aromatic</i>	
<i>Eugenol</i>	97-53-0	<i>Aromatic</i>	<i>Oxygenated aromatic</i>	<i>Phenylpropanoid</i>
<i>Furfural</i>	98-01-1	<i>Aromatic</i>	<i>Oxygenated aromatic</i>	<i>Furan</i>
<i>Guaiacol</i>	90-05-1	<i>Aromatic</i>	<i>Oxygenated aromatic</i>	<i>Guaiacol</i>
<i>Isoeugenol</i>	97-54-1	<i>Aromatic</i>	<i>Oxygenated aromatic</i>	<i>Guaiacol</i>
<i>Methoxyeugenol</i>	6627-88-9	<i>Aromatic</i>	<i>Oxygenated aromatic</i>	<i>Syringol</i>
<i>m-Ethylphenol</i>	620-17-7	<i>Aromatic</i>	<i>Oxygenated aromatic</i>	<i>Phenol</i>
<i>o-Cresol</i>	95-48-7	<i>Aromatic</i>	<i>Oxygenated aromatic</i>	<i>Phenol</i>
<i>o-Ethylphenol</i>	90-00-6	<i>Aromatic</i>	<i>Oxygenated aromatic</i>	<i>Phenol</i>
<i>o-Xylenol</i>	526-75-0	<i>Aromatic</i>	<i>Oxygenated aromatic</i>	<i>Phenol</i>
<i>Phenol</i>	108-95-2	<i>Aromatic</i>	<i>Oxygenated aromatic</i>	<i>Phenol</i>
<i>p-Creosol</i>	93-51-6	<i>Aromatic</i>	<i>Oxygenated aromatic</i>	<i>Phenol</i>
<i>p-Vinylguaiacol</i>	7786-61-0	<i>Aromatic</i>	<i>Oxygenated aromatic</i>	<i>Guaiacol</i>
<i>Pyridine</i>	110-86-1	<i>Aromatic</i>		<i>Heterocyclic Aromatic</i>
<i>Pyrimidine</i>	289-95-2	<i>Aromatic</i>		<i>Heterocyclic Aromatic</i>
<i>Styrene</i>	100-42-5	<i>Aromatic</i>		
<i>Syngaldehyde</i>	134-96-3	<i>Aromatic</i>	<i>Oxygenated aromatic</i>	<i>Aromatics Aldehyde</i>
<i>Syringol</i>	91-10-1	<i>Aromatic</i>	<i>Oxygenated aromatic</i>	<i>Syringol</i>
<i>Toluene</i>	108-88-3	<i>Aromatic</i>		
<i>trans-m-Propenyl guaiacol</i>	19784-98-6	<i>Aromatic</i>	<i>Oxygenated aromatic</i>	<i>Guaiacol</i>
<i>Vanillin</i>	121-33-5	<i>Aromatic</i>	<i>Oxygenated aromatic</i>	<i>Aromatics Aldehyde</i>
<i>Vanillyl methyl ketone</i>	2503-46-0	<i>Aromatic</i>	<i>Oxygenated aromatic</i>	<i>Aromatics Ketone</i>
<i>Acetic acid</i>	64-19-7	<i>Organic acid</i>	<i>Carboxylic acid</i>	
<i>1-Hydroxy-2-butanone</i>	5077-67-8	<i>Ketone</i>		<i>Alpha Ketoaldehyde</i>

<i>1-Methyl-1-cyclopenten-3-one</i>	<i>2758-18-1</i>	<i>Ketone</i>	<i>Cyclic ketone</i>
<i>2-Cyclopenten-1-one, 2-hydroxy-3-propyl</i>	<i>25684-04-2</i>	<i>Ketone</i>	<i>Cyclic ketone</i>
<i>2-Methyl-2-cyclopentenone</i>	<i>1120-73-6</i>	<i>Ketone</i>	<i>Cyclic ketone</i>
<i>3-Ethyl-2-hydroxy-2-cyclopenten-1-one</i>	<i>21835-01-8</i>	<i>Ketone</i>	<i>Cyclic ketone</i>
<i>3-Ethyl-2-hydroxy-2-cyclopenten-1-one</i>	<i>21835-01-8</i>	<i>Ketone</i>	<i>Cyclic ketone</i>
<i>3-Methyl-1,2-cyclopentanedione</i>	<i>765-70-8</i>	<i>Ketone</i>	<i>Cyclic ketone</i>
<i>3-Methyl-2-cyclopenten-1-one</i>	<i>2758-18-1</i>	<i>Ketone</i>	<i>Cyclic ketone</i>
<i>Acetoin</i>	<i>513-86-0</i>	<i>Ketone</i>	
<i>Acetonyl acetone</i>	<i>110-13-4</i>	<i>Ketone</i>	
<i>Cyclopentanone</i>	<i>120-92-3</i>	<i>Ketone</i>	<i>Cyclic ketone</i>
<i>2-Acetylcyclopentanone</i>	<i>60415-94-3</i>		
<i>2-Hydroxy-3-butanone</i>	<i>52217-02-4</i>	<i>Ketone</i>	

n.a.: not available

8.3 LRR activation

Table 43: Detailed results from the preliminary physical activation of LRR.

Parameter	Feedstock	Pyrochar	PAC 700 °C – 2 h	PAC 800 °C – 2 h
BET surface [$m^2 g^{-1}$]	3.00	370.40	600.36	1078.17
Micropore area [$m^2 g^{-1}$]	< 0	308.91	525.06	948.59
External surface area [$m^2 g^{-1}$]	< 0	61.49	67.75	131.72
Micropore volume [$cm^3 g^{-1}$]	< 0	0.14	0.21	0.39
Total pore volume [$cm^3 g^{-1}$]	0.01	0.19	0.28	0.54
DFT surface area [$m^2 g^{-1}$]	2.37	334.61	567.78	1074.10
DFT pore volume [$cm^3 g^{-1}$]	0.01	0.18	0.25	0.49
DFT avg. Pore width [nm]	50.23	1.61	1.10	1.14
Avg. Pore diameter [nm]	17.27	2.06	1.84	2.00
Micropore area (%)	Null	83	87	88
Micropore volume (%)	Null	71	77	72

Table 44: Detailed results from the preliminary chemical activation of LRR.

Parameter	Feedstock	CAC 600 °C – 1:1	CAC 600 °C – 2:1	CAC 700 °C -1:1	CAC 700 °C – 2:1	CAC 800 °C 1:1	CAC 800 °C 2:1
BET surface [$m^2 g^{-1}$]	3.00	675.34	988.58	1436.73	1187.79	1484.42	557.97
Micropore area [$m^2 g^{-1}$]	< 0	622.74	806.96	1233.78	861.14	793.30	243.76
External surface area [$m^2 g^{-1}$]	< 0	45.77	173.60	188.01	319.02	691.12	314.20
Micropore volume [$cm^3 g^{-1}$]	< 0	0.24	0.34	0.55	0.39	0.35	0.11
Total pore volume [$cm^3 g^{-1}$]	0.01	0.31	0.61	0.73	0.75	1.39	1.02
DFT surface area [$m^2 g^{-1}$]	2.37	766.87	979.03	1348.26	1065.67	1328.23	490.14
DFT pore volume [$cm^3 g^{-1}$]	0.01	0.27	0.52	0.66	0.65	1.19	0.76
DFT avg. Pore width [nm]	50.23	0.97	1.01	1.05	1.10	1.01	1.01
Avg. Pore diameter [nm]	17.27	1.82	2.47	2.03	2.52	3.73	7.29
Micropore area (%)	Null	92	82	86	72	53	44
Micropore volume (%)	Null	79	56	75	52	25	10

Table 45: Detailed results from the physical and chemical activation of LRR-hydrochar.

Parameter	PAC	PAC	PAC	PAC	PAC	CAC	CAC	CAC	CAC	CAC
	700 °C-2 h	200 °C-2 h	200 °C-4 h	270 °C-2 h	270 °C-4 h	600 °C-1:1	200 °C-2 h	200 °C-4 h	270 °C-2 h	270 °C-4 h
<i>BET surface [m² g⁻¹]</i>	600.36	630.56	540.25	161.33	77.27	675.34	501.58	599.86	229.56	81.02
<i>Micropore area [m² g⁻¹]</i>	525.06	596.81	523.94	139.16	57.95	622.74	451.71	541.30	185.03	49.45
<i>External surface area [m² g⁻¹]</i>	67.75	36.38	29.21	22.17	19.32	45.77	49.87	58.56	44.53	31.58
<i>Micropore volume [cm³ g⁻¹]</i>	0.21	0.23	0.20	0.06	0.03	0.24	0.18	0.22	0.08	0.02
<i>Total pore volume [cm³ g⁻¹]</i>	0.28	0.27	0.23	0.08	0.05	0.31	0.27	0.32	0.22	0.08
<i>DFT surface area [m² g⁻¹]</i>	567.78	713.61	650.10	144.60	54.00	766.87	581.39	672.25	275.83	72.64
<i>DFT pore volume [cm³ g⁻¹]</i>	0.25	0.25	0.21	0.08	0.04	0.27	0.23	0.27	0.19	0.07
<i>DFT avg. Pore width [nm]</i>	1.10	1.05	5.19	1.61	1.30	0.97	5.19	1.01	1.73	2.05
<i>Avg. Pore diameter [nm]</i>	1.84	1.72	1.72	2.11	2.42	1.82	2.18	2.15	3.89	3.83
<i>Micropore area (%)</i>	0.87	0.95	0.97	0.86	0.75	92	0.90	0.90	0.81	0.61
<i>Micropore volume (%)</i>	0.77	0.85	0.87	0.73	0.60	79	0.66	0.67	0.34	0.30

8.4 Assessment of digestate compacting (briquetting)

In order to feed a fixed bed pyrolysis reactor, the feedstock needs to be compacted in uniform pieces and, to assess the feasibility of digestate compacting, a test was made with RE-CORD milling and briquetting machines. Due to the high amount of required biomass, the sample used in this test was different from the one used in the thermochemical experiments, being produced in another AD plant, but still representative. After the digestate was dried and milled, it was put into the briquetting machine, whose extruder temperature was set to 250 °C, in order to soften the material and facilitating the process. Higher temperatures have to be avoided for limiting biomass degradation. Once the digestate was extruded, the so-obtained cylinder was broken in briquettes by a specific obstacle, as can be seen in Figure 107.



Figure 107: Dried digestate extrusion during briquetting.

The produced briquettes had an outer diameter of about 50 mm and an average length, which can be varied by moving the cutting-obstacle, approximately of 250 mm. By assuming their shape as a perfect hollow cylinder, their density was about 1100 kg m⁻³; their bulk density was approximately 770 kg m⁻³. The briquettes had some cracks on their surface (Figure 108), but they were robust and, considering the heterogeneity of the material, the results were satisfactory: digestate can be briquetted and so fed to a fixed bed pyrolysis reactor.



Figure 108: Briquettes produced from digestate.

8.5 Proposed P&ID for a pilot rotary plant for physical activation

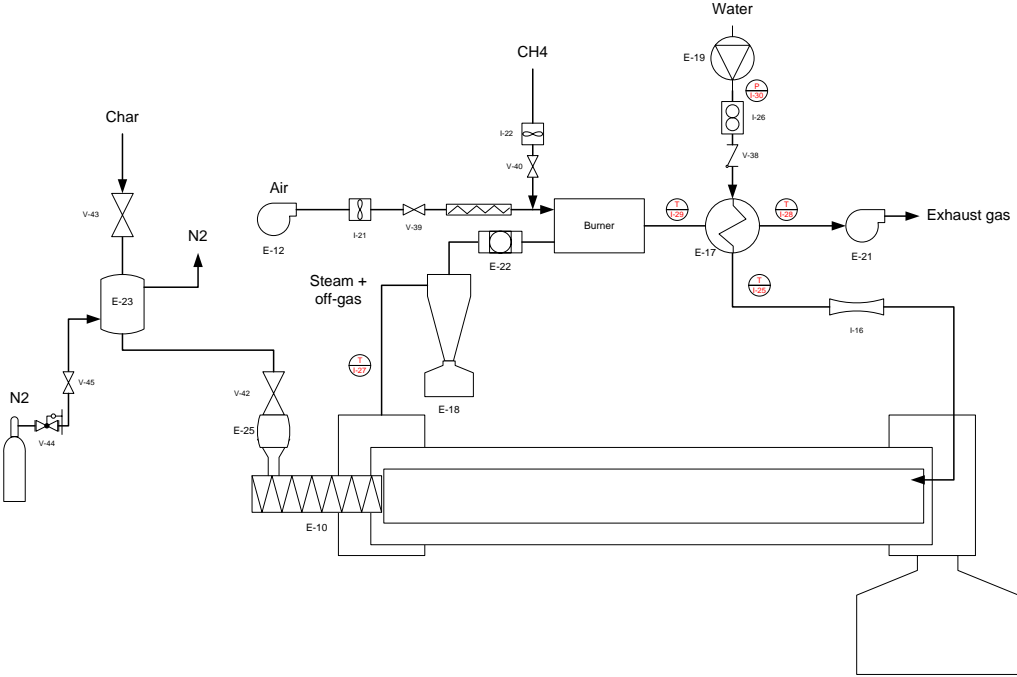


Figure 109: P&ID of a physical activation pilot unit.

9. References

- [1] L.R. Lynd, The grand challenge of cellulosic biofuels, *Nat. Biotechnol.* 35 (2017) 912–915. doi:10.1038/nbt.3976.
- [2] European Biogas Association, EBA Statistical Report 2017, (2017). <http://european-biogas.eu/2017/12/14/eba-statistical-report-2017-published-soon/>.
- [3] Z. Yu, M. Morrison, F.L. Schanbacher, Production and Utilization of Methane Biogas as Renewable Fuel, in: A.A. Vertès, N. Qureshi, H.P. Blashek, H. Yukama (Eds.), *Biomass to Biofuels Strateg. Glob. Ind.*, John Wiley & Sons, Ltd, Oxford, UK, 2010: pp. 403–433. doi:10.1002/9780470750025.ch20.
- [4] S.K. Khanal, Overview of anaerobic technology, in: S.K. Khanal, C.S. Jones (Eds.), *Anaerob. Biotechnol. Bioenergy Prod. Princ. Appl.*, Wiley-Blackwell, 2008: pp. 1–32. http://samples.sainsburysebooks.co.uk/9780813804569_sample_416019.pdf.
- [5] European Commission, State of play on the sustainability of solid and gaseous biomass used for electricity, heating and cooling in the EU, Brussels, 2014. http://ec.europa.eu/energy/sites/ener/files/2014_biomass_state_of_play_.pdf.
- [6] City Life Magazine - Energia Media Srl, Trasformare gli scarti in biometano, (2014). <http://www.citylifemagazine.net/bup-trasforma-gli-scatti-in-biometano/>.
- [7] ARPAT - Agenzia regionale per la protezione ambientale della Toscana, Utilizzo agronomico del digestato, ARPAT News. (2015). <http://www.arpat.toscana.it/notizie/arpatnews/2015/213-15/213-15-utilizzo-agronomico-del-digestato> (accessed January 25, 2017).
- [8] S. Lee, J.G. Speight, S.K. Loyalka, *Handbook of Alternative Fuel Technologies*, CRC Press, Taylor & Francis Group, LLC, Boca Raton, FL, 2007. doi:10.1201/9781420014518.
- [9] A. Aden, M. Ruth, K. Ibsen, J. Jechura, K. Neeves, J. Sheehan, B. Wallace, L. Montague, A. Slayton, J. Lukas, *Lignocellulosic Biomass to Ethanol Process Design and Economics Utilizing Co-Current Dilute Acid Prehydrolysis and Enzymatic Hydrolysis for Corn Stover*, Golden, Colorado, 2002. <https://www.nrel.gov/docs/fy02osti/32438.pdf>.
- [10] M. Marmiroli, U. Bonas, D. Imperiale, G. Lencioni, F. Mussi, N. Marmiroli, E. Maestri, Structural and Functional Features of Chars From Different Biomasses as Potential Plant Amendments, *Front. Plant Sci.* 9 (2018) 1–13. doi:10.3389/fpls.2018.01119.
- [11] F. Verheijen, S. Jeffery, a C. Bastos, M. Van Der Velde, I. Diafas, Biochar application to soils: a critical review of effects on soil properties, processes and functions, 2010. doi:10.2788/472.
- [12] J. Lehmann, S. Joseph, Biochar for environmental management : An introduction, in: *Biochar Environ. Manag. - Sci. Technol.*, 2nd ed., Routledge, 2012: pp. 1–12. doi:10.1016/j.forpol.2009.07.001.
- [13] S.P. Sohi, E. Krull, E. Lopez-Capel, R. Bol, A Review of Biochar and Its Use and Function in Soil, *Adv. Agron.* 105 (2010) 47–82. doi:10.1016/S0065-2113(10)05002-9.
- [14] N. Papaioannou, Biomass derived carbon dots using hydrothermal carbonisation, in: *1st Int. Symposium Hydrothermal Carbonization*, Queen Mary University, London, 2017.
- [15] A. Jain, R. Balasubramanian, M.P. Srinivasan, Hydrothermal conversion of biomass waste to activated carbon with high porosity: A review, *Chem. Eng. J.* 283 (2016) 789–805. doi:10.1016/j.cej.2015.08.014.
- [16] C.R. Correa, M. Bernardo, R.P.P.L. Ribeiro, I.A.A.C. Esteves, A. Kruse, Evaluation of Hydrothermal

Carbonization as a Preliminary Step for the Production of Functional Materials from Biogas Digestate, *J. Anal. Appl. Pyrolysis*. 124 (2017) 461–474. doi:10.1016/j.jaap.2017.02.014.

- [17] C. Rodríguez Correa, M. Stollovsky, T. Hehr, Y. Rauscher, B. Rolli, A. Kruse, Influence of the Carbonization Process on Activated Carbon Properties from Lignin and Lignin-Rich Biomasses, *ACS Sustain. Chem. Eng.* 5 (2017) 8222–8233. doi:10.1021/acssuschemeng.7b01895.
- [18] K. Mochidzuki, N. Sato, A. Sakoda, Production and characterization of carbonaceous adsorbents from biomass wastes by aqueous phase carbonization, *Adsorption*. 11 (2005) 669–673. doi:10.1007/s10450-005-6004-6.
- [19] C. Purnomo, D. Castello, L. Fiori, Granular Activated Carbon from Grape Seeds Hydrothermal Char, *Appl. Sci.* 8 (2018) 331. doi:10.3390/app8030331.
- [20] M. Puccini, E. Stefanelli, M. Hiltz, M. Seggiani, Activated Carbon from Hydrochar Produced by Hydrothermal Carbonization of Wastes, *Chem. Eng. Trans.* 57 (2017) 169–174. doi:10.3303/CET1757029.
- [21] L. Wang, Y. Guo, B. Zou, C. Rong, X. Ma, Y. Qu, Y. Li, Z. Wang, High surface area porous carbons prepared from hydrochars by phosphoric acid activation, *Bioresour. Technol.* 102 (2011) 1947–1950. doi:10.1016/j.biortech.2010.08.100.
- [22] D. Woolf, J.E. Amonette, F.A. Street-Perrott, J. Lehmann, S. Joseph, Sustainable biochar to mitigate global climate change, *Nat. Commun.* 1 (2010) 1–9. doi:10.1038/ncomms1053.
- [23] A. Galieni, F. Stagnari, G. Visioli, N. Marmiroli, S. Specca, G. Angelozzi, S. D'Egidio, M. Pisante, Nitrogen fertilisation of durum wheat: a case study in Mediterranean area during transition to conservation agriculture, *Ital. J. Agron.* 10 (2016) 12. doi:10.4081/ija.2016.662.
- [24] S. Steinbeiss, G. Gleixner, M. Antonietti, Effect of biochar amendment on soil carbon balance and soil microbial activity, *Soil Biol. Biochem.* 41 (2009) 1301–1310. doi:10.1016/j.soilbio.2009.03.016.
- [25] K. Karhu, T. Mattila, I. Bergström, K. Regina, Biochar addition to agricultural soil increased CH₄ uptake and water holding capacity - Results from a short-term pilot field study, *Agric. Ecosyst. Environ.* 140 (2011) 309–313. doi:10.1016/j.agee.2010.12.005.
- [26] G. Visioli, F.D. Conti, C. Menta, M. Bandiera, A. Malcevschi, D.L. Jones, T. Vamerali, Assessing biochar ecotoxicology for soil amendment by root phytotoxicity bioassays, *Environ. Monit. Assess.* 188 (2016) 166. doi:10.1007/s10661-016-5173-y.
- [27] Grand View Research Inc., Activated Carbon Market Size, Share & Trends Analysis Report By Product (Powdered Activated Carbon, Granular Activated Carbon), By Application, By End-use, And Segment Forecasts, 2018 - 2024, (2018). <https://www.grandviewresearch.com/industry-analysis/activated-carbon-market>.
- [28] H. Marsh, F.R. Reinoso, *Activated Carbon*, Elsevier, 2006.
- [29] M.J. Antal, M. Grønli, The Art, Science, and Technology of Charcoal Production, *Ind. Eng. Chem. Res.* 42 (2003) 1619–1640. doi:10.1021/ie0207919.
- [30] F. Ronsse, Commercial biochar production and its certification, *Biochar-Interreg4B.Eu.* (2013) 22. http://www.biochar-interreg4b.eu/images/file/02_Presentation-Frederik-Ronsse.pdf%5Cnpapers2://publication/uuid/0A8C3957-9ACA-4807-A0B7-52DA14D80A89.
- [31] M. Garcia-Perez, T. Lewis, C. Kruger, Methods for Producing Biochar and Advanced Biofuels in Washington State. Part 1: Literature Review of Pyrolysis Reactors. First Project Report., Department of Biological Systems Engineering and the Center for Sustaining Agriculture and Natural Resources,

Washington State University, Pullman, WA, 2010.

- [32] L. Zajec, Slow pyrolysis in a rotary kiln reactor: Optimization and experiment, *Sch. Renew. Energy Sci.* (2009) 1–78. https://www.google.com/url?sa=t&rct=j&q=&esrc=s&source=web&cd=6&cad=rja&uact=8&ved=0ahUKewiysMO4xsfNAhUMK48KHeSuBE8QFghBMAU&url=http://skemman.is/stream/get/1946/7005/17751/1/Luka_Zajec.pdf&usg=AFQjCNFp6QUQSIQFEF_1T0OPWnkkcRxzPQ&sig2=xajnHkV96M7Yuzp wM-0zg.
- [33] A.A. Boateng, *Rotary Kilns*, Butterworth-Heinemann, Boston, 2016.
- [34] S. Kern, M. Halwachs, T. Proll, G. Kampichler, H. Hofbauer, Rotary kiln pyrolysis - First results of a 3 MW pilot plant, in: *18th Eur. Biomass Conf. Exhib.*, Lyon, France, 2010: pp. 3–7. doi:10.5071/18thEUBCE2010-VP2.8.7.
- [35] A.A. Peterson, F. Vogel, R.P. Lachance, M. Fröling, M.J. Antal, Jr., J.W. Tester, Thermochemical biofuel production in hydrothermal media: A review of sub- and supercritical water technologies, *Energy Environ. Sci.* 1 (2008) 32–65. doi:10.1039/b810100k.
- [36] M.M. Titirici, A. Funke, A. Kruse, Hydrothermal Carbonization of Biomass, in: *Recent Adv. Thermo-Chemical Convers. Biomass*, Elsevier, 2015: pp. 325–352. doi:10.1016/B978-0-444-63289-0.00012-0.
- [37] I. Pavlovič, Ž. Knez, M. Škerget, Hydrothermal reactions of agricultural and food processing wastes in sub- and supercritical water: a review of fundamentals, mechanisms, and state of research., *J. Agric. Food Chem.* 61 (2013) 8003–25. doi:10.1021/jf401008a.
- [38] J. a Libra, K.S. Ro, C. Kammann, A. Funke, N.D. Berge, Y. Neubauer, M.M. Titirici, C. Fühner, O. Bens, J. Kern, K.-H. Emmerich, Hydrothermal carbonization of biomass residuals: a comparative review of the chemistry, processes and applications of wet and dry pyrolysis, *Biofuels.* 2 (2011) 71–106. doi:10.4155/bfs.10.81.
- [39] A. Funke, F. Ziegler, Hydrothermal carbonization of biomass: A summary and discussion of chemical mechanisms for process engineering, *Biofuels, Bioprod. Biorefining.* 4 (2010) 160–177. doi:10.1002/bbb.198.
- [40] J. Akhtar, N.A.S. Amin, A review on process conditions for optimum bio-oil yield in hydrothermal liquefaction of biomass, *Renew. Sustain. Energy Rev.* 15 (2011) 1615–1624. doi:10.1016/j.rser.2010.11.054.
- [41] D.L. Barreiro, W. Prins, F. Ronsse, W. Brilman, Hydrothermal liquefaction (HTL) of microalgae for biofuel production : State of the art review and future prospects, *Biomass Bioenergy.* 3 (2012) 15. doi:10.1016/j.biombioe.2012.12.029.
- [42] D.C. Elliott, Hydrothermal Processing, in: R.C. Brown (Ed.), *Thermochem. Process. Biomass Convers. into Fuels*, Chem. Power, John Wiley & Sons, Ltd, Chichester, UK, 2011: pp. 200–231. doi:10.1002/9781119990840.ch7.
- [43] D.C. Elliott, P. Biller, A.B. Ross, A.J. Schmidt, S.B. Jones, Hydrothermal liquefaction of biomass: Developments from batch to continuous process, *Bioresour. Technol.* (2014). doi:10.1016/j.biortech.2014.09.132.
- [44] S.S. Toor, L. Rosendahl, A. Rudolf, Hydrothermal liquefaction of biomass: A review of subcritical water technologies, *Energy.* 36 (2011) 2328–2342. doi:10.1016/j.energy.2011.03.013.
- [45] Y. Matsumura, T. Minowa, B. Potic, S.R.A. Kersten, W. Prins, W.P.M. van Swaaij, B. van de Beld, D.C. Elliott, G.G. Neuenschwander, A. Kruse, Biomass gasification in near- and super-critical water: Status

and prospects, *Biomass Bioenergy*. 29 (2005) 269–292. doi:10.1016/j.biombioe.2005.04.006.

- [46] O. Yakaboylu, J. Harinck, K.G. Smit, W. de Jong, Supercritical Water Gasification of Biomass: A Literature and Technology Overview, *Energies*. 8 (2015) 859–894. doi:10.3390/en8020859.
- [47] S.N. Reddy, S. Nanda, A.K. Dalai, J.A. Kozinski, Supercritical water gasification of biomass for hydrogen production, *Int. J. Hydrogen Energy*. 39 (2014) 6912–6926. doi:10.1016/j.ijhydene.2014.02.125.
- [48] T. Bridgwater, *Biomass Pyrolysis, Task 34 Overview*, (2007) 1–20.
- [49] D. Knorr, J. Lukas, P. Schoen, N. Technical, M. Mary, *Production of Advanced Biofuels via Liquefaction - Hydrothermal Liquefaction Reactor Design*, Atlanta, Georgia, 2013.
- [50] F. Goudriaan, J. Naber, E. van der Berg, *Conversion Of Biomass Residues To Transportation Fuels With The HTU® Process*, n.d.
- [51] E. Miliotti, *Analysis, study and design of a biomass hydrothermal liquefaction plant*, University of Florence, 2015.
- [52] D. Elliott, D. Santosa, C. Valkenburg, G. Neuenschwander, S. Jones, T. Hart, L.J. Rotness, S. Tjokro Rahardjo, A. Zacher, *Catalytic Hydrothermal Gasification of Lignin-Rich Biorefinery Residues and Algae Final Report*, 2009. http://www.pnl.gov/main/publications/external/technical_reports/PNNL-18944.pdf.
- [53] N. Boukis, U. Galla, P. D’Jesus, H. Müller, E. Dinjus, Gasification of wet biomass in supercritical water. Results of pilot plant experiments, in: *14th Eur. Biomass Conf.*, Paris, France, 2005: pp. 964–967.
- [54] A.N. Stranges, Germany’s Synthetic Fuel Industry 1927-45, *Energieia*. 12 (2001) 1–13. doi:10.1007/978-94-015-9377-9_7.
- [55] F. Bergius, Chemical reactions under high pressure, in: *Nobel Lect. Chem. 1922-1941*, Elsevier, Amsterdam, 1966: pp. 244–276.
- [56] F. Bergius, *Die Anwendung hoher Drucke bei chemischen Vorgängen und eine Nachbildung des Entstehungsprozesses der Steinkohle.*, (1913) 58 S. file://catalog.hathitrust.org/Record/001425415.
- [57] J. Fohl, W. Lugscheider, G. Tessmer, F. Wallner, Entfernen von Wasser aus der Braunkohle. II: Thermische Entwässerungsverfahren, *Braunkohle*. 39 (n.d.) 78–87.
- [58] M.C. Mensinger, Wet carbonization of peat: state-of-the-art review, in: *IGT Symp. Peat as an Energy Altern.*, IIT Center, Chicago, IL, United States, 1980. <http://www.osti.gov/scitech/servlets/purl/6798156>.
- [59] Q. Wang, H. Li, L. Chen, X. Huang, Monodispersed hard carbon spherules with uniform nanopores, *Carbon N. Y.* 39 (2001) 2211–2214. doi:10.1016/S0008-6223(01)00040-9.
- [60] B. Hu, K. Wang, L. Wu, S.-H. Yu, M. Antonietti, M.M. Titirici, Engineering carbon materials from the hydrothermal carbonization process of biomass., *Adv. Mater.* 22 (2010) 813–28. doi:10.1002/adma.200902812.
- [61] B. Hu, S.-H. Yu, Functional carbonaceous materials from hydrothermal carbonization of biomass: an effective chemical process, *Dalt. Trans.* 9226 (2008) 5414–5423. doi:10.1039/b804644c.
- [62] M.M. Titirici, M. Antonietti, Chemistry and materials options of sustainable carbon materials made by hydrothermal carbonization, *Chem. Soc. Rev.* 39 (2010) 103–116. doi:10.1039/B819318P.
- [63] M.-M. Titirici, A. Thomas, M. Antonietti, Back in the black: hydrothermal carbonization of plant

material as an efficient chemical process to treat the CO₂ problem?, *New J. Chem.* 31 (2007) 787. doi:10.1039/b616045j.

- [64] Y. Zhang, *Hydrothermal Liquefaction to Convert Biomass into Crude Oil*, Blackwell Publishing, 2010. <http://age-web.age.uiuc.edu/bee/research/IntroHTL.pdf>.
- [65] A. Kruse, N. Dahmen, Water – A magic solvent for biomass conversion, *J. Supercrit. Fluids.* 96 (2015) 36–45. doi:10.1016/j.supflu.2014.09.038.
- [66] Ingelia Italia, Ingelia Italia website, (n.d.). <http://www.ingelia.it> (accessed February 8, 2017).
- [67] Ingelia, Ingelia website, (n.d.). <http://www.ingelia.com/?lang=en> (accessed February 8, 2017).
- [68] CREO-HTC, CREO-HTC website, (n.d.). <http://www.creo-htc.it/> (accessed February 8, 2017).
- [69] M.L. Hernandez, Hydrothermal Carbonisation of Organic fraction Municipal Solid Waste, in: 1st Int. Symposium Hydrothermal Carbonization, Queen Mary University, London, 2017.
- [70] M. Manobianco, Osservazioni al PRGRU – CUP 7769, (2016). http://vias.regione.campania.it/opencms/export/sites/default/VIAVAS/download/allegati/Del_Piano/7769/Ingelia_Italia_OSSERVAZIONI_AL_PRGRU_REVMAX_PP.pdf.
- [71] M.L. Hernandez, Ingelia Solid HTC biofuel from Hydrothermal Carbonization, in: Expobioenergía, Valladolid, Spain, 2011.
- [72] SunCoal Industries GmbH, Making Energy from Organic Waste | SunCoal Industries, (n.d.). <http://www.suncoal.de/en> (accessed February 9, 2017).
- [73] M. Child, Industrial-Scale Hydrothermal Carbonization of Waste Sludge Materials for Fuel Production, Lappeeranta University of Technology, 2014.
- [74] Valmet Corporation, Biotechnology at the edge Reducing carbon footprint and creating new revenue streams, (2016). http://www.suncoal.de/uploads/20161012_Valmet_SunCoal_Partnership.pdf.
- [75] D. Siemon, SunCoal Company Presentation, in: IFAT, Munich, 2014. http://www.bv-htc.de/stuff/downloads/ifta2014/9_SunCoal.pdf.
- [76] CS CarbonSolutions GmbH, CS carbonSolutions - Hydrothermale Carbonisierung, (n.d.). <http://www.cs-carbonsolutions.de/> (accessed February 6, 2017).
- [77] Grenol GmbH, Grenol visions into future, (n.d.). <http://www.grenol.org/index.php?id=8&L=1> (accessed February 2, 2017).
- [78] Grenol GmbH, Hydrothermal carbonization - Key Technology in biomass waste treatment, (2012). http://ecoexpoasia.com/pdf/2012/30.10_Waste_Management-_Tina_External.pdf.
- [79] Grenol GmbH, Hydrothermal carbonization - Key Technology in biomass waste treatment, (2016). http://philippinen.ahk.de/uploads/media/Grenol_Alfons_Kuhles_Maite_Dittke.pdf.
- [80] T. Guenther, K. Serfass, Hydrothermal Carbonization The path to an energy autonomous sewage plant, in: IWAMA 2nd Int. Capacit. Dev. Work. Energy Prod. WWT, Boltenhagen, Germany, 2017: pp. 1–23. http://www.iwama.eu/sites/iwama/files/materials/6_gunther_htc_energy_autonomous_sewage_plant.pdf.
- [81] T. Dolden, Loritus Hydrothermal Carbonization - Waste to Biocoal, Waste to Biochar, (2015). <http://tdolden.wixsite.com/loritus-htc/technology>.

- [82] Loritus, Loritus website, (2015). <http://tdolden.wixsite.com/loritus-htc/technology>.
- [83] TerraNova Energy GmbH, TerraNova Energy – renewable fuel | systems for hydrothermal carbonization, (n.d.). <http://terranova-energy.com/en/> (accessed February 6, 2017).
- [84] TerraNova Energy GmbH, The TerraNova@ Ultra Process, (n.d.) 200. doi:10.1017/CBO9781107415324.004.
- [85] TerraNova Energy GmbH, Process Flow TerraNova@ Ultra with integral Phosphorous-Recovery, (n.d.). <http://terranova-energy.com/pdf/TNEPrecoveryen.pdf>.
- [86] A. Kruse, D. Baris, N. Tröger, P. Wiecek, Scale-Up in Hydrothermal Carbonization, in: Maria Magdalena Titirice (Ed.), Sustain. Carbon Mater. from Hydrothermal Process., John Wiley & Sons, Ltd, Oxford, UK, 2013: pp. 341–353. doi:10.1002/9781118622179.ch9.
- [87] Businesswire.com, AVA-CO2 Introduces the First Industrial-Size Hydrothermal Carbonisation (HTC) Plant in the World | Business Wire, (2010). <http://www.businesswire.com/news/home/20101026006679/en/AVA-CO2-Introduces-Industrial-Size-Hydrothermal-Carbonisation-HTC-Plant> (accessed February 1, 2017).
- [88] T.M. Kläusli, Hydrothermal Carbonisation Energy from Biomass, (2013). <http://duene-greifswald.de/doc/rrr2013/talks/HTC.pdf>.
- [89] sustainabilityconsult.com, Press Release: AVALON Industries Takes Over All Bio-based Chemistry Activities From AVA-CO2, (2016). <http://www.sustainabilityconsult.com/news/229-press-release-avalon-industries-takes-over-all-bio-based-chemistry-activities-from-ava-co2> (accessed February 1, 2017).
- [90] AVA Biochem, Press release - First Industrial Production for Renewable 5-HMF, Muttenz, Switzerland, 2014. http://www.ava-biochem.com/media/downloads_EN/press_releases/First_Industrial_Production_For_Renewable_5_HMF.pdf.
- [91] AVA-CO2 Schweiz AG, Press release - HTC-1: The First Industrial Plant for hydrothermal carbonization Worldwide by AVA-CO2 Begins Trial Operations, (2012). http://www.ava-co2.com/web/media/downloads_EN/medienmitteilungen/PressRelease_EN_HTC-1_Relzow.pdf.
- [92] K. Suwelack, N. Dostert, D. Wüst, A. Kruse, Economics of Hydrothermal Carbonization of Biogas Digestate in a Hybrid AD-HTC Plant, in: 24th Eur. Biomass Conf. Exhib., Amsterdam, The Netherlands, 2016: pp. 1727–1733. doi:10.5071/24thEUBCE2016-3DO.9.4.
- [93] Agrokraft, HTC - Artec biotechnologie, (2015). <http://www.agrokraft.de/projekte/htc/> (accessed January 31, 2017).
- [94] M. Klemm, A. Clemens, R. Blümel, F. Kietzmann, Hydrothermale Carbonisierung (HTC) biogener Reststoffe, (2014).
- [95] Leibniz-Institut für Agrartechnik und Bioökonomie e.V., SmartCarbon AG, (n.d.). <https://www.atb-potsdam.de/?id=1317>.
- [96] SmartCarbon AG, Die hydrothermale Carbonisierung, (2014). http://www.bv-htc.de/stuff/downloads/ifta2014/8_Smart_Carbon.pdf.
- [97] Antaco UK Ltd, Antaco - Innovative biofuel technology, converting organic waste into fuel, (2017). <http://www.antaco.co.uk/> (accessed February 2, 2017).
- [98] J.R. Pels, P.C.A. Bergman, TORWASH Proof of Principle -Phase 1, ECN-E--06-021, 2006.

- [99] ECN, ECN: FGV collaborates with ECN to create high-quality fuel pellets, (2015). <https://www.ecn.nl/news/item/fgv-collaborates-with-ecn-to-create-high-quality-fuel-pellets/> (accessed October 10, 2017).
- [100] A.J. Grootjes, J.R. Pels, M.C. Carbo, H. Kuipers, J. Vogelaar, J.H.A. Kiel, TORWASH® sewage sludge treatment, in: 25th Eur. Biomass Conf. Exhib., Stockholm, Sweden, 2017.
- [101] Japan External Trade Organization(JETRO), Turning Trash Into Treasure Shinko Tecnos. Co., Ltd., (2016). https://www.jetro.go.jp/en/mjcompany/shinko_tecnos/ (accessed May 10, 2017).
- [102] K. Yoshikawa, Commercial – scale demonstration of high quality solid fuel and fertilizer production from biomass and wastes employing HTC, in: 1st Int. Symposium Hydrothermal Carbonization, Queen Mary University, London, 2017.
- [103] United Nations Industrial Development Organization Investment and Technology Promotion Office Tokyo, Waste management: Hydrothermal Treatment Technology, (n.d.). http://www.unido.or.jp/en/technology_db/2349/ (accessed May 10, 2017).
- [104] M. Toufiq Reza, C.J. Coronella, A. Nasr, Lab-scale Batch-to-Continuous reactor systems for hydrothermal carbonization of cow manure, (2016). doi:10.13140/RG.2.2.13607.34723.
- [105] Water Environment & Reuse Foundation, Technology Spotlight 2-18-16, (2016). http://www.werf.org/lift/docs/LIFT_Notes_Docs/2016/Technology_Spotlight/Technology_Spotlight_2-18-16.aspx (accessed October 10, 2017).
- [106] Kevin Coss, Two U Startups Named Among Best University Startups 2017, (2017). <https://research.umn.edu/inquiry/post/two-u-startups-named-among-best-university-startups-2017> (accessed October 10, 2017).
- [107] Frances White, PNNL: News - 3 small energy firms to collaborate with PNNL, (2017). <http://www.pnnl.gov/news/release.aspx?id=4387> (accessed October 10, 2017).
- [108] K.M. Bolin, B. Dooley, R.J. Kearney, Carbonization technology converts biosolids to an economical, renewable fuel, in: R.J. LeBlanc, P.J. Laughton, R. Tyagi (Eds.), Wastewater Biosolids Sustain. Tech. Manag. Public Synerg., Moncton, New Brunswick, Canada, 2007: pp. 591–597.
- [109] D.L. Bodde, Intentional Entrepreneur: Bringing Technology and Engineering to the Real New Economy., Taylor and Francis, 2016.
- [110] WaterWorld, EnerTech, HDR begin construction of first full-scale SlurryCarb facility, (2007). <http://www.waterworld.com/articles/2007/04/enertech-hdr-begin-construction-of-first-full-scale-slurrycarb-facility.html> (accessed December 31, 2017).
- [111] altenergymag.com, TIGER GROUP ANNOUNCES SALE OF ENERTECH RENEWABLE ENERGY PLANT, (2013). <https://www.altenergymag.com/news/2013/12/19/tiger-group-announces-sale-of-enertech-renewable-energy-plant-31733> (accessed December 31, 2017).
- [112] Josh Dulaney, EnerTech energy plant in Rialto closes – San Bernardino Sun, (2012). <https://www.sbsun.com/2012/11/01/enertech-energy-plant-in-rialto-closes/> (accessed December 31, 2017).
- [113] CarboREM, CarboREM website, (2018). <http://www.carborem.com/it/>.
- [114] E. Miliotti, D. Casini, G. Lotti, L. Bettucci, S. Pennazzi, A.M. Rizzo, D. Chiamonti, Valorization of solid residues from anaerobic digestion through thermal and hydrothermal carbonization process, in: 25th Eur. Biomass Conf. Exhib., Stockholm, Sweden, 2017: pp. 1063–1069. doi:10.5071/25thEUBCE2017-3DO.3.4.

- [115] E. Miliotti, D. Casini, M. Prussi, G. Lotti, L. Bettucci, A.M. Rizzo, D. Chiamonti, Lab-scale pyrolysis and hydrothermal carbonization of biomass digestate : Characterization of solid products, in: F. Berruti, R. Ocone, O. Masek (Eds.), *Biochar Prod. Charact. Appl.*, ECI Symposium Series, Alba, Italy, 2017. <http://dc.engconfintl.org/biochar/54>.
- [116] R.K. Garlapalli, B. Wirth, M.T. Reza, Pyrolysis of hydrochar from digestate: Effect of hydrothermal carbonization and pyrolysis temperatures on pyrochar formation, *Bioresour. Technol.* 220 (2016) 168–174. doi:10.1016/j.biortech.2016.08.071.
- [117] I. Oliveira, D. Blöhse, H.-G. Ramke, Hydrothermal carbonization of agricultural residues, *Bioresour. Technol.* 142 (2013) 138–146. doi:10.1016/j.biortech.2013.04.125.
- [118] A. Funke, J. Mumme, M. Koon, M. Diakité, Cascaded production of biogas and hydrochar from wheat straw: Energetic potential and recovery of carbon and plant nutrients, *Biomass Bioenergy.* 58 (2013) 229–237. doi:10.1016/j.biombioe.2013.08.018.
- [119] J. Mumme, L. Eckervogt, J. Pielert, M. Diakité, F. Rupp, J. Kern, Hydrothermal carbonization of anaerobically digested maize silage, *Bioresour. Technol.* 102 (2011) 9255–9260. doi:10.1016/j.biortech.2011.06.099.
- [120] D. Chiamonti, M. Buffi, A.M. Rizzo, G. Lotti, M. Prussi, Bio-hydrocarbons through catalytic pyrolysis of used cooking oils and fatty acids for sustainable jet and road fuel production, *Biomass Bioenergy.* 95 (2016) 424–435. doi:10.1016/j.biombioe.2016.05.035.
- [121] P.J. Valdez, J.G. Dickinson, P.E. Savage, Characterization of product fractions from hydrothermal liquefaction of *Nannochloropsis* sp. and the influence of solvents, *Energy and Fuels.* 25 (2011) 3235–3243. doi:10.1021/ef2004046.
- [122] S.R. Villadsen, L. Dithmer, R. Forsberg, J. Becker, A. Rudolf, S.B. Iversen, M. Glasius, Development and Application of Chemical Analysis Methods for Investigation of Bio-Oils and Aqueous Phase from Hydrothermal Liquefaction of Biomass, *Energy Fuels.* 26 (2012) 6988–6998. doi:10.1021/ef300954e.
- [123] MIPAAF - ICQRF, Decreto 31 maggio 2016 n.7276 “Approvazione dei Metodi ufficiali di analisi per i fertilizzanti - Supplemento n. 13, (2016).
- [124] Gazzetta Ufficiale, Decreto Legislativo 29 aprile 2010, n.75: “Riordino e revisione della disciplina in materia di fertilizzanti, a norma dell’articolo- lo 13 della legge 7 luglio 2009, n. 88”, (2010). <http://www.camera.it/parlam/leggi/deleghe/10075dl.htm> (accessed June 8, 2017).
- [125] European Biochar Foundation (EBC), European Biochar Certificate - Guidelines for a Sustainable Production of Biochar, (2016). doi:10.13140/RG.2.1.4658.7043.
- [126] International Biochar Initiative, Standardized Product Definition and Product Testing Guidelines for Biochar That Is Used in Soil, (2014) 1–60. https://www.biochar-international.org/wp-content/uploads/2018/04/IBI_Biochar_Standards_V2.1_Final.pdf.
- [127] S.A. Channiwala, P.P. Parikh, A unified correlation for estimating HHV of solid, liquid and gaseous fuels, *Fuel.* 81 (2002) 1051–1063. doi:10.1016/S0016-2361(01)00131-4.
- [128] A. Sluiter, B. Hames, R. Ruiz, C. Scarlata, J. Sluiter, D. Templeton, Determination of Sugars , Byproducts , and Degradation Products in Liquid Fraction Process Samples, 2008.
- [129] J. Mumme, L. Eckervogt, J. Pielert, M. Diakité, F. Rupp, J. Kern, Hydrothermal carbonization of anaerobically digested maize silage., *Bioresour. Technol.* 102 (2011) 9255–60. doi:10.1016/j.biortech.2011.06.099.
- [130] M. Sevilla, A.B. Fuertes, The production of carbon materials by hydrothermal carbonization of

cellulose, Carbon N. Y. 47 (2009) 2281–2289. doi:10.1016/j.carbon.2009.04.026.

- [131] E. Dinjus, A. Kruse, N. Tröger, Hydrothermal carbonization - 1. Influence of lignin in lignocelluloses, Chem. Eng. Technol. 34 (2011). doi:10.1002/ceat.201100487.
- [132] S. Kang, X. Li, J. Fan, J. Chang, Characterization of hydrochars produced by hydrothermal carbonization of lignin, cellulose, d-xylose, and wood meal, Ind. Eng. Chem. Res. 51 (2012) 9023–9031. doi:10.1021/ie300565d.
- [133] J.J. Manyà, Pyrolysis for biochar purposes: A review to establish current knowledge gaps and research needs, Environ. Sci. Technol. 46 (2012) 7939–7954. doi:10.1021/es301029g.
- [134] H. Huang, S. Wang, K. Wang, M.T. Klein, W.H. Calkins, A. Davis, Thermogravimetric and Rock-Eval studies of coal properties and coal rank, Energy and Fuels. 13 (1999) 396–400. doi:10.1021/ef980088q.
- [135] S.S. Toor, L. Rosendahl, A. Rudolf, Hydrothermal liquefaction of biomass: A review of subcritical water technologies, Energy. 36 (2011) 2328–2342. doi:10.1016/j.energy.2011.03.013.
- [136] A. Sinağ, S. Gülbay, B. Uskan, M. Güllü, Comparative studies of intermediates produced from hydrothermal treatments of sawdust and cellulose, J. Supercrit. Fluids. 50 (2009) 121–127. doi:10.1016/j.supflu.2009.05.009.
- [137] A. Kruse, P. Bernolle, N. Dahmen, E. Dinjus, P. Maniam, Hydrothermal gasification of biomass: consecutive reactions to long-living intermediates, Energy Environ. Sci. 3 (2010) 136–143. doi:10.1039/B915034J.
- [138] E. Miliotti, L. Bettucci, G. Lotti, S. Dell’Orco, A.M. Rizzo, D. Chiamonti, Hydrothermal carbonization and activation of lignin-rich ethanol co-product, in: 26th Eur. Biomass Conf. Exhib., Copenhagen, Denmark, 2018: pp. 969–972. doi:10.5071/26thEUBCE2018-3CO.3.4.
- [139] A. A. Sluiter, R. Ruiz, C. Scarlata, J. Sluiter, D. Templeton, Determination of Extractives in Biomass: Laboratory Analytical Procedure (LAP); Issue Date 7/17/2005 - 42619.pdf, Tech. Rep. NREL/TP-510-42619. (2008) 1–9. doi:NREL/TP-510-42621.
- [140] A. Sluiter, B. Hames, R. Ruiz, C. Scarlata, J. Sluiter, D. Templeton, D.C. Nrel, Determination of Structural Carbohydrates and Lignin in Biomass Determination of Structural Carbohydrates and Lignin in Biomass, 2011 (2012). doi:NREL/TP-510-42618.
- [141] A. Sluiter, B. Hames, R.O. Ruiz, C. Scarlata, J. Sluiter, D. Templeton, D. of Energy, A. Dötsch, J. Severin, W. Alt, E. a Galinski, J.-U. Kreft, Determination of Ash in Biomass, Microbiology. 154 (2004) 2956–69. doi:TP-510-42622.
- [142] J. Rouquerol, P. Llewellyn, F. Rouquerol, Is the bet equation applicable to microporous adsorbents?, Stud. Surf. Sci. Catal. 160 (2007) 49–56. doi:10.1016/S0167-2991(07)80008-5.
- [143] M. Thommes, K. Kaneko, A. V. Neimark, J.P. Olivier, F. Rodriguez-Reinoso, J. Rouquerol, K.S.W. Sing, Physisorption of gases, with special reference to the evaluation of surface area and pore size distribution (IUPAC Technical Report), Pure Appl. Chem. 87 (2015) 1051–1069. doi:10.1515/pac-2014-1117.
- [144] J. Rodriguez-Mirasol, T. Cordero, J.J. Rodriguez, Preparation and Characterisation of Activated Carbons from Eucalyptus Kraft Lignin, Carbon N. Y. 31 (1993) 87–95. doi:10.1016/0008-6223(93)90160-C.
- [145] S. Kang, X. Li, J. Fan, J. Chang, Characterization of hydrochars produced by hydrothermal carbonization of lignin, cellulose, d-xylose, and wood meal, Ind. Eng. Chem. Res. 51 (2012) 9023–9031.

doi:10.1021/ie300565d.

- [146] D. Castello, A. Kruse, L. Fiori, Low temperature supercritical water gasification of biomass constituents: Glucose/phenol mixtures, *Biomass Bioenergy*. 73 (2015) 84–94. doi:10.1016/j.biombioe.2014.12.010.
- [147] M.C. Schiff, A. Apruzzese, Produrre biogas, *Suppl. Di Agric.* 48 (2011).
- [148] GE Power, Jenbacher type 4 datasheet, (2007). <https://www.ge.com/power/gas/reciprocating-engines/jenbacher/type-4>.
- [149] H. Reichhalter, A. Bozzo, S. Dal Savio, T. Guerra, Analisi energetica, ambientale ed economica di impianti a biogas in Provincia di Bolzano - Relazione conclusiva -, Bolzano, 2011. http://orizzontenergia.it/download/Appr/BIOMASSA/2011_12_30_Analisi_energetica_ambientale_ed_economica_di_impianti_a_Biogas_Bilancio_ecologico_di_impianti_a_biogas_Bolzano_TIS_Innovation.pdf.
- [150] J. Bacenetti, Digestione anaerobica e energia termica, (n.d.). <https://studylibit.com/doc/3402221/digestione-anaerobica-e-energia-termica---master>.
- [151] K.L. Bothi, Characterization of biogas from anaerobically digested dairy waste for energy use, Cornell University, 2007. <https://ecommons.cornell.edu/handle/1813/5329>.
- [152] R. Zhang, Biogas Production Technologies, Biogas and Fuel Cell Workshop, National Renewable Energy Laboratory, 2012.
- [153] U. Bertelè, V. Chiesa, Biomass Energy Report, 2011.
- [154] S. Sutanto, J.W. Dijkstra, J.A.Z. Pieterse, J. Boon, P. Hauwert, D.W.F. Brillman, CO₂ removal from biogas with supported amine sorbents: First technical evaluation based on experimental data, *Sep. Purif. Technol.* 184 (2017) 12–25. doi:10.1016/j.seppur.2017.04.030.
- [155] F. Malpei, R. Canziani, Criteri di dimensionamento e tipologie di impianti per la produzione di biogas, (2011). http://www.xylemwatersolutions.com/scs/italy/it-it/Angolo_del_tecnico/atti_convegni/biogas_Cremona/Documents/malpei_canziani_rev1.pdf.
- [156] S. Castelli, S. Segato, Energia da biogas, Maggioli editore, 2014.
- [157] Centro Ricerche Produzioni Animali C.R.P.A. S.p.A., Stato dell'arte delle tecnologie di trattamento di tipo anaerobico e aerobico degli scarti organici, (2006) 1–106. <http://www.ilbiogas.it/biogas-ricerche-e-studi/impianti-crpa-modelli.pdf>.
- [158] F. Cecchi, D. Bolzonella, F. Fatone, V. Facchin, N. Frison, Mass & Energy balances around full scale plants for food waste anaerobic digestion, *Biotechnology*. (2011).
- [159] P. Fuksa, D. Kocourková, J. Hakl, J. Kalista, Influence of weed infestation on the calorific value and chemical composition of maize (*Zea mays* L.), *J. Plant Dis. Proctectio, Suppl.* 830 (2006) 823–830.
- [160] Pettorali Marco, Biomass Carbonization in Fixed-Bed Oxidative Reactor : Experimental Campaign and Technological developments, University of Florence, 2018. <http://hdl.handle.net/2158/1127793>.
- [161] L. D'Apote, D. Migliardi, Valorizzazione energetica del Biogas, Roma, 2010. <http://www.progettobiomasse.it/it/pdf/booklet/blu.pdf>.
- [162] W.L. McCabe, J.C. Smith, P. Harriott, Unit operations of chemical engineering, Fifth edit, McGraw Hill, 1993.

- [163] A. Onofri, Insilamento dei foraggi, Dipartimento di scienze Agrarie ed Ambientali, Università degli studi di Perugia, 2011. http://www.casaonofri.it/sistemiforaggeri/presentations/insilamento_s.pdf.
- [164] M. Lucian, L. Fiori, Hydrothermal carbonization of waste biomass: Process design, modeling, energy efficiency and cost analysis, *Energies*. 10 (2017). doi:10.3390/en10020211.
- [165] G. Kaletunç, Prediction of specific heat of cereal flours: A quantitative empirical correlation, *J. Food Eng.* 82 (2007) 589–594. doi:10.1016/j.jfoodeng.2007.03.028.
- [166] Great Wall Machinery Corporation, Cement Rotary Kiln, (2015). <http://www.greatwallcorporation.com/product/rotary-kiln/cement-rotary-kiln.html#a2>.
- [167] C. Remy, J. Warneke, B. Lesjean, J. Chauzy, C. Sardet, Energiebilanz und Carbon footprint von Referenztechnologien und HTC-Prozess bei der Klärschlammentsorgung, in: HTC-Workshop, Kompetenz Zentrum Wasser Berlin, 2013.
- [168] X. Lu, B. Jordan, N.D. Berge, Thermal conversion of municipal solid waste via hydrothermal carbonization: Comparison of carbonization products to products from current waste management techniques, *Waste Manag.* 32 (2012) 1353–1365. doi:10.1016/j.wasman.2012.02.012.
- [169] Therminol - Eastman, Therminol 66 technical data sheet, (n.d.). <https://www.therminol.com/products/Therminol-66>.
- [170] S. Hall, Rules of Thumb for Chemical Engineers, Elsevier, 2012. doi:10.1016/C2010-0-65782-8.
- [171] Metcalf & Eddy, G. Tchobanoglous, H.D. Stensel, R. Tsuchihashi, F.L. (Franklin L. Burton, M. Abu-Orf, G. Bowden, W. Pfrang, Wastewater engineering : treatment and resource recovery, Fifth edit, McGraw Hill Education, London, n.d.
- [172] F. Dilek, W. Sanin, W. Clarkson, P. Aarne, Sludge Engineering The Treatment and Disposal of Wastewater Sludges, (n.d.) 122.
- [173] J.R. Couper, W. Penney, J. Fair, W. M, Chemical engineers' equipment, Elsevier, 2009.
- [174] Flygt Industries, Slurry handbook Guidelines for slurry pumping, (2003) 1–48. http://www.hidrotecaguas.com/catalogos/Bombas_para_liquididos_abrasivos.pdf.
- [175] A. Ragazzoni, Analisi della redditività degli impianti per la produzione di biogas alla luce delle nuove tariffe incentivanti, in: BIOGAS E BIOMETANO UNA FILIERA Bioenerg. SOSTENIBILE, Ravenna, 2013. http://www.crupa.it/media/documents/crupa_www/Convegni/20130314_BiogasBiometano_RA/Ragazzoni_RA_14-3-2013.pdf.
- [176] R. W. Whitesides, Process Equipment Estimating by Ratio and Proportion, PHD Course G127. (2012) 1–8.
- [177] Autorità per l'energia elettrica il gas e il sistema idrico, Prezzi medi di vendita al mercato finale al dettaglio, (2017). <http://www.autorita.energia.it/it/dati/gp36.htm>.
- [178] Autorità per l'energia elettrica il gas e il sistema idrico, Prezzi finali dell'energia elettrica per i consumatori industriali - UE e area Euro, (2017). <http://www.autorita.energia.it/it/dati/eepcfr2.htm>.
- [179] GSE, GSE - Tariffa onnicomprensiva, (2016). http://www.gse.it/it/Qualifiche_e_certificati/Tariffa_omnicomprensiva/Pages/default.aspx.
- [180] H. Li, Q. Chen, X. Zhang, K.N. Finney, V.N. Sharifi, J. Swithenbank, Evaluation of a Biomass Drying Process Using Waste Heat From Process Industries: a Case Study, *Appl. Therm. Eng.* 35 (2012) 71–80.

- [181] W.A. Amos, Report on Biomass Drying Technology Report on Biomass Drying Technology, 1998.
- [182] R. Perry, D. Green, J. Maloney, Perry's chemical engineers' handbook, 1997. doi:10.10360071422943.
- [183] M. Krokida, D. Marinos-kouris, A.S. Mujumdar, Rotary Drying, in: *Handb. Ind. Dry.*, 2006: pp. 151–171. doi:10.1080/07373938808916399.
- [184] T. Hatakeyama, K. Nakamura, H. Hatakeyama, Studies on heat capacity of cellulose and lignin by differential scanning calorimetry, *Polymer (Guildf)*. 23 (1982) 1801–1804. doi:10.1016/0032-3861(82)90125-2.
- [185] J. Sameni, S. Krigstin, D. dos S. Rosa, A. Leao, M. Sain, Thermal characteristics of lignin residue from industrial processes, *BioResources*. 9 (2014) 725–737. doi:10.15376/biores.9.1.725-737.
- [186] M.T. Reza, *Hydrothermal Carbonization of Lignocellulosic Biomass*, University of Nevada, Reno, 2011.
- [187] Z. Ma, S. Li, W. Qiao, S. Ren, Hydrothermal Degradation of Enzymatic Hydrolysis Lignin in Water-Isopropyl Alcohol Co-Solvent, *BioResources*. 11 (2016) 6867–6879. doi:10.15376/biores.11.3.6867-6879.
- [188] B. El Khaldi-hansen, M. Schulze, B. Kamm, Qualitative and Quantitative Analysis of Lignins from Different Sources and Isolation Methods for an Application as a Biobased Chemical Resource and Polymeric Material, in: S. Vaz Jr. (Ed.), *Anal. Tech. Methods Biomass*, Springer International Publishing, 2016. doi:10.1007/978-3-319-41414-0.
- [189] A. Barlassina, Studio della lignina nel campo dei trattamenti superficiali di substrati metallici, Politecnico di Milano, Dipartimento di Chimica, Materiali e Ingegneria Chimica "Giulio Natta," 2015.
- [190] M. Milhé, L. Van De Steene, M. Haube, J.M. Commandré, W.F. Fassinou, G. Flamant, Autothermal and allothermal pyrolysis in a continuous fixed bed reactor, *J. Anal. Appl. Pyrolysis*. 103 (2013) 102–111. doi:10.1016/j.jaap.2013.03.011.
- [191] S.-Q. Li, L.-B. Ma, W. Wan, Q. Yao, A Mathematical Model of Heat Transfer in a Rotary Kiln Thermo-Reactor, *Chem. Eng. Technol*. 28 (2005) 1480–1489. doi:10.1002/ceat.200500241.
- [192] S.-Q. Li, J.-H. Yan, R.-D. Li, Y. Chi, K.-F. Cen, Axial transport and residence time of MSW in rotary kilns Part I. Experimental, *Powder Technol*. 126 (2002) 217–227. doi:10.1016/S0032-5910(02)00014-1.
- [193] S.-Q. Li, J.-H. Yan, R.-D. Li, Y. Chi, K.-F. Cen, Axial transport and residence time of MSW in rotary kilns: Part II. Theoretical and optimal analyses, *Powder Technol*. 126 (2002) 228–240. doi:10.1016/S0032-5910(02)00014-1.
- [194] W.F. Fassinou, L. Van de Steene, S. Toure, G. Volle, P. Girard, Pyrolysis of Pinus pinaster in a two-stage gasifier: Influence of processing parameters and thermal cracking of tar, *Fuel Process. Technol*. 90 (2009) 75–90. doi:10.1016/j.fuproc.2008.07.016.
- [195] S.A. Benson, C.R.C.R. Zaman, S.K.H.M.A.M.E.S. Olson, Activated Carbon Production from North Dakota Lignite, 2008. <https://www.osti.gov/servlets/purl/951063>.
- [196] N. Arena, J. Lee, R. Clift, Life Cycle Assessment of activated carbon production from coconut shells, *J. Clean. Prod*. 125 (2016) 68–77. doi:10.1016/j.jclepro.2016.03.073.
- [197] O.A. Ortiz, N.D. Martínez, C.A. Mengual, L.M. Petkovic, Performance analysis of pilot rotary kiln for activated carbon manufacture, using a steady state mathematical model, *Lat. Am. Appl. Res*. 33 (2003) 295–300.
- [198] C. Ng, W. Marshall, R.M. Rao, R.R. Bansode, J.N. Losso, R.J. Portier, Granular Activated Carbons from

Agricultural By-products : Process Description and Estimated Cost of Production, 2003.